The Pennsylvania State University
The Graduate School
College of Engineering

SEGMENTAL DYNAMICS AND ION ASSOCIATION IN POLY(ETHYLENE OXIDE) BASED SINGLE ION CONDUCTORS

A Dissertation in
Chemical Engineering
by
Kokonad Sinha

Submitted in Partial Fulfillment
of the Requirements
for the Degree of

Doctor of Philosophy

May 2012

The dissertation of Kokonad Sinha was reviewed and approved* by the following:

Janna K. Maranas
Associate Professor of Chemical Engineering and Materials Science and Engineering
Dissertation Advisor, Chair of Committee

Michael Janik
Assistant Professor of Chemical Engineering and Chair of the Brennan Clean Energy Early Career Professorship

Scott T. Milner
Joyce Chair Professor of Chemical Engineering

James S. Vrentas
Dow Professor of Chemical Engineering

James Runt
Professor of Materials Science and Engineering

Andrew Zydney
Walter H. Robb Chair, Professor, and Department Head of Chemical Engineering

*Signatures are on file in the Graduate School.

Abstract

Increased use of hand held electronic devices have fueled the need for smaller and more flexible lithium ion batteries. The mechanical flexibility of currently used batteries is reduced because of the use of liquid electrolytes, which require a rigid casing. Therefore, scientists are turning to replacing the liquid electrolyte with a solid polymer electrolyte (SPE), thereby eliminating the need for the casing. SPEs contain a polymer host such as polyethylene oxide (PEO) and a lithium salt, which provides the cation. Ionic conductivity in SPEs is coupled to the polymer mobility. The cation is solvated by ether oxygen atoms (EO) and the lithium moves by hopping from one EO-rich site to another. This movement is aided by the segmental mobility of the polymer. However, high anion mobility contributes to conductivity and results in reverse electrode polarization which degrades battery life. We therefore use single ion conductors (ionomers) where only the cation conducts. In this case a sulfonate anion is covalently bonded to a PEO backbone through an isophthalate comonomer unit. We use the nomenclature PEOx-Y%M for these ionomers (e.g. PEO400-50%Li). These samples allow us to vary the degree of sulfonation (Y, the percentage of sulfonated isophthalate groups), the spacer length (x, molecular weight of PEO between isophthalate groups) and the cation identity (M, which could be Li^+, Na^+ and Cs^+).

We use quasi-elastic neutron scattering (QENS) to study the PEO backbone dynamics of these ionomers as a function of ion content and ion identity. The ion content, defined as the molar ratio of cations to EO atoms, can be changed in two ways - by varying the degree of sulfonation ($Y \in [0,100\%]$), and by changing the MW of the spacer (x = 400, 600, or 1100). When we compare the dynamics of nonionic polymers (i.e. no acid groups - PEO600-0%) to that of pure PEO, we observe that the isophthalate group reduces the mobility of its neighboring atoms. Therefore, the overall dynamics is composed of two fractions - a fast fraction in the mid-region of the spacer away from the effect of the isophthalate group (bridge

atoms), and a slow fraction which neighbors the isophthalate group (anchor atoms). When we introduce ions by increasing the degree of sulfonation (PEO600-Y%Na), no new relaxations are observed, but the two fractions are affected differently. The bridge atoms appear to saturate at a low ion content of 0.01. In contrast, the anchor atoms have considerably reduced mobility when the ion content is above 0.01 due to crosslinking between ionic groups at the isophthalate units. Correspondingly, the anchor atom relaxation determines the glass transition temperature of the ionomer. We also compare the results to the PEO/$LiClO_4$ system, by comparing both polymer dynamics and conductivity as a function of ion content. The optimal ion content for ionomers is half that of the salt system, which we explain based on the differing behavior of polymer dynamics in the two systems. We further investigate the effects of changing ion content on the component dynamics by changing the spacer length (at 100% sulfonation). The trend in bridge and anchor atom dynamics depends mainly on the absolute ion content, and not on the way it is varied. On comparing the dynamics and conductivities of two samples which have similar ion content, we conclude that it is better to achieve a particular ion content by varying the spacer length (at 100% sulfonation) rather than having partial sulfonation.

Using QENS to calculate the ionic composition of bridge and anchor atoms, we incorporate the findings of small angle X-ray scattering (SAXS) and present a visual schematic of the dynamic patterning of bridge and anchor atoms. SAXS measurements also show that formation of ionic aggregates is characteristic of these ionomers and in some cases microphase separation occurs.

We also study the effect of different cations (Li^+, Na^+ and Cs^+) on the bridge and anchor atom dynamics of PEOx-100%M ionomers. The ion content of these systems is above 0.01, therefore, the bridge atom relaxation times are similar, and ion identity primarily affects the anchor atom relaxations. By correlating QENS data with SAXS measurements, we study the effect of aggregate size and extent of microphase separation on anchor atom dynamics. Li based samples have high extent of microphase separation, whereas Na and Cs based samples display a distribution of aggregate sizes. These morphological differences affect the nature of interaction between the cation and the anchor atoms. Based on the binding energies and atomic radii of these cations, we identify the factors which govern the anchor atom dynamics at different temperatures. We conclude that when the reduced temperature [T - T_g] is less than 60°C, the anchor atom dynamics are controlled by the cation coordination number (number of EO atoms that solvate a cation in a PEO environment). Comparatively, when [T - T_g] is greater than 60 °C, the dynamics are controlled by the cation-EO binding energies. Using QENS data, we further investigate the effect of spacer length on the degree of microphase separation in these samples.

We conclude by identifying conditions that are favorable for conductivity in single ion conductors. Molecular dynamics (MD) simulations on PEO600-100%Na show the existence of string like aggregates which assist in charge transfer. We recognize that to improve the conductivity of single ion conductors and solid polymer electrolytes in general, we need to focus on both favorable cation coordination states (like string like aggregates) as well as high polymer host mobility. While the presence of favorable cation coordination states help in charge transport, amorphous polymer domains are necessary for ion transport from one coordination state to another. We finally propose a sample design that allows this partial decoupling of ion transport and conductivity. This design can help us create string like aggregates as a function of several variables (such as length, concentration, chain length etc.). By studying the effect of such factors on dynamics and conductivity, we can build better single ion conductors.

Table of Contents

List of Figures

List of Tables

Acknowledgments

First and foremost, I would like to thank my advisor, Janna Maranas for giving me this enriching opportunity to work with her. Thank you for helping me through my doctoral work, exhibiting patience, always encouraging me and believing in me. You have made me more efficient and have greatly improved my writing and presentation skills. Thank you for encouraging me to go to conferences and meetings to showcase my work. You pushed me in the right direction when things were bleak and guided me through several bouts of frustration. I am particularly thankful to you for introducing me to neutron scattering; understanding the science and analyzing the data were the most challenging aspects, yet my favorite parts of my doctoral experience. I also deeply appreciate your allowing me enough time to recuperate from my surgery in 2009.

I would like to thank Ralph Colby, Jim Runt, Karen Winey and Karl Mueller and their students for helpful discussions. In particular I would like to thank Greg Tudryn for your timely help with sample preparation and interpretation of DRS data. I would also like to thank Wenqin Wang and Karen Winey for being very helpful with the interpretation of SAXS data.

I would like to thank all my committee members - James Vrentas, Mike Janik, Scott Milner and Jim Runt, who helped me identify the strengths and weaknesses in my research, both in terms of content and approach.

I would like to thank my colleagues Susan Fullerton Shirey, Ryan Bradley, María Antonieta Sánchez Farrán and Kan-Ju Lin for all your help and support. Grad school was definitely a lot of fun because you all were a significant part of it.

I would like to thank John Copley (NIST) and Eugene Mamontov (ORNL) for helpful discussions regarding the DCS and BASIS respectively. Thank you for being patient with my questions and experiment related requests.

I would also like to thank my friends at State College and around; the past five years are easily the most memorable ones in my life because of you. I would like to thank my friends, Sunando, Swayamjit and Amit, for being my comrades in the war against graduate school slump. Susan, from our trip to NIST together

in 2008 we have come a long way; I think of you as my mentor and I thank you for your friendship. María, I have learned a lot from your commendable work ethic and I thank you for being there as a friend, always encouraging me. I also express my heartfelt gratitude to Ipsa for your exceptional emotional support throughout and especially in the last few weeks; it means more to me than words can express. Your going over my thesis content was the icing on the cake.

Last and not the least, I would like to thank my parents, my brother and sister-in-law, and my dearly loved ones. My father, for setting high standards for my academics right at a young age. My mother, for consistently making sure I have eaten breakfast, lunch and dinner for the past 10 years that I have lived away from home. My brother, for being there for me as a guide and friend, and invariably making me laugh when I was under pressure. My sister-in-law, who treated me like her little brother and making sure I wasn't buckling under stress. Your care, affection, support and the remarkable ability to deal with me has given me strength and resolve to wade through tough times.

This work is supported by the Department of Energy, Office of Basic Energy Sciences, under Grant No. DEFG02-07ER46409. This work utilized facilities supported in part by the National Science Foundation under Agreement No. DMR-0454672. We acknowledge the support of the National Institute of Standards and Technology, U.S. Department of Commerce, and in providing the neutron research facilities used in this work. A portion of this research at Oak Ridge National Laboratory's Spallation Neutron Source was sponsored by the Scientific User Facilities Division, Office of Basic Energy Sciences, U. S. Department of Energy.

"No problem can withstand the assault of sustained thinking"
- Voltaire -

I dedicate this dissertation to my friends and family
Thank you for being there for me

Chapter 1

Single Ion Conductors as Solid Polymer Electrolytes

1.1 Solid polymer electrolytes

Lithium-ion batteries are one of the most popular types of batteries for portable electronics because of their high energy densities and the fact that they can be designed to be rechargeable. They also have a low self-discharge rate, and do not have a memory effect (loss of battery life due to incomplete charge-discharge cycles) that is prevalent in rechargeable Ni-Cd batteries. Beyond consumer electronics, lithium ion batteries are also growing in popularity for electric vehicles. Research is yielding a stream of improvements to traditional lithium battery technology, focusing on energy density, durability, cost, and intrinsic safety.

A typical lithium ion battery (see Figure 1.1) contains an electrolyte, which is a mixture of ethylene carbonate or diethyl carbonate and varying lithium complexes such as $LiPF_6$, $LiAsF_6$, $LiClO_4$, $LiBF_4$, and $LiCF_3SO_3$. The electrodes are intercalation compounds (e.g. Li_xCoO_2 and graphite intercalation compounds) that allow the lithium ions to reside in the structure during charge and discharge cycles. Originally, lithium metal was used as the electrode; however, the growth of lithium metal dendrites from the anode to the cathode led to short circuiting and explosions.[15] This led to the use of intercalation compounds, where lithium was present in its ionic rather than metallic state.

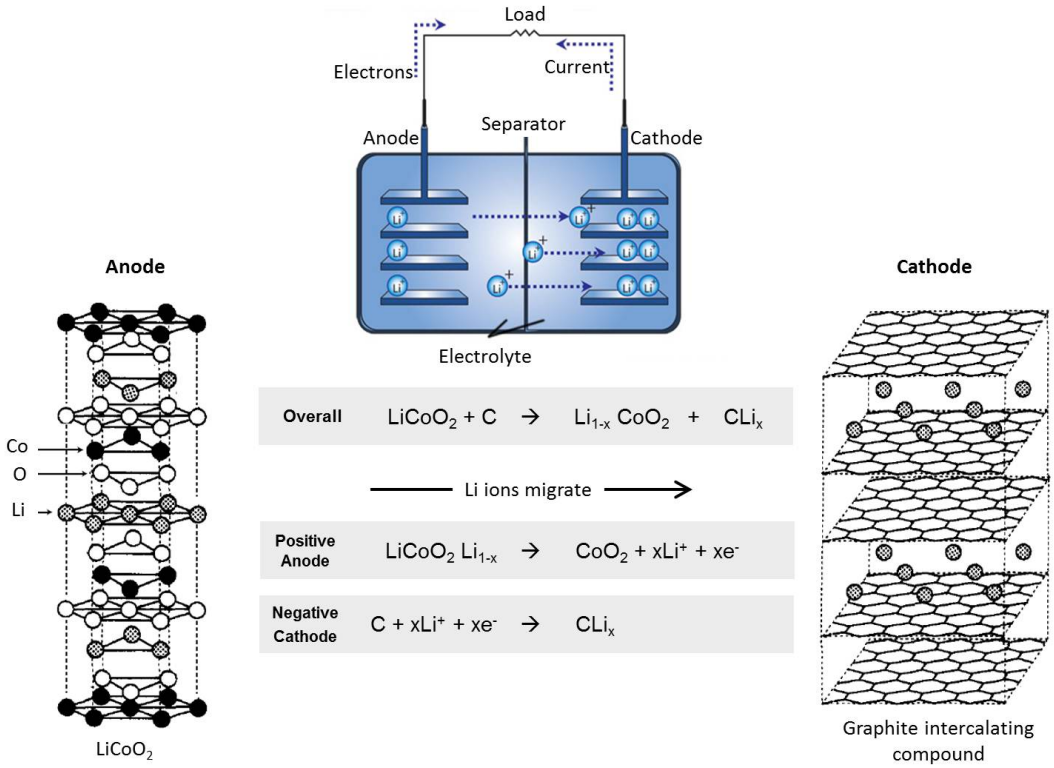

Figure 1.1. Schematic of a lithium ion battery

One of the primary practical disadvantages of lithium ion batteries (and other batteries in general) is the presence of the liquid electrolyte that is not only toxic but also requires a hard casing to house it. The rigid casing adds bulkiness to the size, shape and weight of electronic gadgets. Scientists are therefore turning to the use of solid polymer electrolytes (SPEs) which are non-toxic and do not require a casing. It was first shown in 1975 that polyethylene oxide (PEO) can act as a host for sodium and potassium salts, thus producing a solid polymer/salt complex.[16] Later in 1979, these complexes were proposed as SPEs by using them with appropriate electrodes.[17] Experiments and detailed mechanistic studies in 1983 established that the ionic motion in salt-polymer complexes is not due to transfer of charges (like metals), but is a continuous motion of the cation in the amorphous region of the polymeric material.[18,19]

The major challenge facing the use of solid polymer electrolytes for lithium batteries is the low conductivity. An ionic conductivity of more than 10^{-4} S/cm is necessary for batteries to generate a current density of 0.5-5 mA/cm^2 at room

temperatures,[20] which is attainable by electrolytes with solvent containing gels.[21] Currently, at room temperature and below, the conductivity of solid polymer electrolytes ranges from 10^{-9} to 10^{-7} S/cm and climbs up to practically useful values only at elevated temperatures of 80-100 °C. Many new polymer electrolytes have been synthesized in an effort to minimize the crystallinity and to achieve even lower T_g values, thus enhancing chain dynamics and hence increasing the level of ionic conductivity. However, these attempts have been mostly unsuccessful. PEO serves as a good host in this situation because the ether oxygen atoms solvate the cation, and the low glass transition temperature makes it amorphous at room temperature. However, from a practical viewpoint, PEO is not an ideal electrolyte; it has several shortcomings. Since it crystallizes easily, modifications are required to prevent it from happening and to retain/extend the amorphous domain to enable ion transport. Crosslinked polymer networks and comb polymers have been used to prevent crystallization,[22–24] and small-molecule plasticizers have been added to improve polymer mobility,[25–28] but with varied success. The use of ceramic nanoparticles is promising, because they succeed in raising the level of conductivity by several orders of magnitude to 10^{-5}-10^{-4} S/cm at room temperature.[2,29,30] Ideally, a solid polymer electrolyte would have the conducting properties of a liquid and the mechanical properties of a solid. Such a material would serve both as electrolyte and separator, and be mechanically flexible.

1.2 Single ion conductors

One of the major disadvantages of amorphous polymer/salt systems is that the fraction of conductivity from the cation (transference number) can be as low as 20-30%,[31] implying a larger contribution from the anion. This can pose a practical problem for lithium ion batteries, because anion accumulation at the electrode can cause reverse polarization within the battery, greatly increasing cell resistance and degrading peformance.[29,32] To remove this problem, the mobility of the anion should be reduced or eliminated, eventually obtaining "single ion conduction" state.[3,5,8,33–48] Three general methods have been identified to achieve single ion conduction in polymers[20] - (1) a blend of polyelectrolyte and ion conductive polymer host;[49,50] (2) the copolymerization of ion conductive monomer host and carrier

(cation) source monomer;[3,8,40,42,46,47,51] and (3) the polymerization of an ion conductive monomer which is also a cation source.[42]

Our focus in this study lies on the second category of ionomers, where the anion is covalently bonded to the polymer backbone through a comonomer unit, and then polymerized. We refer to single ion conductors as "ionomers" in this work, as a moniker for "ion containing polymers." Ionomers are characterized by the formation of ionic moieties that interact with the polymer backbone in varying degrees. Some studies postulate that the ions are distributed throughout the sample in a very low state of aggregation, i.e. in ion pairs or quadrupoles (ion quartets), whereas other studies postulate the existence of sizable aggregates $\sim$ 100Å.[52–54] It has been shown that the nature of ionic moieties depends on the dielectric constant of the medium. In media of low dielectric constant, ion associations such as pairs, triplets, quartets etc. are expected to exist, and the charges are as close to each other as physically possible.[53]

Since the anion is covalently bonded to the polymer backbone, the mobility of the polymer immediately surrounding the aggregates is reduced relative to the bulk material. This is called the *region of reduced mobility*, the dynamics of which depends on several factors - size of the aggregates, mobility of the backbone, length of the polymer chain, binding energies of the cations to the polymer and to the anion, temperature etc. Several ionomers show the presence of thermally stable ionic aggregates, where the extent of microphase separation increases as the temperature increases.[6,7,55–59] Because of the difference in properties of the bulk and reduced mobility regions, microphase separated ionic aggregates in ionomers have been shown to be analogous to microphase separated block copolymers. Studies have shown that longer segments in block copolymers with immiscible blocks tend to facilitate phase separation.[60–62] Smaller cations with stronger binding energies have also shown to increase the extent of microphase separation in single ion conductors.[63,64] Thus we see that though single ion conductors serve a practical purpose of eliminating anion mobility, these systems are more complicated to study compared to PEO/Li-salt systems. The crosslinking of the polymer through the aggregates presents an additional dimension to the investigation of the cation-polymer interaction.

1.3 Ion transport mechanisms in polymers

Lithium migration from one site to another can take place (without the need for significant polymer displacement) if the physical separation between cation favored sites is small, and the energy barriers between the sites are low.[21] There are two broad categories of ion conduction mechanisms. In the first, the cation requires the mobility of host as a medium of transport and is therefore *coupled* to the polymer mobility. Comparatively, in a *decoupled* mechanism, the cation migration occurs from one site to another without assistance from the host mobility. In SPEs, both coupled and decoupled modes of ion transport can take place, and the tendency for an SPE to allow either is denoted by the decoupling index (R), given by the ratio of mechanical relaxation time and the conductivity relaxation time.[11–14,65] For systems that have decoupled ion conduction, R $\sim 10^{12}$. Comparatively, glass forming systems such as PEO/$LiClO_4$ has R $\sim 10^4$ at T_g; and they have coupled conduction.

Ionic conductivity in amorphous solid polymer electrolytes is strongly coupled to polymer mobility. For PEO/Li-salt systems, lithium ions are solvated by 5-7 ether oxygen (EO) atoms on the PEO chains (see Figure 1.2a) and hop from one site to another in the presence of an electric field.[66–69] This hopping is facilitated by the segmental motion of the polymer. A simplified depiction is shown in Figure 1.2b. As the ion content increases, the coordination of the cations with EO atoms increases, resulting in lower polymer host mobility,[66,67,70,71] which in turn reduces conductivity. Thus most studies on SPEs strive to increase the ion mobility to a practical value by boosting the polymer mobility.

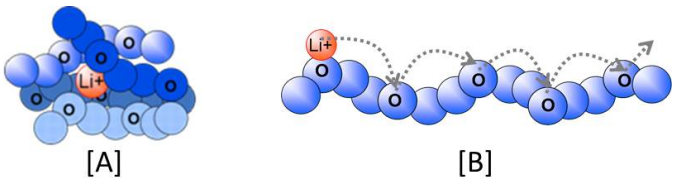

Figure 1.2. (A) Lithium cation coordinating with several ether oxygen atoms; (B) Motion of lithium ion by hopping along oxygen rich sites

The lithium ion can exist in several coordination states, of which the "single" state (Li coordinating with EO atoms alone, as shown in Figure 1.2a) is believed

to contribute the most to conductivity. Comparatively, lithium in clusters or pairs (neutral) contribute little. Charged clusters (e.g. triple ions: positive or negative) have the potential to contribute to conductivity either by transport or by charge transfer. For PEO based SPEs, the single ion content ranges from 20-60% (for ion contents near maximum conductivity) depending on the temperature and anion.[57,58,68,72] The fraction of single ions also depends on the size of the cation. Larger cations have smaller surface charge densities and therefore interact weakly with both anions and ether oxygen atoms.[20,40,41,73–78] Accordingly, larger cations can move faster in polymer solids through the fast exchange between sites owing to easy dissociation from anions and ether oxygen atoms. These systems therefore have higher conductivity. Note that larger organic cations such as tetraalkyl ammonium do not show high ionic conductivity (as expected from the above discussion) because the surface charge density of the ammonium cation is not completely delocalized through the alkyl groups. Quasi-elastic neutron scattering (QENS) has been used extensively to study the motion of the polymer in polymer/Li-salt systems. The polymer mobility of SPEs above their melting temperature has been measured using QENS for PEO/LiI,[70] PEO/$LiClO_4$,[2,79] PEO/LiTFSI[80] and PEO/$LiN(SO_2C_2F_5)_2$.[67,81] For all SPEs, as discussed before, the segmental mobility of PEO decreases with the addition of lithium salt because the lithium cations coordinate with multiple ether oxygen atoms. In most cases, it is important for the polymer host not to crystallize. This is because most crystalline phases of the polymer are pure, and do not incorporate the ion, thereby forcing the ion to stay in the amorphous phase. this leads to a higher ion content in the amorphous phase which in turn reduces the mobility and conductivity. For those systems in which the most stable crystal phase is PEO_6 with 6 PEO ether oxygens for each Li ion [PEO/LiTFSI,[80] PEO/$LiClO_4$[82] and PEO/$LiN(SO_2C_2F_5)_2$[83]] a process additional to segmental relaxation was observed.[2,66,67,81,84,85] Some authors attribute this to the formation and breaking of "crosslinks" between Li^+ and ether oxygen atoms.[67,85] These serve as transient states, with a life time estimated at 13-40 ns from computer simulations.[72,86] As discussed before, amorphous polymers have low conductivity for practical use because the ion motion is limited to depending on the segmental dynamics of the host polymer.

Comparatively, systems which support decoupled ion conduction mechanisms

report higher conductivity values than the coupled counterparts. While the common theme in decoupled systems is the availability of conduction pathways, most studies report the existence of crystal structures that involve the cation.[80,87–89] This is based on the idea that ionic conductivity is expected to be especially favored in a static environment where permanent pathways for ion transport are present.[90] In contrast to amorphous systems, if the sites to which an ion migrates are already present (like in a favored crystal structure), cation migration will occur if the vibrating ion gains sufficient energy to hop. By implication, designing more organized or ordered polymer electrolytes should enhance conductivity.[73,90–93] Crystalline materials have advantages over amorphous materials in this regard, as crystalline ionic conductors can be designed with identical pathways of appropriate size for ionic transport. On the other hand, the disordered nature of an amorphous material has an unpredictable number of ion transport sites. One such favorable structure which gives high conductivity even at room temperatures (by 2-4 orders of magnitude) is the PEO_6 crystal structure, which has two helical chains of PEO around a center of Li ions.[90,94,95] The Li ions use the PEO channels for conduction, while the anions lie between two PEO_6:Li structures. The conduction mechanism in crystalline systems is similar to ceramic ionic conductors. While certain kinds of deliberate impurities and imperfections can boost the conductivity of ceramic ionic conductors in more than one dimension, unwanted impurities and imperfections can severely restrict ion motion. These can arise from accidental mechanical stress among other factors; therefore one needs to be cautious about using them in practical situations.

A study of the PEO/$LiClO_4$ system shows that even above T_m, fragments of the PEO_6 crystalline phase discussed above can remain.[79] This has also been observed for PEO/LiTFSI[80] and in PEO/LiI.[89] The remnants of these crystalline phases rotate, and serve as conduction pathways for cations, resulting in higher conductivity.[2] This shows that even a partially decoupled ion transport mechanism can assist in achieving higher conductivity in amorphous polymers. We therefore need to explore this possibility as a viable solution for elevating ion conductivity in SPEs.

For single ion conductors, the conductivity values are generally low (about 2 orders of magnitude less than the polymer/salt counterparts[20]). This partly arises

from the ion content of ionomers, which is generally low because of limitations posed by the chemical structure. The alternative is to increase the frequency of the anion (and cation) occurring on the polymer backbone, but the aggregation of ions results in very high T_gs and therefore low conductivity. The stability of the aggregate also affects the overall conductivity of the ionomer, because the ion transference number and mobility does not depend solely on the amorphous region any more. The single ion fraction for ionomers is quite low because cations that are part of stable aggregates do not leave the aggregates, and rarely participate in conduction.[74] However, one cannot rule out one possible advantage of aggregates, some of which can potentially allow charge transfer (as opposed to actual cation motion) across the aggregate. There is also a possibility of small charged aggregates that are mobile and can contribute to conduction.[48,96–98] A good single ion conductor should consist of all three requirements - flexible structure, favorable ion conductive mechanism and the source of the carrier ion in one repeating unit,[20] and this study involves the investigation of one such PEO based single ion conductor.

1.4 Samples investigated in this study

We study systems where sulfonate groups (SO_3^- anion) are covalently bonded to a PEO chain by means of isophthalate groups (comonomer), as shown in Figure 1.3. We refer to these systems as PEOx-Y%M and they allow us to change three variables: (a) the ratio of isophthalate groups ionized with SO_3^- to the overall number of isophthalate groups, called the degree of sulfonation (Y%); (b) the length of the polymer between isophthalate groups, or the spacer unit (x); and (c) the identity of the cation. The degree of sulfonation and length of the spacer unit control the ion content of the sample. Variation of ion identity allows us to explore the effect of ion association energies on the cation-polymer interaction strength. The value x (400,600,1100) refers to the molecular weight in g/mol of the PEO spacer corresponding to N (9,13,25).

This study is a part of a collaboration investigating ionic transport in PEO-based single ion conductors. By combining results obtained from quasi-elastic neutron scattering (QENS), dielectric relaxation spectroscopy (DRS),[3,5,8] NMR,[99]

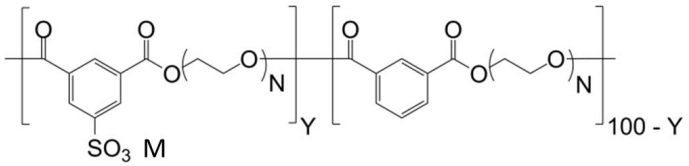

Figure 1.3. Chemical structure of PEOx-Y%M where x = 400/600/1100 and M = Li/Na/Cs

FTIR,[100] X-ray scattering,[5–7] *ab initio* calculations[6] and molecular dynamics simulations,[9,101,102] we address cation-polymer interactions through the interplay of dynamics, morphology, and ionic conductivity. ***The objective of this investigation is to study ionomer dynamics as a function of ion content and cation identity, and investigate the interplay of the PEO backbone mobility, conductivity, and morphology.*** We expect that the presence of ions will lower the mobility of the polymer like in PEO/Li-salt systems, but with some additional considerations. The presence of a comonomer every N repeat units means that a significant fraction of the PEO spacer could be influenced by the comonomer, should its dynamics vary considerably from PEO. When ions are present, they may not solvate all parts of the PEO spacer equally (for example, they may prefer locations near the anions), leading to interesting changes in dynamics with ion content and ion identity. These samples show little or no crystallinity, so we can expect that the polymer dynamics is tied to conductivity.

These ionomers offer an additional advantage due to its chemical structure: by varying the spacer length and ion content, we can potentially examine both, coupled and decoupled forms of ion conduction. The ions in these ionomers tend to segregate and eventually microphase separate into ion-rich domains that are thermally stable as shown by SAXS measurements.[6,7] The extent of aggregate formation and microphase separation determines the nature of interaction between the cation and the polymer, which in turn affects conductivity. The single ion content of these ionomers has been estimated to be less than 1% using DRS measurements,[47] and FTIR detects no single ions.[100] As discussed previously, ionic aggregation in these samples greatly complicates the investigation of polymer behavior because ions crosslink the polymer chain through the isophthalate comonomer units. The study of the region of reduced mobility (created due to crosslinking) can

greatly enhance our understanding of conductivity mechanisms in these ionomers, because the majority of the cations directly interact with the polymer in this region. The region of reduced mobility can potentially have a T_g that is higher than the bulk, but there are two aspects which prevent the detection of a distinct T_g for this region - (1) the domain size may not be large enough to register a T_g, and (2) the boundary between this region and the bulk is not sharp, leading to a detection of a large range in T_g rather than two individual T_g values.

This disadvantage can be overcome by dielectric relaxation spectroscopy (DRS), but with some limitations. DRS measurements on PEO600-100%Li[3,103] and poly (ethylene oxide)-based polyurethane ionomers[47] show that segmental dynamics are slowed down by increasing ion content, reflected by the increase of the glass transition temperature.[3,103] For the PEO600-Y%Li system, four dielectric relaxations were observed. The segmental α process slows down with increasing ion content above a critical concentration. Two slower processes are present, the ion mode α_2, assigned to rotation of separated ion pairs, and a weak low-frequency α_3 process. The local β relaxation, due to local twisting of PEO segments, is not significantly affected by complexation of ether oxygens with Li cations. The origin of the α_3 process is not clear, but is attributed to the formation of local ion-rich structures pertaining to these ionomers.

Small-angle X-ray scattering (SAXS) suggests that the ions in this system occupy a wide range of local environments that depend on the ion content, ion identity and spacer length, and include microphase separated ionic aggregates, small clusters, ion pairs, and ions solvated by the PEO spacer.[6,7] The presence of ions affects the α_2 process, which in some cases dominates the DRS signal to the extent that the segmental relaxation is no longer visible. Since QENS primarily measures hydrogen atom motion and is not affected by the presence of ionic moieties in this system, it serves as an excellent technique to isolate the dyanmics of the polymer backbone. 95% of the hydrogen atoms are located on the polymer chains and we observe segmental motion of the PEO spacer. QENS has been applied to understanding the polymer dynamics of pure PEO and PEO/Li-salt systems, as discussed in the previous section. However, no QENS measurements have been made for studying the backbone dynamics of ionomers. Studies on ionomers using QENS have focused on the dynamics of the cation. Available stud-

ies include water dynamics and its influence on cation hopping and ion aggregation in NAFION ionomers,[104–107] and the dynamics of hydrogen-rich cations in PTFE based ionomers. In the latter case, the onset of cation mobility has been linked with the alpha relaxation of the polymer.[108] In the following section, we present an overview of the QENS measurements used to investigate the backbone dynamics in these PEO based single ion conductors.

1.5 Overview of investigation

In this study we investigate the polymer backbone dynamics of the PEOx-Y%Na ionomers by varying three features in the chemical structure - (a) degree of sulfonation, (b) spacer length, and (c) ion identity. We use quasi-elastic neutron scattering (QENS) to study the dynamics at three temperatures - 298 K, 323 K and 348 K. The measurement technique, instrument details and corresponding data treatment are discussed in *Chapter 2* and *Chapter 3*. In *Chapter 4* we identify the constituent dynamics of the polymer backbone. We first compare the dynamics of the non-ionic polymer (PEO600-0%) to pure PEO, and observe that the isophthalate group introduces a slower segmental relaxation in addition to that seen by pure PEO. The spacer segments far from the effect of the isophthalate group undergo a faster relaxation, and are similar to pure PEO dynamics. We refer to the slow fraction as anchor atoms, and the fast fraction as bridge atoms. We then increase the degree of sulfonation to study how the presence of ions affects the two processes for the PEO600-Y%Na system (where Y $\in$ [0,100]). We initially choose this system because it does not microphase separate in the temperature range of our study, in contrast to the Li ionomers, which show evidence of ion segregation at all temperatures of measurement.[3,6,8,47]

We further establish a comparison of this observation to the PEO/$LiClO_4$ system based on previous work in our group.[2] The ion content of PEO salt systems is defined by the ether oxygen (EO) to Li ratio and falls in the range of 4:1 to 50:1, although 8:1 - 14:1 are the most frequent targets because conductivity is maximized in this range. To connect the degree of sulfonation to this ratio, we consider the ion content, defined as the molar ratio of cations to EO atoms. This is the inverse of the ratio that is normally quoted, so that the nonionic polymer has

a well-defined ion content of 0. In *Chapter 5* we study the dynamics by changing the ion content in a different way - by varying the spacer length, while keeping the sulfonation at 100% (PEOx-100%Na where x = 400/600/1100). The respective trends of relaxation time vs. ion content for bridge and anchor atoms remain the same regardless of how we change the ion content. We further evaluate the ion content of the bridge and anchor atoms and collaborate this data with SAXS measurements to obtain the spatial organization of bridge and anchor atoms. This dynamic patterning is presented as a visual array varying with temperature and spacer length for PEOx-100%Na.

We then discuss the impact of ion identity on the dynamics of these samples (PEOx-100%M where x = 400/600/1100 and M = Li/Na/Cs) in *Chapter 6*. We investigate a hypothesis that governs the ionomer dynamics at different temperatures. It is expected that small cations such as Li conduct poorly because of their strong binding energy and vice versa for Cs, as discussed earlier in this chapter. However, deviations from the expected behavior show that the conductivity and ion transport not only depend on the amorphous region, but also on different cation coordination states that arise from aggregation. By comparing the dynamics to conductivity at different temperatures, we identify scenarios that facilitate conduction in single ion conductors. Based on these observations we present a conduction mechanism that partially decouples charge transport and polymer mobility. In conclusion, we present a sample design that can potentially utilize the conduction mechanism mentioned above. The samples studied in this thesis are listed in Table 1.1, along with their ion content values, glass transition temperature (T_g) and molecular weight (MW). The key results of this study and some thoughts about the future direction of this research are outlined in *Chapter 7*.

Table 1.1. Properties of PEOx-Y%M samples (where x = 400/600/1100, Y ∈ [0,100] and M = Li/Na/Cs) and PEO/$LiClO_4$[2]

Sample	Cation:EO ratio	Ion content	T_g (K)	Molecular Weight (g/mol)
PEO600-0%Na	0	0	229	5800
PEO600-6%Na	1:217	0.005	230	5800
PEO600-11%Na	1:118	0.008	232	5800
PEO600-17%Na	1:76	0.013	233	8700
PEO600-49%Na	1:26	0.038	245	4700
PEO600-100%Na	1:13	0.077	267	6300
PEO400-100%Li	1:09	0.111	285	3300
PEO600-100%Li	1:13	0.077	258	4600
PEO1100-100%Li	1:25	0.04	236	4500
PEO400-100%Na	1:09	0.111	295	3300
PEO600-100%Na	1:13	0.077	267	4600
PEO1100-100%Na	1:25	0.04	236	4500
PEO400-100%Cs	1:09	0.111	294	3300
PEO600-100%Cs	1:13	0.077	270	4600
PEO1100-100%Cs	1:25	0.04	238	4500
PEO/$LiClO_4$	1:30	0.033	251	500000
PEO/$LiClO_4$	1:14	0.071	257	500000
PEO/$LiClO_4$	1:10	0.01	246	500000
PEO/$LiClO_4$	1:8	0.125	256	500000
PEO/$LiClO_4$	1:4	0.25	264	500000

Chapter 2

Experimental Techniques

The purpose of this chapter is to briefly discuss the techniques used for this study. We will also briefly discuss the details of neutron scattering instruments used at National Institute of Standards and Technology (NIST) at Gaithersburg, MD and Oak Ridge National Labs (ORNL) in Oak Ridge, TN.

2.1 Quasi Elastic Neutron Scattering Fundamentals

Quasi Elastic Neutron Scattering serves as a useful tool to study the dynamics of polymers, proteins and several other soft materials. Since polymer dynamics occurs on the length scale of angstroms (Å) and time scales of picoseconds (ps), neutrons serve as a good probe because they have the wavelength of interatomic distances and energy of interatomic interactions. The combination of these properties helps to quantify polymer dynamics (with a characteristic time) as a function of spatial scale. Neutrons have the most penetration compared to other waves used to study materials.[1] Electron waves are deflected by the electron cloud around an atom, and therefore penetrate the least. X-rays penetrate more, but are affected by electromagnetic fields around the atom. Since a neutron has no charge and negligible electric dipole, it is unaffected by these fields. Since nuclear forces are short range forces, a nucleus is detected by a neutron only when it passes within 10^{-15} m of the nucleus. Most of the atom is empty space; the distance between

nuclei is 100,000 times the size of the neutron, resulting in high penetration by neutrons. For example, the signal attenuation per mm of aluminum for X-rays is 99%, whereas for neutrons is only 1%. Neutrons, like electrons and X-rays, respond differently to elements of different atomic numbers. However, unlike eletrons and X-rays, neutrons have a random dependence of penetration depth with different atomic numbers, as shown in Figure 2.1.

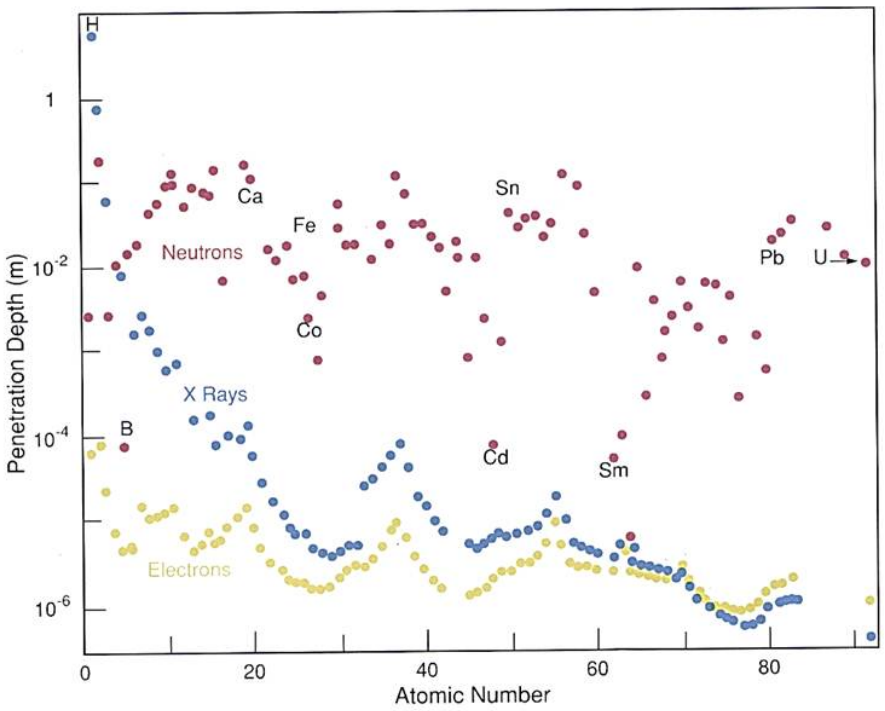

Figure 2.1. Dependence of penetration depth on atomic number for electrons, X-rays and neutrons, till the beam's intensity is reduced by a factor of 1/e, that is, to about 37% of its original intensity.[1]

Some atoms that scatter X-rays weakly, such as hydrogen, can scatter neutrons strongly. The extent of scattering is also dependent on the isotope of the element. For example, hydrogen scatters more strongly than deuterium. The extent of interaction between a neutron and the nucleus of an atom is determined by the effective area presented by the nucleus to the passing neutron. The scattering cross section, σ, is determined by

$$\sigma = 4\pi b^2 \tag{2.1}$$

where b is the scattering length of an atom. The total scattering signal is further

subdivided into coherent and incoherent contributions. The coherent scattering signal arises when the incident neutrons interact with all the nuclei in a coordinated fashion. The scattered waves have definite relative phases and can interfere with each other. Comparatively, the incoherent scattering contribution comes from the incident neutrons interacting with the nuclei independently of the other. The corresponding scattered waves have random, indeterminate relative phases and don't interfere with one another. Simply put, the coherent scattered signal contains information of the position of one atom relative to another, whereas the incoherent scattered signal contains information about one atom alone. The coherent and incoherent scattering lengths and cross sections for elements and their isotopes are available on the website of the NIST Center for Neutron Research (NCNR).[109] Neutrons can scatter elastically (no loss of energy) or inelastically (some loss/gain of energy) depending on whether it encounters immobile or mobile atoms in the sample. Structure can be measured with an instrument that detects the angle of the scattered neutrons, but does not detect an energy change between the neutron and the nucleus of the atom. In this case, the elastic scattering signal and coherent contribution provides information on the structure of the sample while the incoherent contribution adds a structureless background. Conversely, mobility can be measured if an energy change is detected by the instrument (either the neutron gains energy from or loses energy to the atom), and this type of scattering is inelastic. If the atoms in the sample scatter mostly incoherently, then the "self" motion is measured, whereas collective motion is measured if the atoms scatter mostly coherently. Figure 2.2 summarizes the different types of scattering, and the controlling variables. The instruments used in this study measure self motion (incoherent, inelastic).

For elastic scattering, the final enery of the scattered neutrons equals the initial energy; a plot of scattered neutron intensity vs. the difference of energy (δE = 0) gives a delta peak at 0, as shown in Figure 2.3a. For inelastic scattering, the initial and final energies are not equal, leading to peaks at non-zero values of δE. The location of peaks depends on the nature of motion by the molecule. The schematic shown in Figure 2.3b represents inelastic features arising from rotation of a small molecule such as CH_3I about the C-I axis. Quasi Elastic Neutron Scattering [QENS] is a special type of inelastic scattering where neutrons that would otherwise

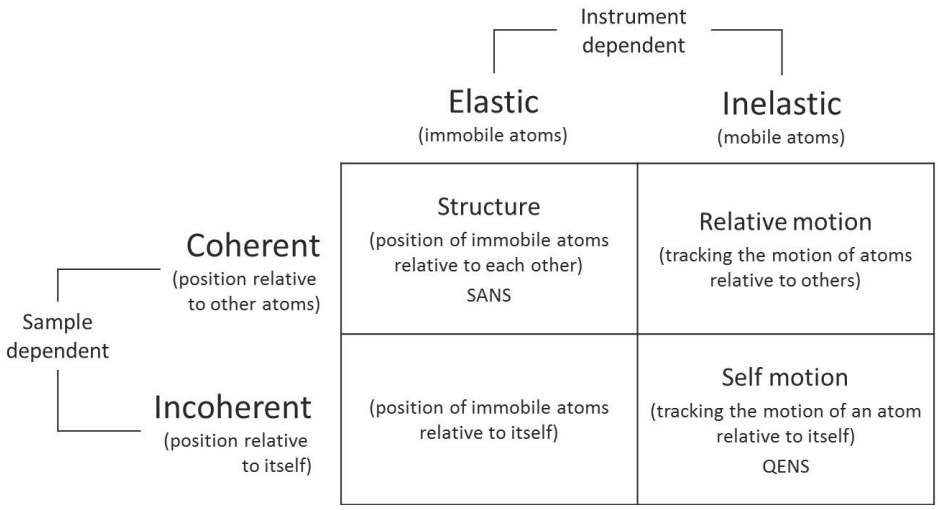

Figure 2.2. Types of neutron scattering measurements

scatter elastically undergo a small change in energy due to molecular rotations or diffusive motions. This causes a broadening of the elastic peak as shown in Figure 2.3c, implying that the deviation from an elastic feature quantifies molecular motion.

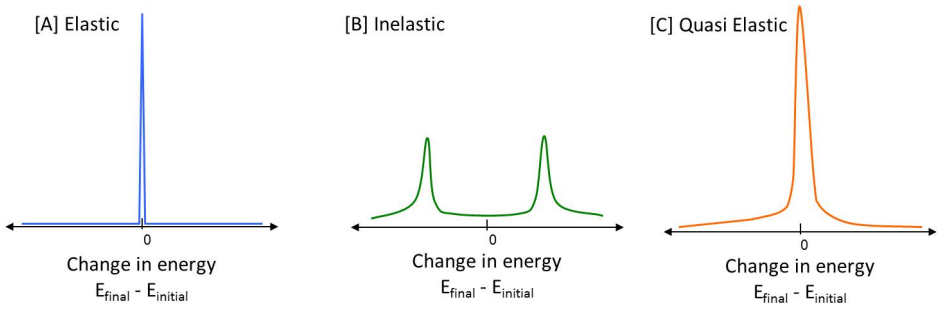

Figure 2.3. Examples of elastic, inelastic and quasi elastic neutron scattering

2.2 Neutron Scattering Instruments

In this section we discuss three instruments, two of which (Disc Chopper Spectrometer and High Flux Backscattering Spectrometer) are at the NIST, Gaithersburg, MD and one instrument (Backscattering Spectrometer) is at ORNL, Oak Ridge, TN.

2.2.1 Disk Chopper Time-of-flight Spectrometer [DCS]

The DCS (see Figure 2.4) is one of the two instruments used for this work at the NIST Center for Neutron Research (NCNR) at the National Institute of Standards and Technology (NIST), Gaithersburg, MD.[110] Pulses of neutrons with well

Figure 2.4. The DCS instrument at NCNR, NIST

defined incident energy (E_i) are scattered by the sample. Of the scattered neutrons, some do not exchange energy with the sample and are scattered elastically, whereas others exchange energy and are scattered inelastically. The energies that the neutrons gain or lose during the scattering are determined by the time they taken to arrive at an array of detectors, and hence these instruments are referred to as having time-of-flight geometries. This time can be calculated based on the arrival time at the sample (t_S) and at the detector (t_D). The scattered neutron velocity is calculated using the time-of-flight and the distance between the sample and detector. This velocity, along with the incident energy is used to calculate the final energy, E_f. The final energy is subtracted from the initial energy to give the energy transfer, $\hbar\omega$, where $\hbar$ is Planck's constant and ω is the frequency. Based on the value of the scattering angle, we can calculate the energy exchange as a function of the momentum transfer, Q. A schematic of time-of-flight geometry is

illustrated in Figure 2.5.

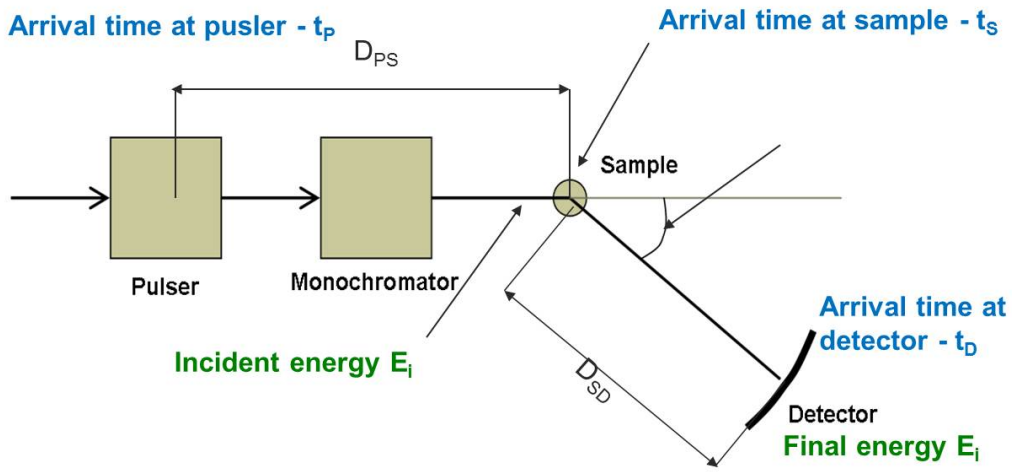

Figure 2.5. Schematic of time-of-flight geometry

We use an incident wavelength λ of 4.8 Å for our experiments, which corresponds to an energy resolution (medium) E_{res} of 57 μeV.[110] This gives an upper bound on the time range t_{max} at 72 ps, which is calculated using Planck's constant h (4.135 x 10^{-15} eV.s).

$$\begin{aligned} t_{max} &= \frac{1}{\nu} = \frac{h}{E_{res}} \\ &= \frac{4.135 \times 10^{-15}}{57 \times 10^{-6}} \\ &= 7.254 \times 10^{-11} s \sim 72\ ps \end{aligned}$$

Though 72 ps is the limit established by the above calculation, the measurement error of the instrument is unacceptable at this value. We therefore set the limit to about 50 ps. The lower bound on the time range, arises from the interplay of the scattering vector and energy. This is depicted using the Kinematically Allowed Region (KAR) in Figure 2.6. The red line at 1.55 meV represents the maximum energy loss measured by the system in this configuration. The accessible Q range is established by the limits of the region (blue lines) when the energy loss is zero (elastic peak). To calculate the lower time limit, we draw a horizontal line depicting fixed Q (e.g. Q = 1.04 $Å^{-1}$). The point 'x' which corresponds to an energy gain (ΔE) of 7.5 meV for this Q value. We calculate the lower time limit using the

following equations.

$$\begin{aligned} t_{min} &= \frac{1}{\nu} = \frac{h}{\Delta \mathrm{E}} \\ &= \frac{4.135 \times 10^{-15}}{7.8 \times 10^{-3}} \\ &= 5.3 \times 10^{-13} s \sim 0.53\ ps \end{aligned}$$

For Q values higher than 1.3 Å^{-1}, we use the limit -10.55 meV. The t_{min} values differ for every Q from 0.4 to 1 ps, and we report the accessible time range of DCS as 1 - 50 ps. In this configuration, the DCS instrument accesses a spatial scale ranging from from 3 to 11 Å.

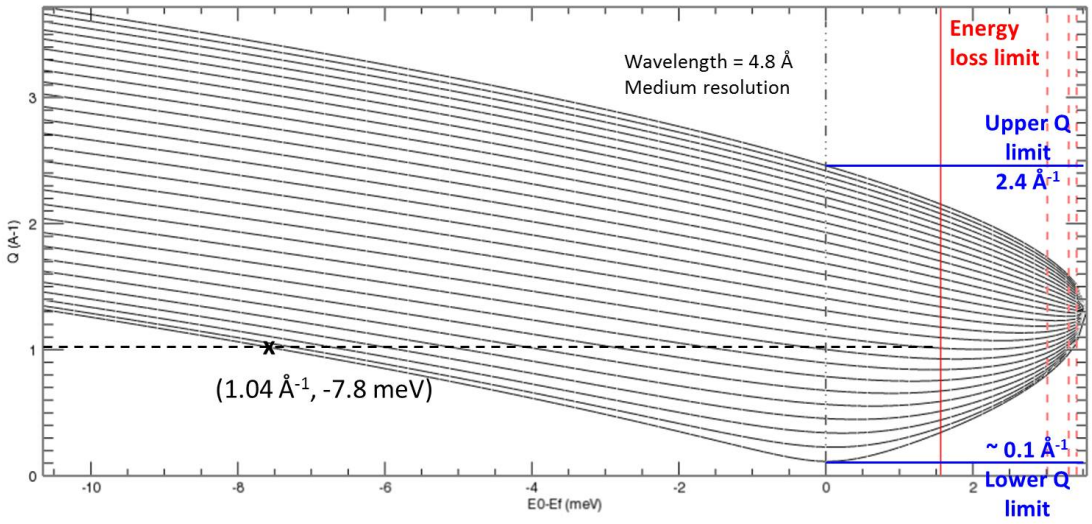

Figure 2.6. The kinematically allowed region for DCS at $\lambda = 4.8$ Å, medium resolution

2.2.2 High Flux Backscattering Spectrometer [HFBS]

To extend the energy window of our measurements, we compliment the DCS measurements with data from HFBS. The HFBS is an instrument with backscattering geometry, and is also located at the NCNR, NIST (see Figure 2.7).[111] The working schematic of the instrument is illustrated in Figure 2.8. The incident neutron beam encounters a phase space transformation [PST] chopper that Doppler-shifts the incident neutron wavelength distribution to the one desired for backscattering.

This shifting helps to maintain a high flux by correcting the velocity of neutrons that are too fast or too slow. After the PST, the neutrons are backscattered from a monochromator driven by a Doppler drive which alters the distribution of neutron energies (±17 in our case). The neutrons then strike the sample and backscatter from the analyzer before they finally reach the detectors. This way, the neutrons pass through the sample twice. The analyzers only backscatter neutrons of a specific wavelength; therefore, only neutrons with this wavelength are detected. Since the initial range of energies is known (E_i), and the final energy is constant (E_f), we can calculate the energy transfer as a function of scattering angle. We choose the dynamic range of the instrument (ΔE) to be ± 17 μeV, with an energy resolution of 1 μeV.[111] As with the DCS, the upper time limit is set by the resolution of the instrument, and the lower time limit is set by the accessible energy window.

$$\begin{aligned} t_{max} &= \frac{1}{\nu} = \frac{h}{E_{res}} \\ &= \frac{4.135 \times 10^{-15}}{1 \times 10^{-6}} \\ &= 4.135 \times 10^{-9} s \sim 4135\ ps \end{aligned}$$

$$\begin{aligned} t_{min} &= \frac{1}{\nu} = \frac{h}{\Delta \mathrm{E}} \\ &= \frac{4.135 \times 10^{-15}}{17 \times 10^{-6}} \\ &= 2.43 \times 10^{-10} s \sim 243\ ps \end{aligned}$$

Since the measurement error close to instrument resolution is very high, we set the upper limit at 2500 ps. Therefore, the time range accessible by HFBS is 250 - 2500 ps. The accessible spatial range is set by 16 detectors, and is similar to that of DCS: 3 - 11 Å.

2.2.3 Backscattering Spectrometer [BASIS]

We also conducted QENS experiments in BASIS at the Spallation Neutron Source (SNS), Oak Ridge National Labs (ORNL) (see Figure 2.9).[112] BASIS is a near-backscattering, crystal-analyzer spectrometer. The schematic of the instrument is

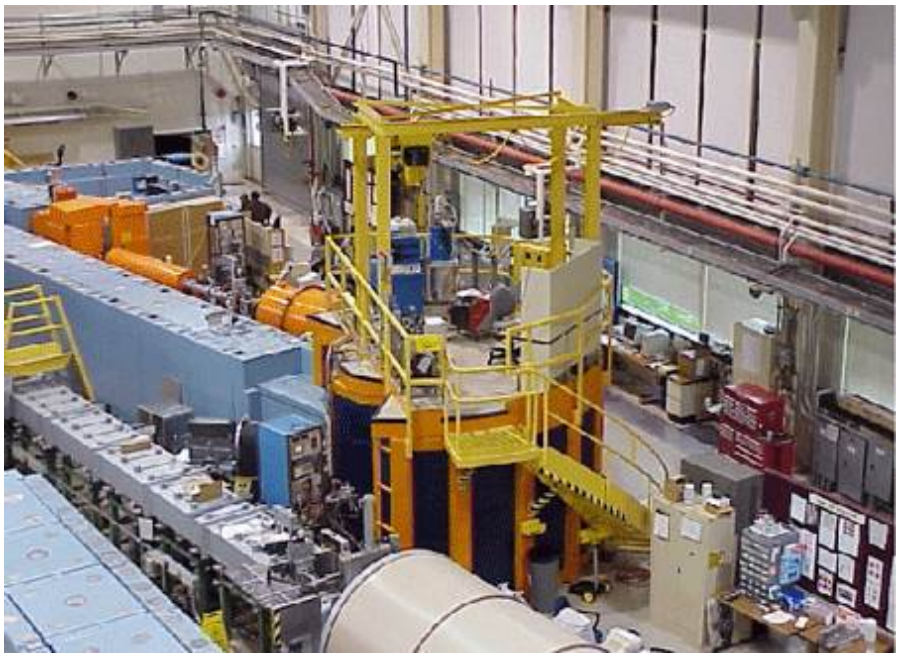

Figure 2.7. HFBS at NCNR, NIST

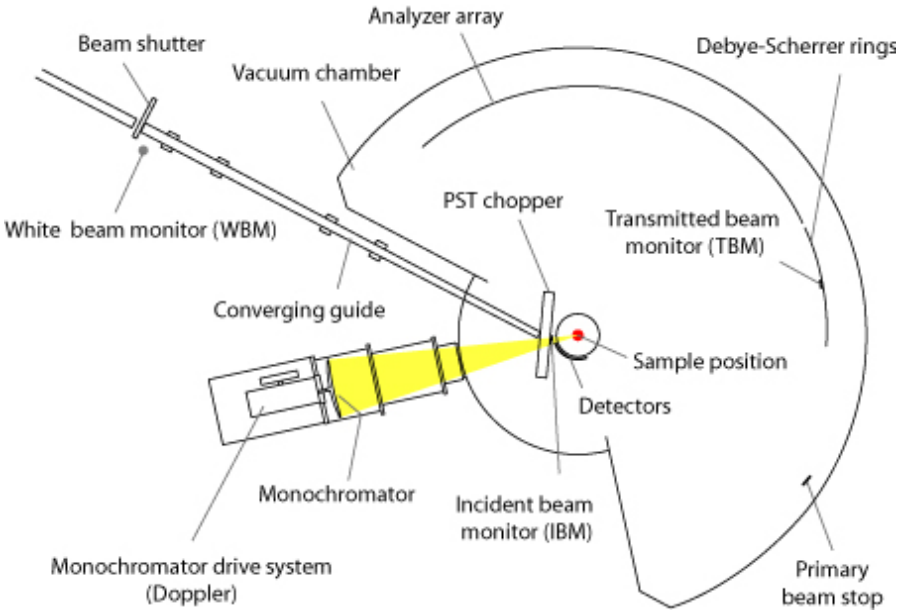

Figure 2.8. Schematic for HFBS

shown in Figure 2.10. Neutrons are focused onto the sample scattering through a supermirror funnel towards the analyzer crystals. These are strained perfect Si (111) crystals that reflect the neutrons with a very narrow distribution of energies centered around 2.08 meV onto the detectors. The final energy E_f is known from the Bragg reflection from the analyzer crystals. The energy change is evaluated by calculating the time taken to traverse the distance from the sample to analyzer to detector. The accessible dynamic range is ± 110 μeV (ΔE) and the energy resolution is 3.4 μeV. Using these values we evaluate the time limits accessible by the instrument. As with the DCS and HFBS, the error near the resolution is high, and we report 40 - 800 ps as the time range accessible by BASIS.

$$\begin{aligned} t_{max} &= \frac{1}{\nu} = \frac{h}{E_{res}} \\ &= \frac{4.135 \times 10^{-15}}{3.4 \times 10^{-6}} \\ &= 1.216 \times 10^{-9} s \sim 1216\ ps \end{aligned}$$

$$\begin{aligned} t_{min} &= \frac{1}{\nu} = \frac{h}{\Delta \mathrm{E}} \\ &= \frac{4.135 \times 10^{-15}}{110 \times 10^{-6}} \\ &= 3.75 \times 10^{-11} s \sim 37\ ps \end{aligned}$$

2.2.4 Choosing Q values

To combine data from all three instruments, we treat the accessible Q range of the instrument differently. For the HFBS, 16 Q values are accessible by the detectors are therefore fixed. The DCS and BASIS instruments have banks of detectors which can be grouped to match the HFBS values closely. The software DAVE handles the grouping for DCS by specifying the limits (0 to 2.4 Å^{-1}) and step size (0.155 Å^{-1}). For BASIS, the Q values of each set is calculated using the formula

$$Q_i = Q_{min} + \frac{Q_{max} - Q_{min}}{N} \times \frac{2i - 1}{2} \tag{2.2}$$

Figure 2.9. Schematic for BASIS

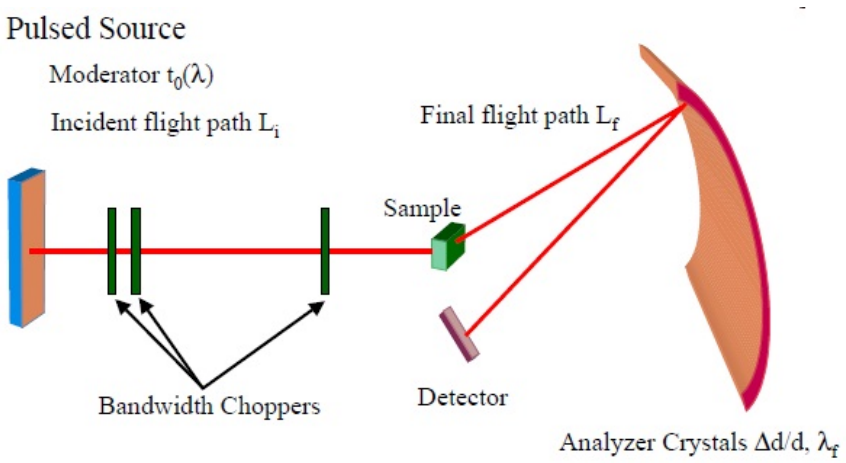

Figure 2.10. Schematic for BASIS

where Q_{min} and Q_{max} are 0.2 and 2.0 Å^{-1} respectively, N is the number of detector sets, and Q_i is the Q value for the i^{th} detector. Based on comparisons for 8, 9, or 10 detectors for BASIS (corresponding to step sizes of 0.225, 0.2, or 0.18 Å^{-1} respectively), we concluded that binning to 10 detectors gives Q values that match the best with DCS/HFBS. The grouping of detectors is summarized in Table 2.1. The highlighted cells are Q values that match across the three instruments.

Table 2.1. Grouping of detectors in DCS and BASIS to match HFBS Q values

HFBS		DCS		BASIS	
Detector #	Q (Å^{-1})	Detector #	Q (Å^{-1})	Detector #	Q (Å^{-1})
1	0.25	1	0.16	1	0.29
2	0.36	2	0.29	2	0.47
3	0.47	3	0.42	3	0.65
4	0.56	4	0.58	4	0.83
5	0.62	5	0.73	5	1.01
6	0.75	6	0.89	6	1.19
7	0.87	7	1.04	7	1.37
8	0.99	8	1.19	8	1.55
9	1.11	9	1.35	9	1.73
10	1.22	10	1.51	10	1.91
11	1.32	11	1.67		
12	1.42	12	1.82		
13	1.51	13	1.98		
14	1.60	14	2.13		
15	1.68	15	2.28		
16	1.75	16	2.38		

2.2.5 Changes in the DCS instrument

Changes made in the DCS instrument (2008) increased the error in Detector #4 (Q = 0.57 Å^{-1}); we therefore stopped using this Q value after 2008. The changes also resulted in a slight modification of the curves in Figure 2.6 because of which

the lower limit of the time scale for each Q got modified. The details of this finding and its impact on our data treatment is discussed in Appendix A.

Chapter 3

Experimental Details

3.1 Sample Synthesis

The ionomers were synthesized using poly-(ethylene glycol) (PEG) oligomer diols and dimethyl 5-sulfoisophthalate sodium (DM5SIS) salt in a two-step melt transesterification process. The details of the preparation are established in previous publications.[3,8] We use ^{1}H NMR to verify the molecular weight of the PEO spacers (400, 600 and 1100 g/mol in this study). The ionomers are purified by exhaustive diafiltration in deionized water to remove monomers, polymerization catalyst, and any ionic impurities. The concentrated ionomer solution is then freeze-dried and then vacuum-dried at 120 °C to constant mass. To control the degree of sulfonation, we vary the ratio of sulfonated and neutral isophthalates. The placement of the sulfonated and non-sulfonated isophthalate groups is random. The cation is exchanged from sodium to lithium or cesium by aqueous diafiltration with an excess of LiCl or CsCl salts, then exhaustively dialyzed to remove salt impurities.[3,8]

3.2 Sample Preparation for QENS

We load our polymer based samples as a film in annular geometry. The sample is pressed uniformly between two aluminum foils (which are practically invisible to neutrons) with a thickness that is calculated to allow 10% of the neutrons to be scattered. This gives good signal intensity with low probability of multiple

scattering.

3.2.1 Sample thickness calculation

The scattering strength of a sample is directly proportional to the mass of the sample, and is the sum of the individual contributions of the component elements. By controlling the thickness of the film, we limit the scattering to 10%. Each element has a "subscript" which is a representation of the element mass in the sample. For example, the subscript of the element H in a 70-30% by weight mixture of CH_3CH_2OH (ethanol) and H_2O (water) is given by

$$\text{H-subscript} = 6\left[\frac{70}{MW_{Ethanol}}\right] + 2\left[\frac{30}{MW_{Water}}\right] \tag{3.1}$$

After evaluating the subscripts of each element, we evaluate the number density of each element using the following formulas. For this we need to know the density of the sample.

$$\text{atom fraction} = \frac{\text{subscript}}{\text{total subscript of all elements}}$$

$$\text{mass} = \text{atomic weight} \times \text{subscript}$$

$$\text{mass fraction} = \frac{\text{mass}}{\text{total mass of all elements}}$$

$$\text{number density} = \frac{\text{density} \times \text{mass fraction} \times N_{AV}}{\text{atomic weight}} \tag{3.2}$$

Using coherent, incoherent and absorption cross section values from the NIST website,[109] we evaluate the effective cross section σ which depends on the wavelength used for the instrument (6 Åfor our measurements).

$$\text{total sigma} = \text{coherent} + \text{incoherent} + \left[\text{absorption} \times \frac{\lambda}{1.798}\right] \tag{3.3}$$

We use the number density calculated above to calculate the absorption and attenuation factors, and then use the annulus thickness to evaluate transmittance,

absorbance and % scattering.

$$\text{absorption factor} = \text{number density} \times \left[\text{absorption} \times \frac{\lambda}{1.798}\right]$$

$$\text{attenuation factor} = \text{number density} \times (\text{total sigma})$$

$$\text{transmittance} = \exp\left[-\pi.\begin{pmatrix}\text{attenuation}\\ \text{factor}\end{pmatrix}.\begin{pmatrix}\text{annulus}\\ \text{thickness}\end{pmatrix}\right]$$

$$\text{absorbance} = 1 - \exp\left[-\pi.\begin{pmatrix}\text{absorption}\\ \text{factor}\end{pmatrix}.\begin{pmatrix}\text{annulus}\\ \text{thickness}\end{pmatrix}\right]$$

$$\%\ \text{scatterer} = 100 - (\text{transmittance} \times 100) \tag{3.4}$$

We vary (by iteration) *annulus thickness* to obtain 10% scattering from the sample. Depending on the hydrogen content of our samples, we obtain thicknesses ranging from 60 μ to 90 μ.

3.3 QENS data

3.3.1 Signal components

Among the elements present in our samples - C, H, O, S, Li, Na, and Cs, the scattering is dominated by the incoherent scattering from hydrogen atoms, as shown in Table 3.1. Since the majority of hydrogen atoms are located on the PEO spacer, most of the signal is obtained from incoherent scattering of the H atoms of the spacer (see Table 3.2 for PEO600-100%Na); the QENS measurements reflect the motion of this part of the ionomer. The incoherent scattering contribution from the PEO spacers for PEOx-100%M is shown in Table 3.3.

3.3.2 Data treatment

As discussed in the previous chapter, we conduct QENS measurements on the DCS/HFBS instruments at the NIST Center for Neutron Research (NCNR), NIST

Table 3.1. Scattering cross sections for the different elements in this study in barns (1 barn = 10^{-24} cm^2)

Element	Coherent XS	Incoherent XS	Absorption XS
C	5.56	0	0.00353
H	1.76	80.3	0.333
O	4.23	0	0.0001
S	0.988	0	0.54
Na	1.66	1.62	0.53
Li	0.619	0.78	0.0454
Cs	3.69	0.21	29

Table 3.2. Relative scattering strength (%)of ionomer components for PEO600-100%Na

	isophthalate + ions	PEO spacer	total
coherent	1.56	6.14	7.7
incoherent	5.07	87.23	92.3
total	6.63	93.37	100.0

Table 3.3. Incoherent scattering contribution from spacer for PEOx-100%M

Sample	Li	Na	Cs
PEO400-100%M	84.75	84.71	84.69
PEO600-100%M	87.26	87.23	87.22
PEO1100-100%M	90.14	90.12	90.12

and on the BASIS instrument at the Spallation Neutron Source (SNS), ORNL. The time scales accessed by DCS, BASIS and HFBS instruments are 1-50 ps, 40-800 ps, and 250-2500 ps respectively over a spatial scale of 3 - 11 Å. All sample data are measured against a resolution function obtained from a vanadium standard that is immobile at the conditions of the measurement. The intensity of scattered neutrons is a function of momentum transfer (Q) and frequency (ω). We reduce the raw data from the DCS and HFBS using DAVE (Data Acquisition and Visualization Software), an in-house software developed at NCNR.[113] The data for BASIS is reduced using BSS_Reduction, an in-house software developed at SNS. To give

reduced data $[I(Q,\omega)]$, these softwares use detector efficiencies obtained from the resolution data $[R(Q,\omega)]$and subtracts the background and the sample holder from the raw data. The frequency domain data for DCS, BASIS and HFBS are shown in Figure 3.1 for PEO400-100%Na, PEO600-100%Na and PEO1100-100%Na. The more the data deviates from elastic resolution, higher is its mobility. Based on these deviations, we observe the mobility of the ionomers decreases in the order PEO1100-100%Na > PEO600-100%Na > PEO400-100%Na, consistent with the idea that the presence of ions slows down the polymer.

In order to effectively merge the data from the three instruments and allow for the possibility of using analytical fits with a stretched exponential, we inverse Fourier transform the data to the time domain. The total intensity $I(Q,\omega)$ is a convolution integral of the resolution function $R(Q,\omega)$ and sample dynamics $S(Q,\omega)$.

$$I(Q,\omega) = S(Q,\omega) \otimes R(Q,\omega) \tag{3.5}$$

In the time domain, $I(Q,t)$ is a product of the self-intermediate scattering function of the sample $S(Q,t)$ and resolution $R(Q,t)$.

$$I(Q,t) = S(Q,t) \cdot R(Q,t) \tag{3.6}$$

The self-intermediate scattering function, $S(Q,t)$, plotted in the time domain for both instruments in Figure 3.2 represents the correlation of atom positions at time t relative to their positions at $t = 0$. Note that the data points plotted do not exceed the time corresponding to instrumental resolution. (For a comprehensive discussion on how QENS data was inverse Fourier transformed, see Appendix A. The relevant FORTRAN code for BASIS data transformation is also included.) The locations of the decay curves along the Y-axis are discussed in the following sections.

We fit the decays in Figure 3.2 to obtain a characteristic relaxation time. For this purpose we recognize that the dynamics of polymers and other soft materials often exhibit a distribution of relaxation times, rather than Debye or single relaxation. Thus, we choose the stretched exponential or Kohlrausch-William-Watts

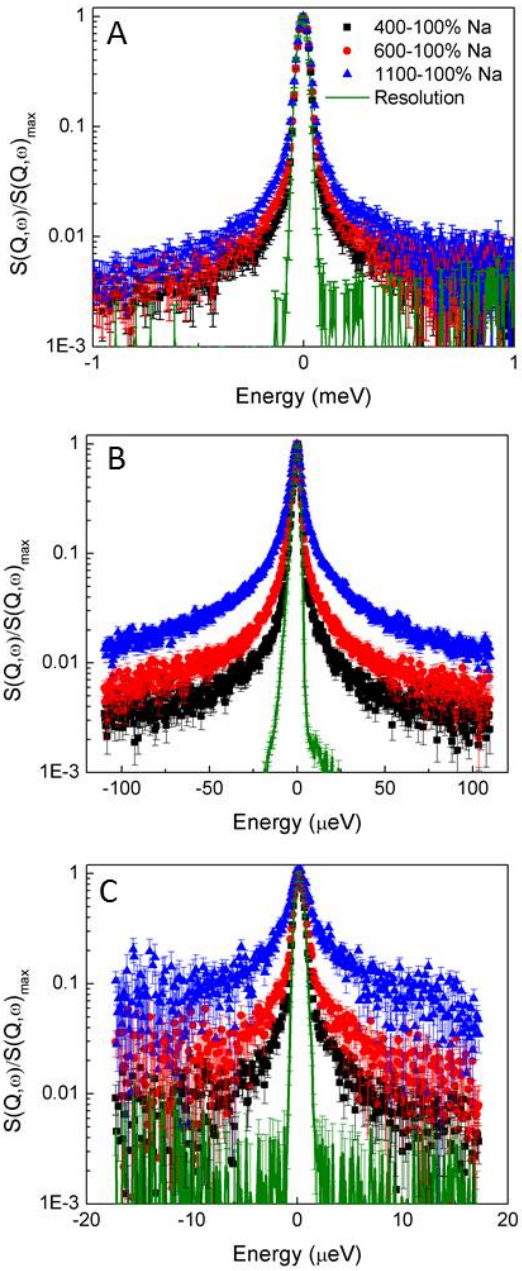

Figure 3.1. Frequency domain data from (A) DCS, (B) BASIS and (C) HFBS for PEO400-100%Na, PEO600-100%Na and PEO1100-100%Na at Q = 1 $Å^{-1}$ and T = 348 K.

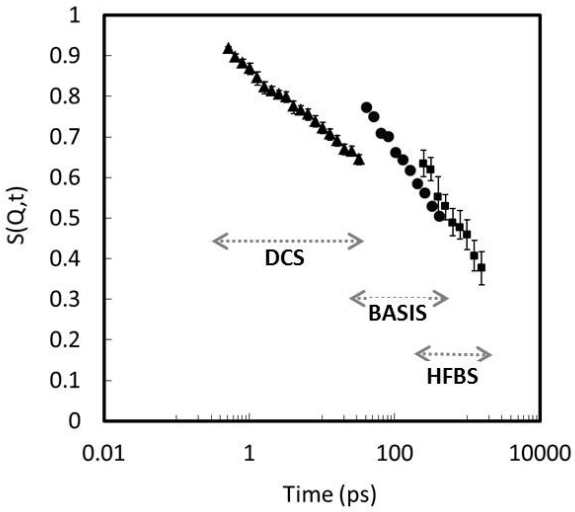

Figure 3.2. Inverse Fourier transformed data from DCS, BASIS and HFBS for PEO600-100%Na at Q = 1 Å^{-1}, T = 348 K.

(KWW) expression[114]

$$S(Q,t) = exp\left[-\left(\frac{t}{\tau(Q)}\right)^{\beta(Q)}\right] \tag{3.7}$$

where τ is the characteristic time, and the stretching exponential β represents the width of the distribution.

We conduct measurements on DCS/HFBS for the sample sets PEO600-Y%Na (Y $\in$ [0,100]) and PEOx-100%Na [x = 400/600/1100], to study the effect of changing ion content. Due to a scheduled shutdown at the NCNR, we performed the next set of measurements at BASIS in SNS, ORNL for PEOx-100%M [x = 400/600/1100 and M = Li/Na/Cs], to study the effect of ion identity. The time scales accessed by DCS/HFBS (1-50 ps and 250-2500 ps respectively) revealed the existence of two fractions of the ionomer that undergo slow and fast relaxations. In Chapters 4 and 5 we study how the dynamics of the two fractions contribute differently to overall mobility and conductivity. In contrast to the large time range accessed by DCS/HFBS, BASIS accesses a time scale of 40-800 ps. This short time range indicates the presence of two relaxations, but does not allow us to fully resolve the dynamics to the constituent processes. We therefore develop a technique for resolving BASIS data to the two processes by comparing the data for samples measured

on both BASIS and DCS/HFBS. We then make logical assumptions about the two fractions and obtain the individual relaxation times. In the following sections we first discuss the QENS data from DCS/HFBS, and then discuss the treatment of BASIS data to obtain the constituent dynamics.

3.3.2.1 Fitting DCS and HFBS data

As with other polymers, amorphous PEO has a fast exponential decay that occurs on times scales of less than 2 ps, attributed to local cage vibrations and torsional librations.[115,116] The simplest possible description of polymer motion over QENS timescales, and the one appropriate for pure PEO, is the fast exponential decay K_{vib}, combined with the segmental relaxation K_{seg}:

$$S(Q,t) = K_{vib}K_{seg} \tag{3.8}$$

where

$$K_{vib} = E_0\left(Q\right) + \left(1 - E_0\left(Q\right)\right) exp\left[-\left(\frac{t}{\tau_{vib}\left(Q\right)}\right)\right] \tag{3.9}$$

and

$$K_{seg} = exp\left[-\left(\frac{t}{\tau\left(Q\right)}\right)^{\beta(Q)}\right] \tag{3.10}$$

E_0 is the elastic incoherent structure factor (EISF) for the vibration and represents the fraction of the decay allocated to segmental motion. Fast vibrations fall outside the HFBS window and thus motion on this instrument reflects only K_{seg}. In Figure 3.3a we have shown how a single process K_{seg} fits the data. This approach is successful for some cases, but not for some others (see Figure 3.3b), where a slower second process is required to describe the data from both instruments simultaneously. We cannot fit the data with a combined decay

$$K_{seg} = K_{FAST}K_{SLOW} \tag{3.11}$$

suggesting that all H-atoms do not undergo both processes. Instead, a weighted sum

$$K_{seg} = X_{FAST}K_{FAST} + \left(1 - X_{FAST}\right)K_{SLOW} \tag{3.12}$$

is required, indicating that some H-atoms belong to a "fast" subset (undergoing K_{FAST}) of the total H atoms and the rest belong to a "slower" subset (undergoing K_{SLOW}). In all the cases where two processes are observed, K_{FAST} has decayed to 0.2 or less before the HFBS window such that HFBS is only sensitive to K_{SLOW}.

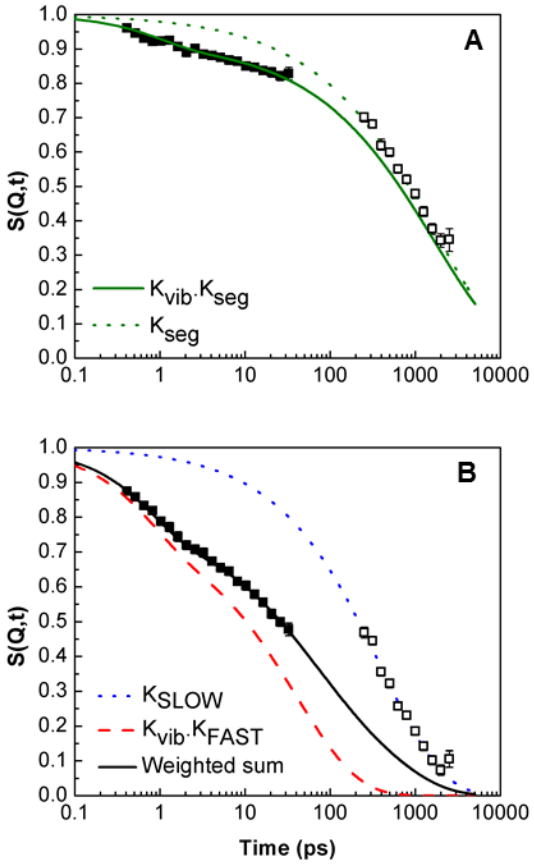

Figure 3.3. (A) Data for PEO600-0%Na at Q = 1.04 Å^{-1}, T = 298 K is fit to a single process K_{seg} (B) Data for PEO600-17%Na at Q = 1.04 Å^{-1}, T = 298 K is fit to a weighted sum of two processes, K_{FAST} and K_{SLOW}

To represent the data on a single plot, we shift the HFBS data such that K_{vib} and K_{FAST} are included in the decay. This is done by algebraic comparison of the full fit line [weighted sum in Figure 3.3] with only K_{SLOW} to determine the amount by which the data must be shifted. The resulting decay curve shows the data as if it was measured on a single instrument and does not affect the fitting algorithm, as shown in Figure 3.4. This data indicates that mobility of the PEO spacer reduces as we increase the ion content in the samples, consistent with PEO-based

SPEs in the amorphous phase.[2,66,79] (in Appendix D we have shown the combined DCS/HFBS S(Q,t) curves for several samples with varying Q, temperature and ion content)

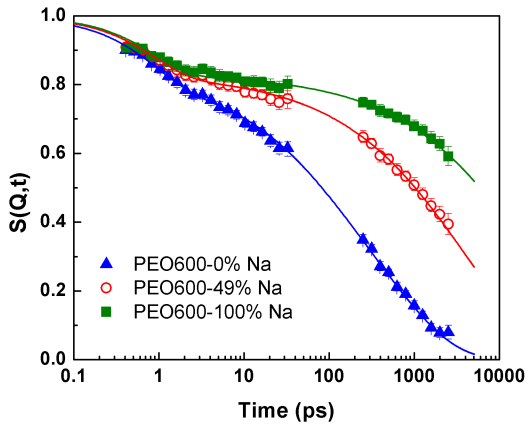

Figure 3.4. DCS data, shifted HFBS data and the corresponding fitting lines for PEO400-100%Na, PEO600-100%Na, and PEO1100-100%Na at T = 298 K, Q = 1.04 $Å^{-1}$

There are two limiting cases where a single process is observed: high temperature and low ion content, in which only K_{FAST} is observed ($X_{FAST} \to 1$), and low temperature and high ion content, in which only K_{SLOW} is observed ($X_{FAST} \to 0$). Scenarios that lie in between these extremes require two processes to describe the data. This is presented pictorially in Figure 3.5 where the different shades show the identities and number of processes that constitute the dynamics.

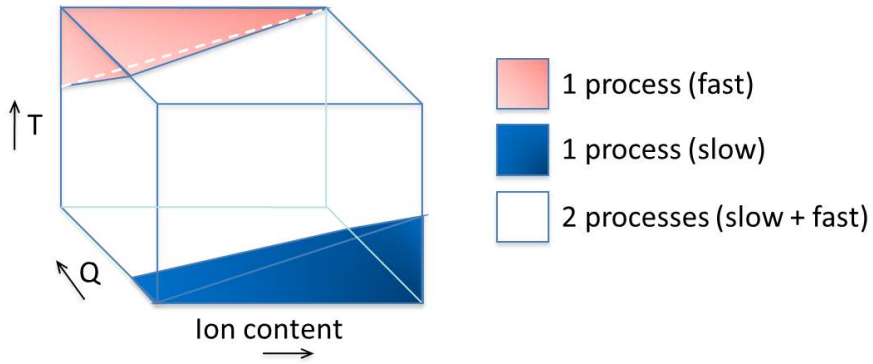

Figure 3.5. Occurrence of slow and fast processes as a function of ion content, Q and temperature. The boundaries are approximate and are meant for visualization only.

The fitting is performed simultaneously on all data sets imposing the restrictions that relaxation times cannot increase with increasing temperature and Q; and τ_{FAST} should not exceed τ_{SLOW}. Due to the small time window of each instrument and the stretched nature of the relaxation, a range of fitting parameters can describe the data. We represent this range in the form of an error bar outside of which the parameter cannot represent the data, regardless of the values of the other parameters. To obtain the error bars, we generate 500 $S(Q,t)$ datasets within the instrument error. Each dataset is fit using Levenberg-Marquardt non-linear least squares fitting program. To probe the entire parameter space, initial guesses for τ_{FAST} and τ_{SLOW} were randomized between 1 ps and 100000 ps. We allowed β_{FAST} and β_{SLOW} to vary between the limits of 0 and 1. X_{FAST} was held at the best fit value while calculating the range of fitting parameters. In the figures presented in this paper, we report mean $\pm$ [*one standard deviation*] for the relaxation times. The outline of the algorithm and the corresponding FORTRAN and BASH scripts used to obtain the error bars on fitting parameters is discussed in Appendix C.

A note on the origins of the two relaxations: In Chapter 4 we identify the physical origins of the two processes and name them bridge atoms (fast fraction) and anchor atoms (slow fraction). In the following section we will be referring to the fast and slow fractions by these names.

3.3.2.2 Fitting BASIS data

The S(Q,t) data for PEO600-100%Na from all three instruments are shown in Figure 3.6a. K_{vib} is observed in DCS but not BASIS and HFBS. The fitting parameters τ and β for bridge and anchor relaxations are the same for all three instruments. The original positions of the S(Q,t) data on the y-axis for the three instruments (filled data points) do not fall in a fit line because they access different energy windows. The instruments observe different fractions of the fast and slow processes, which results in the fraction of bridge atoms (X_{BRIDGE}) to follow the order DCS > BASIS > HFBS. The fraction of bridge atoms observed in HFBS is negligible, as shown in the previous section. Based on the fitting parameters obtained, we can shift the original data to lie on a single curve as if it were measured on a single instrument accessing the entire energy window, as shown by the solid

line in Figure 3.6a. The shifted data (unfilled symbols) is for visualization purposes only, and does affect the fitting parameters.

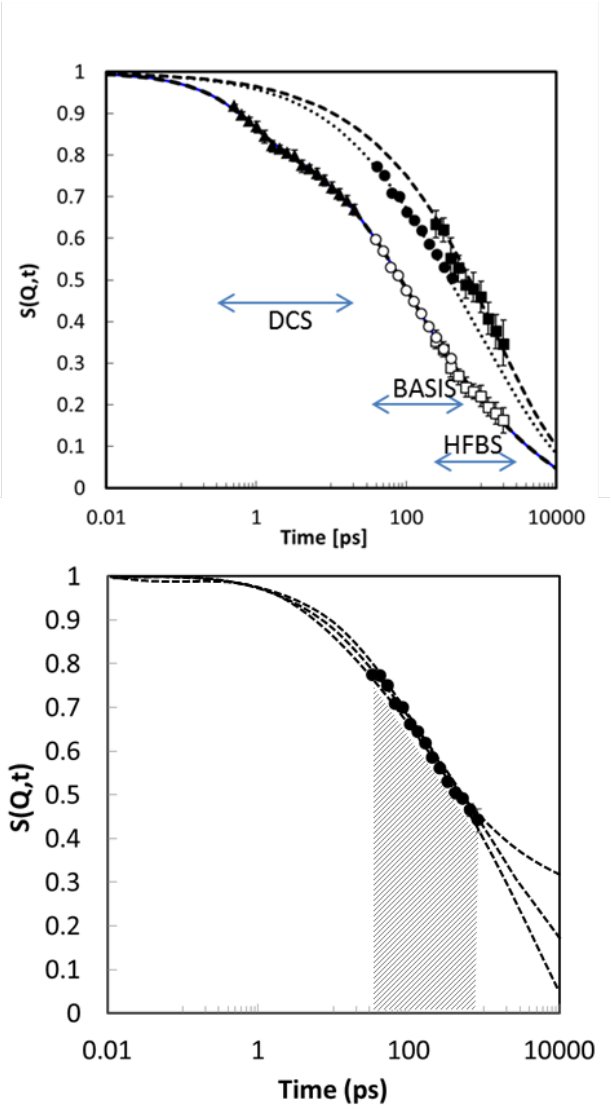

Figure 3.6. (a) S(Q,t) data from DCS, BASIS and HFBS for PEO600-100%Na at T = 348 K and Q = 1 Å^{-1}; (b) S(Q,t) data from BASIS only, showing multiple fit lines and the area under the S(Q,t) curve

For the samples where we have only BASIS data, we can use the KWW equation to fit the S(Q,t) data with an EISF (ϵ), which corresponds to the fraction that is immobile in the window of the instrument, given by

$$K_{seg} = \epsilon\,(Q) + (1 - \epsilon\,(Q))\,exp\left[-\left(\frac{t}{\tau\,(Q)}\right)^{\beta(Q)}\right] \tag{3.13}$$

Using this equation BASIS data can be fit with different sets of $[\tau, \beta, \epsilon]$ parameters as shown by the dotted fit lines in Figure 3.6b. We will represent the loci of fitting parameters in a graph of relaxation times (τ) as a function of EISF (ϵ) as shown in Figure 3.7 for PEOx-100%Na where x = [400, 600, 1100]. The further a locus lies away from (0,0), the slower the dynamics. This is consistent with our observations in Figure 3.4, where the mobility reduces in the order PEO1100-100%Na > PEO600-100%Na > PEO400-100%Na due to increasing ion content.

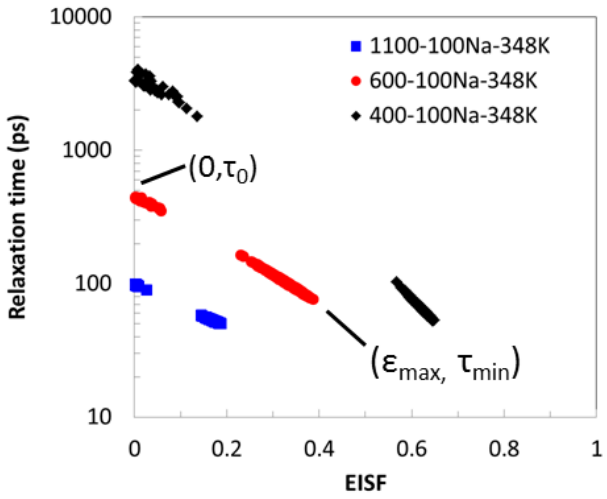

Figure 3.7. $\tau - \epsilon$ loci for PEOx-100%Na at T = 348 K, Q = 1.37 Å^{-1} where x = [400, 600, 1100]

While the $\tau - \epsilon$ curve in Figure 3.7is a good visual representation of the overall dynamics, it fails to provide information about the constituent bridge and anchor relaxation processes. To obtain this information, we need to make reasonable assumptions based on observations made in our previous work. Consider the PEO600-100%Na $\tau - \epsilon$ curve shown in Figure 3.7. In the limit where $\epsilon \rightarrow 0$, we consider the mobility of the entire ionomer, including the immobile portion (i.e. so slow that it lies outside the BASIS energy window). In this case we obtain very low β (< 0.35), implying a very large distribution of relaxation times. This is consistent with the fact that there are two relaxations (bridge and anchor) and

BASIS accesses the decay time scales between these relaxation processes. Since β for the two segmental relaxations is approximately 0.6,[80,82,117] a lower value suggests a very large distribution of relaxation times, consistent with the existence of two processes with different relaxation times. The value of the relaxation time when $\epsilon \rightarrow 0$ is referred to as τ_0. In this limit, Eq 3.13 reduces to

$$K_{seg} = exp\left[-\left(\frac{t}{\tau_0\,(Q)}\right)^{\beta(Q)}\right] \tag{3.14}$$

Since the BASIS data can be fit by both Eq 3.14 and Eq 3.12, the areas under the S(Q,t) (curve shown in Figure 3.6b) obtained from both the equations will be the same. This leads to a relation between τ_0 and the combination of τ_{BRIDGE} and τ_{ANCHOR}, obtained by equating the area under the curve obtained from the two equations:

$$\tau_0 = [\tau_{BRIDGE}]^{X_{BRIDGE}}\,[\tau_{ANCHOR}]^{1-X_{BRIDGE}} \tag{3.15}$$

A comprehensive derivation of Eq (3.15) is discussed in Appendix B. The above eqation has three unknowns, τ_{BRIDGE}, τ_{ANCHOR} and X_{BRIDGE} of which we can make logical estimates of τ_{BRIDGE} and X_{BRIDGE}. We will first estimate X_{BRIDGE} with the help of ϵ_{max}, which is the maximum value of ϵ that can fit the data (see Figure 3.7). Physically it represents the highest fraction of the sample that is seen as immobile in the window of the instrument, and therefore can be used to make a good approximation of the fraction of anchor atoms. On comparing samples which we measured on DCS/HFBS and BASIS, we observed that for $\epsilon_{max} > 0.75$, $X_{ANCHOR} = 1$. Since $X_{BRIDGE} = 1 - X_{ANCHOR}$, we estimate X_{BRIDGE} as

$$X_{BRIDGE} = \begin{cases} 1 - \epsilon_{max} & \text{if } \epsilon_{max} < 0.75 \\ 0 & \text{if } \epsilon_{max} \geq 0.75 \end{cases} \tag{3.16}$$

The values of X_{BRIDGE} are lower than that obtained from DCS, and above those from HFBS ($X_{BRIDGE} = 0$), as expected (see Figure 3.8). We can estimate τ_{BRIDGE} from τ_{min}, which we define as the smallest value of τ that can fit the BASIS data (see Figure 3.7). This parameter is of importance at high Q (1.91 $Å^{-1}$), where the faster bridge region dynamics are more prominently detected. Therefore it is a reasonable assumption to make that τ_{min} is approximately equal

to τ_{BRIDGE} at high Q. For the PEOx-100%Na samples that have been measured previously on DCS/HFBS, the Q dependence of bridge relaxation times varies as $\tau \sim Q^{-n}$, where n ranges from 1.3 to 2 depending on the temperature. Using the τ_{min} value obtained at high Q and the range of n, we can estimate the values of τ_{BRIDGE} at all Q values. Based on these estimates of X_{BRIDGE} and τ_{BRIDGE} we can calculate the range of τ_{ANCHOR} values from the τ_0 values that fit Eq 3.14.

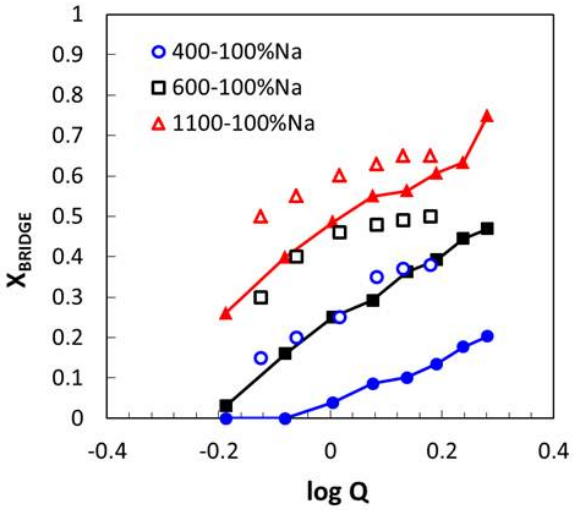

Figure 3.8. Q dependence of bridge atom fraction X_{BRIDGE} for PEOx-100%Na at 348 K. Open symbols - parameters obtained from DCS. Connected filled symbols - parameters obtained from BASIS.

We compared the estimates of τ_{BRIDGE} and τ_{ANCHOR} (from BASIS) to those obtained from DCS/HFBS for samples measured on all three instruments. A summary of these estimates is shown in Figure 3.9 for PEOx-100%Na [x = 400, 600, 1100] at 348 K; the above approximations for τ_{BRIDGE} and τ_{ANCHOR} provide very good estimates for varying spacer lengths. Additional details of this technique and graphs comparing the fitting parameters obtained from DCS/HFBS with those from BASIS (for more temperatures and for PEO600-100%Li) are discussed in Appendix B. Due to the strong agreement between these fitting parameters, we extend the same assumptions for τ_{BRIDGE} and τ_{ANCHOR} to the remaining samples of the PEOx-100%M series.

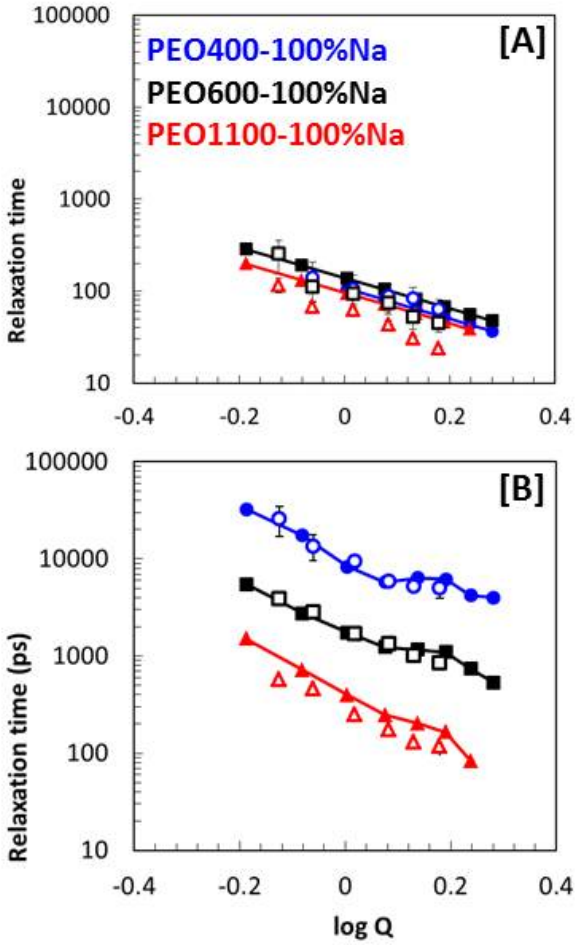

Figure 3.9. Comparing Q-dependence of relaxation times of (a) bridge atoms and (b) anchor atoms for PEOx-100%Na (T = 348 K). Open symbols - parameters obtained from DCS/HFBS. Connected filled symbols - parameters obtained from BASIS.

Chapter 4

Identities of component dynamics in the PEO sulfonate ionomers

In this chapter we identify the physical origins of the two fractions that compose the overall dynamics of the ionomers. Using QENS, we measure polymer mobility as a function of ion content while varying the degree of sulfonation (Y%). We further establish a comparison to PEO/$LiClO_4$ systems based on previous work in our group.[2] To compare the samples on the same basis, we use the ion content, defined as the molar ratio of cations to ether oxygen atoms, as shown in Table 4.1. Ionomers with a PEO spacer of 600 g/mol MW are limited to an ion content of 0.077 (Na:EO = 1:13) or less, which is smaller than the range of ion contents normally studied in PEO/salt systems. The maximum conductivity of PEO600 ionomers occurs at an ion content of 0.013 (Na:EO = 1:76). This is both within the range we investigate and far lower than that of PEO/Li-salt systems which occurs at an ion content between 0.071 (Li:EO = 1:14) and 0.125 (Li:EO = 1:8). We consider the origin of this difference in this chapter.

4.1 Dynamics in the nonionic polymer

We first compare QENS data to other available probes of segmental motion for the nonionic polymer, in this case broadband dielectric relaxation spectroscopy (DRS). In Figure 4.1 we compare the two processes obtained from QENS with DRS[3] data. The DRS experiment measures the reorientation of local dipoles, and

Table 4.1. Properties of PEO600-Y%Na (where Y ∈ [0,100]) and PEO/$LiClO_4$[2] samples

Sample	Cation:EO ratio	Ion content	T_g (K)	Molecular Weight (g/mol)
PEO600-0%Na	0	0	229	5800
PEO600-6%Na	1:217	0.005	230	5800
PEO600-11%Na	1:118	0.008	232	5800
PEO600-17%Na	1:76	0.013	233	8700
PEO600-49%Na	1:26	0.038	245	4700
PEO600-100%Na	1:13	0.077	267	6300
PEO/$LiClO_4$	1:30	0.033	251	500000
PEO/$LiClO_4$	1:14	0.071	257	500000
PEO/$LiClO_4$	1:10	0.01	246	500000
PEO/$LiClO_4$	1:8	0.125	256	500000
PEO/$LiClO_4$	1:4	0.25	264	500000

is not spatially resolved. The lowest Q values in QENS data typically provide the best comparison. For pure PEO, it has been noted that Q = 1.02 $Å^{-1}$ or higher is more segmental in nature than Q= 0.57 $Å^{-1}$.[118] For this comparison, we chose Q = 0.57 $Å^{-1}$ for the slow process, and Q= 0.89 $Å^{-1}$ for the fast process because this process is not present at Q = 0.57 $Å^{-1}$. Note that the difference between the fast and slow processes is larger than differences due to spatial scale. The DRS data includes the α relaxation corresponding to segmental motion, and a β relaxation attributed to local chain twisting in the PEO spacers.[3] As with other studies, the QENS data represents the merged relaxation evident at temperatures greater than 1.3 T_g.[119] Our slow process data is consistent with DRS measurements on the nonionic polymer. The fast process more closely resembles the merged α/β process of pure PEO, also shown in Figure 4.1. Although the β relaxations in pure PEO and the nonionic polymer (the difference being the presence of the isophthalate co-monomer) are nearly coincident, the β relaxation can change slope after merging with the α relaxation.[120] It is not known if this occurs in pure PEO, however, QENS data on pure PEO is consistent with the times obtained for the fast process. The fast process does not appear to coincide with the α relaxation of the ionomer. We conclude that the QENS data is consistent with reported measures of segmental mobility in the nonionic polymer, with the slow process resembling

the ionomer and the fast process resembling pure PEO.

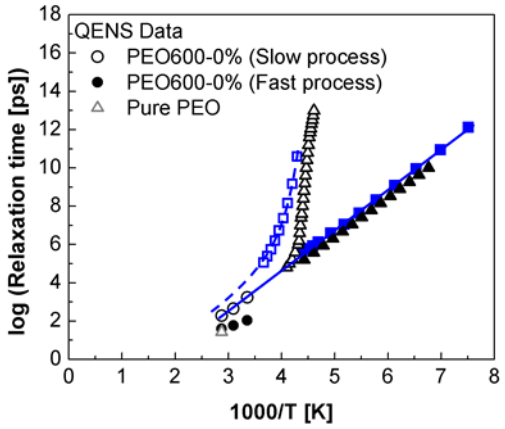

Figure 4.1. Temperature dependence of relaxation times obtained from QENS for PEO600-0%Na (circles), and for amorphous pure PEO (open grey triangle),[2] and DRS for PEO600-0%Na (squares),[3] and for pure PEO (black triangles).[4] For the DRS data, open symbols denote α relaxation, and filled symbols denote β relaxation. Error bars, if smaller than the data markers, are not shown.

We determine the influence of the isophthalate monomer on PEO dynamics by comparing the nonionic polymer to pure PEO. Pure PEO is amorphous at 348 K and undergoes one segmental relaxation.[2,117,121] Segmental relaxation in polymers depends on Q via $\tau \sim Q^{-n}$ where n varies from -2 to -2/β[117,121,122] As shown in Figure 4.2, both K_{FAST} and K_{SLOW} are segmental processes with the same slope as pure PEO. At 348 K, only the faster relaxation (K_{FAST}) is present in the nonionic polymer; it is slowed slightly compared to pure PEO. This slowing reflects the influence of the isophthalate group on segmental relaxation of the PEO spacer. At lower temperatures (298 K and 323 K), we observe the slower, second process (K_{SLOW}) that is also a segmental relaxation.

One possible explanation for two classes of segmental motion is the proximity of the atoms to the co-monomer: H-atoms near the isophthalate group may be slower than those in the mid-segment. In a previous study of disordered diblock copolymers of PEO and PMMA,[123] we determined that mobility of the fast PEO block (T_g = 221 K) is significantly slowed by covalent bonding to the slow PMMA block (T_g = 391 K) for 5-6 backbone atoms adjacent to the bond. This is not observed experimentally in the case of high molecular weight diblocks, because the

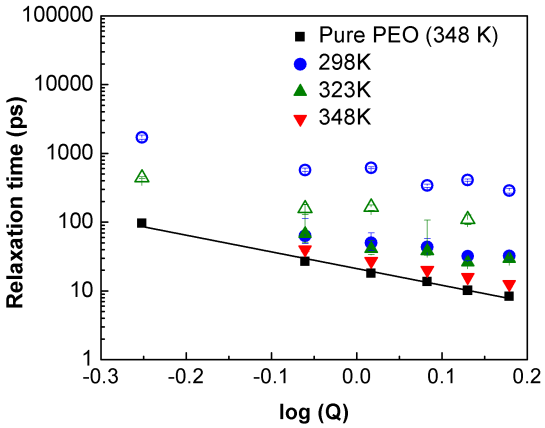

Figure 4.2. Relaxation times from K_{FAST} (filled symbols) and K_{SLOW} (open symbols) for the nonionic polymer. Data for pure PEO is at 343 K. The units of Q are in $Å^{-1}$.

number of atoms influenced by the bond is a small fraction of the total. This is not the case for the PEO 600 ionomer, in which the spacer has 13 repeat units with 39 backbone atoms. If this system behaves as the PEO/PMMA simulation, a reasonable fraction [$\sim$ 30%] of the backbone atoms in the PEO spacer would be slowed by direct connection to the isophthalate group. This depends on the isophthalate group being "slow" compared to PEO, a reasonable assumption since PEO has a T_g of 220K and polymers with repeat units similar to isophthalate have high T_g (e.g. the T_g of polyethylene terephthalate is 343 K). Thus the mobility of the PEO spacer might be influenced by the isophthalate group in a significant enough fraction that it is observed in our experiments. Preliminary results from molecular dynamics simulations on PEO600-100%Na show this behavior: displacements of hydrogen atoms over time intervals of 2-10 ns are smallest near the isophthalate group and reach a maximum at the chain midpoint.[9] From these observations, we suggest that the 'fast' motion (K_{FAST}) corresponds to the mid-region hydrogen atoms, and the 'slow' motion (K_{SLOW}) represents hydrogen atoms close to the isophthalate co-monomer. This is illustrated in Figure 4.3, where we introduce the terms "bridge atoms" and "anchor atoms" to describe the fast and slow fractions. This terminology is used throughout the remainder of the paper. We remind the reader that although the presence of two dynamic processes is an experimental observation, the classification as bridge and anchor atoms is our interpretation of

this observation.

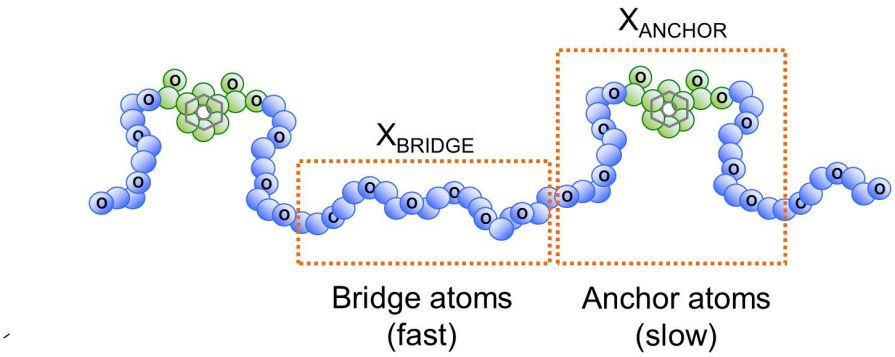

Figure 4.3. Illustration of the spatial location of fast and slow portions of the nonionic polymer.

The interpretation presented above divides mobility of the PEO H-atoms into two classes: bridge atoms (segmental and similar to pure PEO), and anchor atoms (significantly slower but still segmental). The fraction X_{BRIDGE} denotes the fraction of bridge atoms, and is given in Figure 4.4 for all samples. It may appear counterintuitive that the fraction of bridge atoms depends on spatial scale. To understand this observation, we must consider the physical meaning of the spatial scale of the measurements. To a first approximation, the spatial scale Q sets the radius of a sphere centered at each atom, and ask about movement within this sphere: when the atom leaves the sphere, its S(Q,t) falls to zero. At low Q values that correspond to large radii of observation ($\sim$ 11 Å), all atoms appear to be influenced by the isophthalate group ($X_{BRIDGE} = 0$). This is because the observation volume encompasses the entire PEO spacer ($R_g \sim 9$ Å for 13 repeat units[124]) and motion on this scale is controlled by the slowest anchor atoms. As we decrease the size of observation radius, the contribution of bridge atoms becomes more prominent and X_{BRIDGE} increases.

Only a single process is observed at T = 348 K, consistent with bridge atoms. Dynamics of the slower anchor atoms only become distinct when the temperature is lowered. For two processes to be observed, the average relaxation times of anchor atoms must be significantly greater than bridge atoms, and the variation must be sharply divided; otherwise a single relaxation with low β would fit the data. The emergence of two processes as temperature is lowered occurs because the PEO

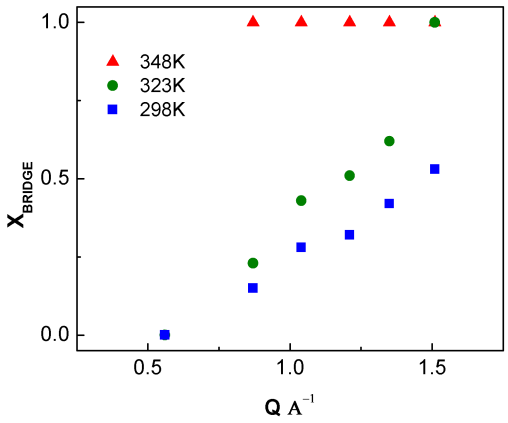

Figure 4.4. Fraction of bridge atoms in the nonionic polymer as a function of Q.

spacer and the more rigid isophthalate group likely have different temperature dependencies. At high temperature, the difference in dynamics between bridge and anchor atoms is not sufficient to resolve into two processes, but as temperature is lowered, anchor atoms slow more than their faster bridge counterparts. This leads to increasing differences between bridge and end segments and the eventual emergence of two processes. In Figure 4.5, we show the increasing difference between bridge and anchor atom relaxation times as temperature decreases.

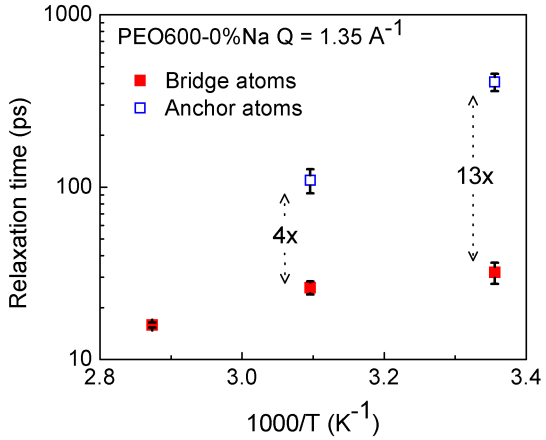

Figure 4.5. Comparison of the temperature dependencies of bridge and anchor atoms in the nonionic polymer.

4.2 Effect of ion content on ionomer dynamics

In the previous section we identified two segmental relaxation processes associated with the PEO hydrogen atoms in the nonionic polymer: bridge atoms in the spacer mid region, and anchor atoms neighboring the isophthalate group. In this section we discuss the effects of ion content on both relaxations.

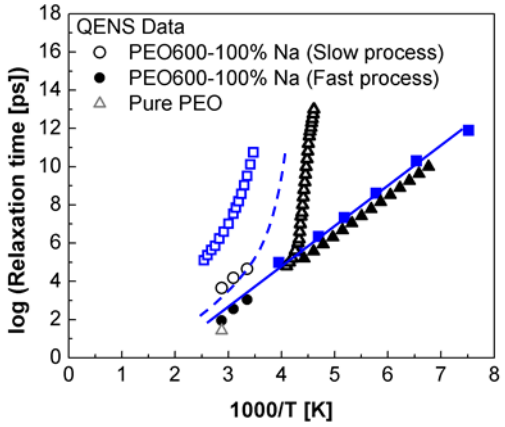

Figure 4.6. Temperature dependence of relaxation times obtained from QENS for PEO600-100%Na (circles), and for amorphous pure PEO (open grey triangle),[2] and DRS for PEO600-100%Na (squares),[3] and for pure PEO (black triangles).[4] For the DRS data, open symbols denote α relaxation, and filled symbols denote β relaxation. The dashed line corresponds to the α relaxation of the nonionic polymer as seen from DRS (Figure 4.1). Error bars, if smaller than the data marker, have not been shown.

In Figure 4.6, we compare relaxation times obtained via QENS with dielectric times for the PEO600-100%Na sample. Spatial scales are selected as described for Figure 4.1. Two processes are evident in the DRS data: the β-relaxation at low temperature, and a slower relaxation, the origin of which is discussed below. Unlike the nonionic polymer, the end atom QENS data do not appear to represent the merger of the two DRS relaxations, but rather the continuation of the β-relaxation. In DRS measurements of the Li analog of this sample, PEO600-100%Li, the local β-relaxation, the segmental α-relaxation and a new process [termed α_2] are evident.[3] The α_2-relaxation process follows the temperature dependence of the segmental relaxation, is two orders of magnitude slower, and is interpreted as the reorientation of dipoles formed by ion pairs. When the ion is changed to sodium, only one process is clearly resolvable,[5] and its timescale more closely follows the

α_2 relaxation. This behavior is consistent with the aggregation behavior of the system as observed via SAXS: in PEO600-100%Li, ionic aggregation is observed at all temperatures, whereas for PEO600-100%Na, well-defined ionic aggregates form upon increasing temperatures from 298K to 393K. This emerges to a lesser extent and only at temperatures above our measurements.[6,7] Apparently, the better dispersion of ions in PEO600-100%Na causes the contribution from ion pairs to overshadow the PEO segmental process to the extent that it is no longer clearly resolvable using DRS. QENS, which does not observe ion or dipole motion, is still able to resolve the segmental relaxation in this sample. As illustrated in Figure 4.7, the presence of ions does not give rise to any new processes, nor does it change the physical origins of the two processes observed in the nonionic polymer. Both processes remain segmental in nature with ion addition, as shown by the Q dependence of relaxation times. It is clear from Figure 4.7 that increasing the ion content has different effects on the dynamics of the two processes.

In Figure 4.8a we plot relaxation times at Q = 1.35 Å^{-1} as a function of ion content. While the relaxation times of bridge atoms increase by a small amount ($\tau_{BRIDGE,100\%}/\tau_{BRIDGE,0\%} \sim 3$), those of anchor atoms increase significantly ($\tau_{ANCHOR,100\%}/\tau_{ANCHOR,0\%} \sim 50$). An ion content of 0.01 divides two regimes with different behavior. In the first regime [ion contents < 0.01], bridge relaxation times vary whereas anchor relaxation times are relatively constant. DRS relaxation times for the PEO600-Li series are insensitive to ion content up to the same value.[3] This suggests that the segmental process, when observable with DRS, better corresponds to anchor atoms, as opposed to bridge atoms. In the second regime [ion contents > 0.01], the trend reverses: relaxation times of bridge atoms are relatively constant, whereas those of anchor atoms increase substantially. Based on these observations and the idea that relaxation times slow when ion content increases, we suggest the following scenario. Ions initially populate the bridge segments. As concentration increases past 0.01 (100 EO per cation), ions populate the end segments. In the extreme case that no further ions populated bridge regions, there would be 1 cation for 100 total EO in the PEO600-100%Na sample. We consider the fraction of bridge atoms as 25% (a representative value at 298 K). Since the entire PEO spacer is 13 EO, there are 3.25 bridge EOs per spacer, meaning that bridge atoms from (100/3.25 $\sim$) 30 PEO spacers share 1

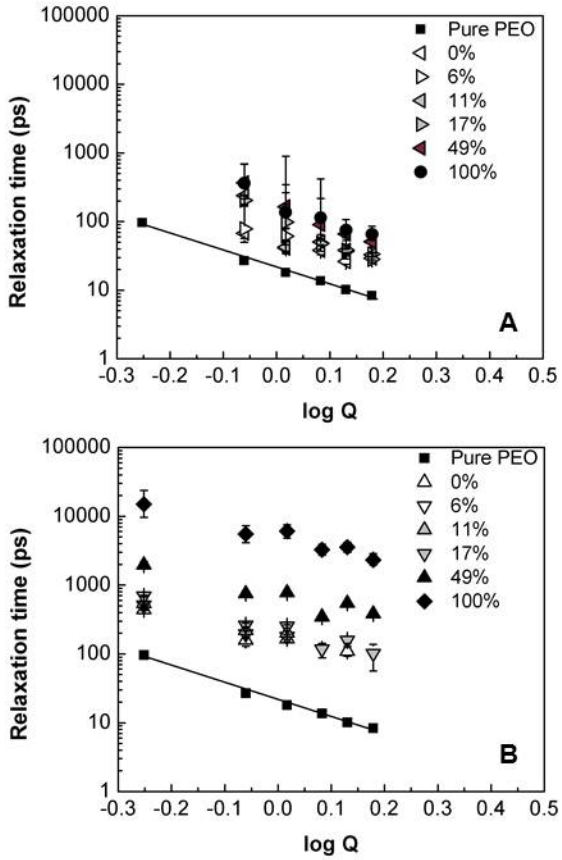

Figure 4.7. Q dependence of the relaxation times for the ionomers at 298 K for (A) bridge atoms, and (B) anchor atoms. The single relaxation for pure PEO is shown in both parts of the figure. The solid line through pure PEO data represents $\tau \sim Q^n$ where n = -1.8. The units of Q are in $Å^{-1}$.

cation. The anchor atoms from these 30 spacers (30 x 9.75 $\sim$ 300 EO atoms) share the remaining 29 cations. This yields an anchor atom ion content of 10 EO per cation. This rough estimate implies that one out of every 30 cations is "'single"' [no association with its anion] whereas the other 29 participate in shared ion pairs, separated ion pairs or larger aggregates. The behavior of the PEO salt system PEO/$LiClO_4$ with ion content is presented in Figure 4.8 for comparison. In this system, the presence of ions slows down the segmental relaxation process by electrostatic coordination between the cation and the ether-oxygen atoms of the PEO chain. The influence of ion content on segmental relaxation times is similar to that of the bridge atoms in the ionomer: between 0.025 and 0.12, the relaxation time

increases by a factor of three. However, the variation is continuous, rather than divided into two regimes. In contrast, the slower processes have distinctly different trends, confirming that the origins of these processes are different. Indeed, the slower process in PEO/$LiClO_4$ is rotational in nature and unrelated to the slower process in the ionomer. PEO/Li-salt systems crystallize into pure PEO and ion-containing structures with EO:Li ratios of 3:1 or 6:1, depending on the electrolyte concentration.[82,83,125] It is the rotation of these structures that defines the slower process. These structures do not exist in the ionomers, as WAXS studies on the PEO600 based ionomers do not show the formation of crystalline structures in the temperature range of measurement.[6,8] Although it is possible that small helical structures exist locally, our results are not consistent with a rotation, for which relaxation times are Q independent.[2]

The increase in relaxation times of anchor atoms exceeds that which is expected from electrostatic coordination of the cation with the PEO spacer. Although the maximum ion content of the ionomers is 0.08, we estimate that for the anchor atoms, the concentration may be as high as 10 EO per cation (0.1). The relaxation times of anchor atoms increase by a factor of 50 over this range, whereas relaxation times of PEO/$LiClO_4$ vary by a factor of nine. This suggests that something other than electrostatic coordination via cations and ether oxygens influences dynamics in the anchor atom region. In PEO/Li salt system, ion pairs or larger aggregates do not involve the polymer chain. This is not the case for the ionomer. Interaction between at least two anions and a cation can form physical cross-links via ionic clusters, which do not occur in PEO/Li salt systems. We know that these clusters are not well defined, large, or of consistent size, because ionic aggregation is not evident in the SAXS data for PEO600-100%Na below 353K.[6,7] However, it is reasonable to assume small, polydisperse clusters with weak boundaries are present in PEO600-100%Na, based on the excess scattering intensity in the SAXS data between the interchain packing peak (amorphous halo) and the ionomer peak evident in the PEO600-100% Li ionomer. This provides a mechanism for slowing in excess of the PEO/Li salt case: ionic cross-linking preferentially slows the chain near the anions, leaving the bridge region unaffected. We also note that X_{ANCHOR} increases with ion content (see Figure 4.9). This could occur if more ether oxygens associate with small ionic clusters.

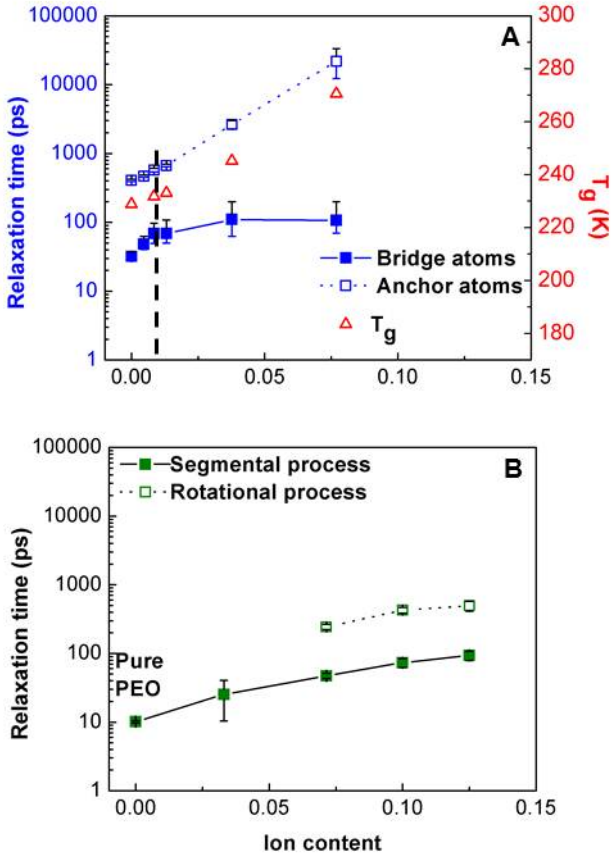

Figure 4.8. (A) Relaxation times for PEO600-Y%Na ionomers [298 K, Q = 1.35 Å^{-1}] and T_g vs ion content (B) Relaxation times for PEO/$LiClO_4$ [348 K, Q = 1.35 Å^{-1}] and T_g vs ion content[2]

The glass transition temperature increases with ion content from 229 K for the nonionic polymer to 271 K for PEO600-100%Na. This is compared to the ion content dependence of bridge and anchor relaxation times in Figure 4.8. It is clear that the anchor atoms control T_g, rather than the bridge atoms. The reason for this is similar to the reason only the slow process is observed at the largest length scales of our experiments. In the concept of the cooperatively rearranging region, the length scale associated with T_g is $\sim$ 100 Å.[126] A region of this size would include multiple PEO spacers and their associated ions, and thus we expect it to encompass multiple dynamic processes. The dynamics of the region will be controlled by the slowest of those processes. In PEO/salt systems, it is established that the segmental motion of the polymer facilitates ion motion. Conductivity depends on

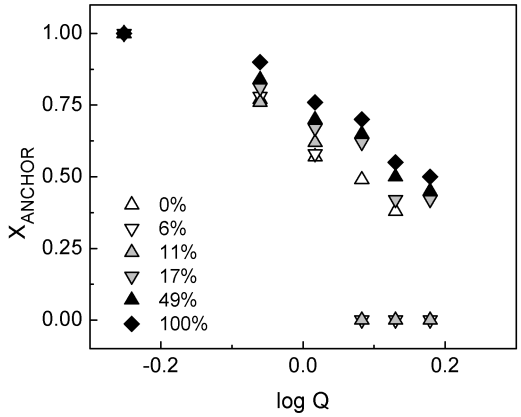

Figure 4.9. Fractions of fast H-atoms, X_{ANCHOR}, as a function of Q for all samples at T = 323 K. The legend entries 'Y%' correspond to PEO600-Y%Na. Darker data points have higher ion content than lighter data points. The units of Q are in $Å^{-1}$.

both the mobility of the host polymer and the ion content. Since increasing ion content both provides more ions for conduction and slows polymer mobility, a peak is observed in conductivity. As shown in Figure 4.10, a peak also occurs in the ionomers. The maximum conductivity occurs at lower ion content in the ionomers than in PEO/$LiClO_4$. This is directly related to the positioning of the anion on the polymer backbone and its influence on polymer mobility. In the ionomers, cations slow the polymer in two ways: coordination with ether oxygen atoms in bridge regions, and ionic cross-linking in end regions. The latter is absent in PEO/$LiClO_4$, as the anion is not bonded to the PEO chain, and thus salt clusters do not crosslink the polymer. As a result, only interaction with PEO ether oxygen atoms (comparable to the bridge region) slows polymer mobility in PEO/salt systems. Because of this difference, higher ion content may be tolerated in PEO/salt systems before sluggish polymer dynamics decreases conductivity. The rapid rise of conductivity for the ionomers and the positioning of optimal conductivity at low ion content may be important in designing low ion content electrolytes. We note however, that the conductivities of these two samples should not be directly compared. The ionomers are essentially single ion conductors, whereas in PEO/$LiClO_4$ both the anions and the cations contribute to conductivity. The identity of the anion is also different, which has been demonstrated to influence conductivity.[127,128]

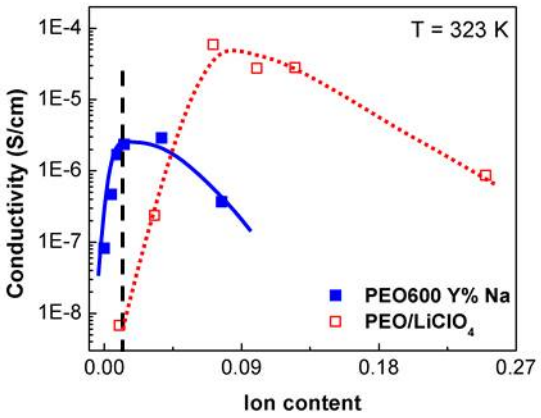

Figure 4.10. Conductivity vs. ion content for the PEO600-Y%Na ionomers[5] and $PEO/LiClO_4$[2] at T = 348 K. The curves through these data points serve as visual aids to identify the conductivity peaks.

We conclude this chapter by discussing several structures that may be important, and their importance in our data and other measurements on PEO600-100%Na. Figure 4.11 proposes four such structures, the single cation, the separated contact pair, the shared contact pair, and a small ionic aggregate. We emphasize that our measurements do not directly reveal these structures, and their connection with our data is our interpretation. Single cations (also sometimes called "free" ions) are solvated by PEO ether oxygens and have limited interaction with anions. The ions interacting with bridge ether oxygens are most likely single cations. Although we estimate no more than 7% single ions, an FTIR study indicates that all of the SO_3 groups are associated with a cation (direct contact pairs or aggregates), with no detectable single cations.[100] In molecular simulations, close to 30% of Na are found as single cations, and 20% are in direct contact pairs.[9] The separated contact pair, in which a PEO segment lies between the anion and cation, occurs regularly in PEO/Li salt systems; this can be classified as free or as a pair, depending on technique. This structure is found in simulation,[9] and there is some evidence it may be present based on DRS.[3] The current data does not require or exclude such structures. Indeed, the techniques used to date (SAXS,[6,7] molecular simulation,[9] DRS,[3,5] and QENS) suggest that at the temperatures of our measurements, a variety of structures are present in PEO600-100%Na. One structure

that appears consistent with all techniques used to date and is also consistent with previous observations on ion containing polymers[33,53,54,129] is the small ionic aggregate. The current measurements suggest that small ionic clusters lead to ionic crosslinks, slowing polymer dynamics in excess of what is expected based on PEO salt systems. Ionic aggregates are not evident in SAXS in PEO600-100%Na at room temperature,[7] indicating that the clusters are small and inconsistent in size. Ionic aggregates become evident via SAXS in PEO600-100%Na above 353 K. In molecular simulations, 50% of Na ions cluster in ionic aggregates of three to twelve ions.[9] Aggregates are also seen in DRS, with their fraction increasing with temperature.[7] It appears that these aggregates are characteristic of PEO-based single ion conductors, and their size and regularity depends on ion identity and temperature.[7] The influence of ion identity on polymer structures has been reported[6,7] and the corresponding influence on polymer dynamics using QENS is the subject of Chapter 6.

4.3 Concluding remarks

In this chapter we studied how QENS was used to measure dynamics in PEO based single ion conductors of the form PEO600-Y%Na where Y $\in$ [0,100]. The presence of the isophthalate group in the nonionic polymers slows segmental relaxation additional to that seen in pure PEO, and introduces an additional segmental relaxation that is slower. Our interpretation associates these relaxations with segments in the mid-region of the repeating unit (bridge atoms) and segments neighboring the isophthalate group (anchor atoms). Ionomers with non-zero ion content also show two segmental relaxations. The presence of ions does not change the origins of the two processes, but does slow them down. The anchor atoms slow significantly more than the bridge atoms as ion content increases. We suggest this is due to the presence of small ionic clusters, which crosslink the polymer chains. These crosslinks are either more stable or more extensive than those formed between bridge ether oxygens and cations, as the influence of ion content on anchor atom dynamics is stronger than in PEO salt systems.

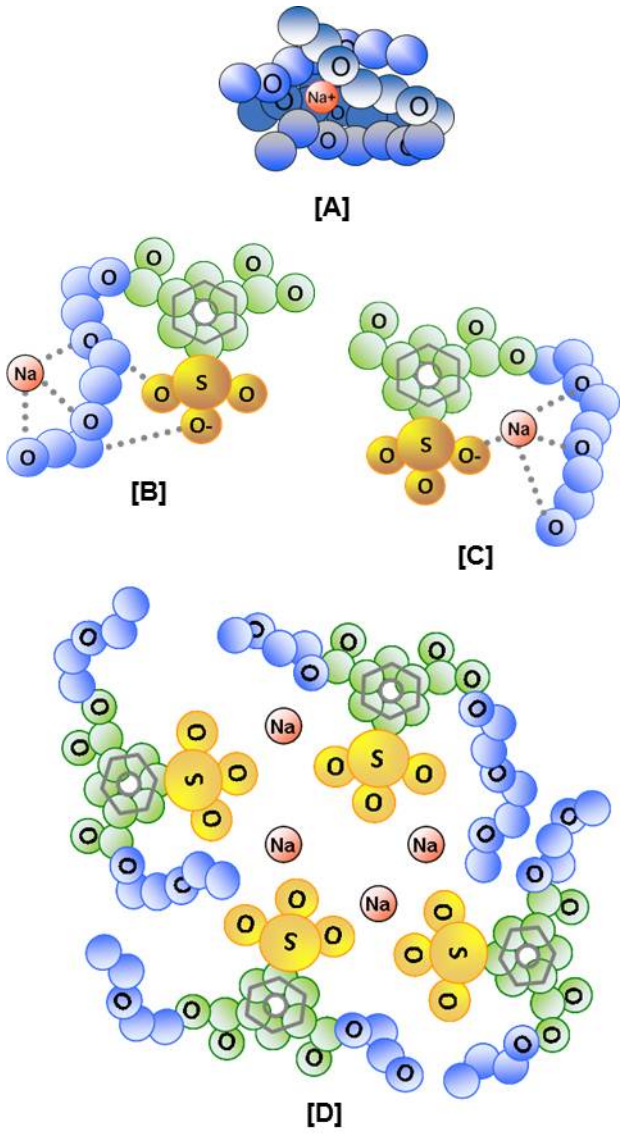

Figure 4.11. Cation coordination states (A) single cation, (B) separated contact pair, (C) shared contact pair, and (D) small ionic aggregate

Chapter 5

Effect of ion content and dynamic patterning in PEO based single ion conductors

5.1 Introduction

In the previous chapter, we used QENS to identify the dynamic processes that govern ionomer mobility and their role in ionic conductivity. We observed that the non-ionic polymer (PEO600-0%Na) has two segmental relaxations, arising from two different fractions of the ionomer (see Figure 5.1a). The slower H-atoms (anchor atoms) belong to the PEO spacer neighboring the isophthalate group and the faster H-atoms (bridge atoms) belong to the mid-spacer section, away from the effect of the isophthalate group.

The addition of ions to the system (by increasing the degree of sulfonation) does not introduce any new processes, but the two fractions are affected differently. The bridge atom relaxation times are independent of ion content above the ion content of 0.01. Comparatively, the anchor atoms slow down significantly with the addition of ions. For example, the bridge relaxation time for PEO600-100%Na is about 3 times that of PEO600-0%Na, whereas the anchor relaxation time for PEO600-100%Na is about 100 times that of PEO600-0%Na (values reported at 298 K, Q = 1.35 $Å^{-1}$). Based on these observations, we identified that the bridge atoms

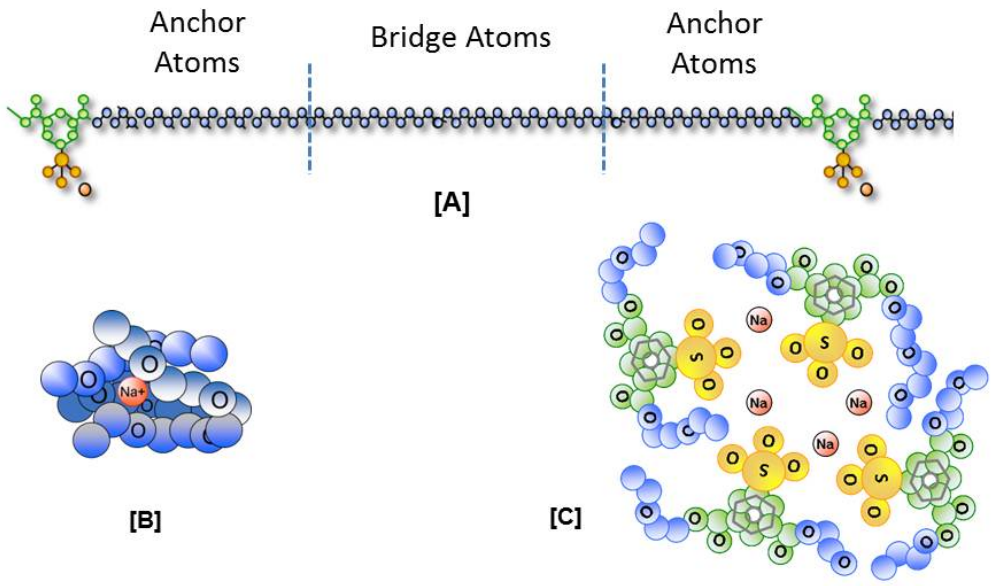

Figure 5.1. (A) Fractions of bridge atoms and anchor atoms in the spacer for PEO600-Y%Na ionomer; (B) "Single (free) cation" coordination with EO atoms that slows down the bridge atoms; and (C) ionic aggregate that cross-links the anchor atoms of the spacer

are slowed down by the coordination with free cations (Figure 5.1b), whereas the anchor atoms are slowed by the crosslinking of isophthalate groups by cations (Figure 5.1c). This behavior is consistent with studies on ionomers which show regions of restricted mobility around ionic clusters.[53,54,129] In this chapter we study the effect of changing ion content by varying the spacer length (400, 600, 1100), while keeping the degree of sulfonation constant at 100% (see Table 5.1). We will investigate the effect on dynamics and conductivity, and conclude that it is better to achieve a particular ion content by changing the spacer length, as opposed to changing the sulfonation level. We will further combine dynamics information obtained from QENS with ion aggregation information from SAXS[6,7] and propose an overall schematic summarizing the dynamic patterning of bridge and anchor atoms in these samples.

Table 5.1. Properties of PEO600-Y%Na samples (where Y ∈ [0,100]) and PEOx-100%Na samples (where x = 400/600/1100)

Sample	Cation:EO ratio	Ion content	T_g (K)	Mol. Wt. (g/mol)	Ions per chain
PEO600-0%Na	0	0	229	5800	0
PEO600-6%Na	1:217	0.005	230	5800	0.6
PEO600-11%Na	1:118	0.008	232	5800	1.1
PEO600-17%Na	1:76	0.013	233	8700	2.5
PEO600-49%Na	1:26	0.038	245	4700	3.8
PEO600-100%Na	1:13	0.077	267	6300	10.5
PEO400-100%Na	1:09	0.111	295	3300	8.5
PEO600-100%Na	1:13	0.077	267	4600	7.7
PEO1100-100%Na	1:25	0.04	236	4500	4.1

5.2 Effect of ion content on dynamics

As in the previous chapter, both bridge and anchor relaxations are segmental processes. This is illustrated in Figure 5.2, where the Q dependence of bridge and anchor relaxation times follow the same slope as those for pure amorphous PEO at (348 K).[2,117,121] Also evident from Figure 5.2 is the different dependencies of the two processes on ion content; the anchor atom relaxation is more ion dependent than the bridge atom relaxation. For example, at Q = 1.35 Å^{-1}, $\tau_{400}/\tau_{1100} \sim 2$ for the bridge atoms, whereas $\tau_{400}/\tau_{1100} \sim 100$ for the anchor atoms.

As the glass transition temperature varies with ion content, it is reasonable to ask which process is associated with T_g. This question is addressed in Figure 5.3, where we include the samples from the current study (PEOx-100%Na) and those from the previos chapter (PEO600-Y%Na). When the glass transition temperature is low [below $T_g \sim 230$ K], the increase in bridge relaxation tracks T_g, shown by the solid black line. For samples with higher T_g (and higher ion content), the bridge atom relaxation does not change much, but the anchor relaxation tracks T_g with the same slope as the bridge atoms below $T_g \sim 230$ K. This T_g corresponds to an ion content of approximately 0.01. The two parts of Figure 5.3 represent different temperatures and Q values; the absence of anchor relaxations for low T_g samples at Q = 1.35 Å^{-1} and T = 348 K (Figure 5.3a) implies that the difference be-

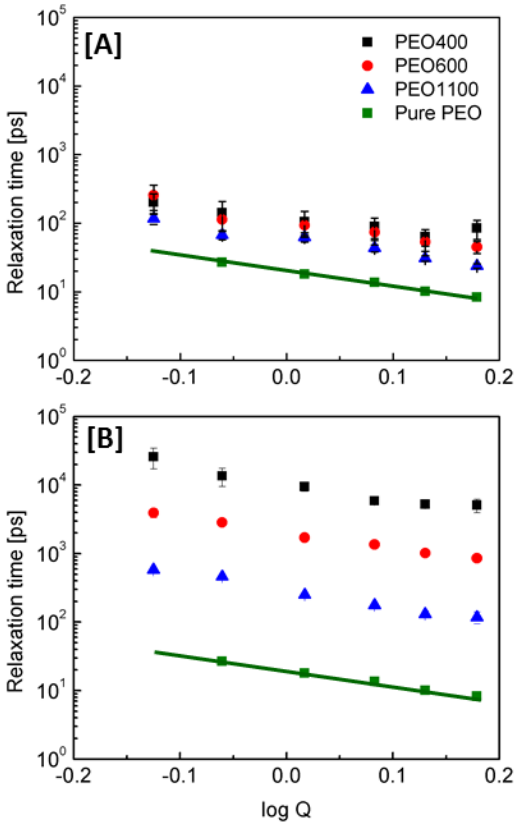

Figure 5.2. Q dependence of relaxation times of (A) bridge atoms, and (B) anchor atoms for PEOx-100%Na at T = 348 K. Data for pure amorphous PEO is at 348 K. The units of Q are in $Å^{-1}$.

tween bridge and anchor atoms is not sufficient to resolve into two processes. This variation in number of processes observed (one or two) depends on temperature, ion content and the observation length scale set by Q, and is discussed in detail in Chapter 3. In Table 5.1, we list the number of ions per chain, which depends on ion content and molecular weight. At ion contents of 0.01 or less, the number of ions per chain is less than 3, consistent with limited ability to slow dynamics via cross-linking. We refer to 0.01 as the cross-over ion content, below which the bridge relaxation governs T_g and above which the anchor relaxation governs T_g.

We now investigate how the ionomer dynamics and conductivity depend on the method of achieving a particular ion content - by changing spacer length or by changing degree of sulfonation. In Figure 5.4a we plot the bridge and anchor relax-

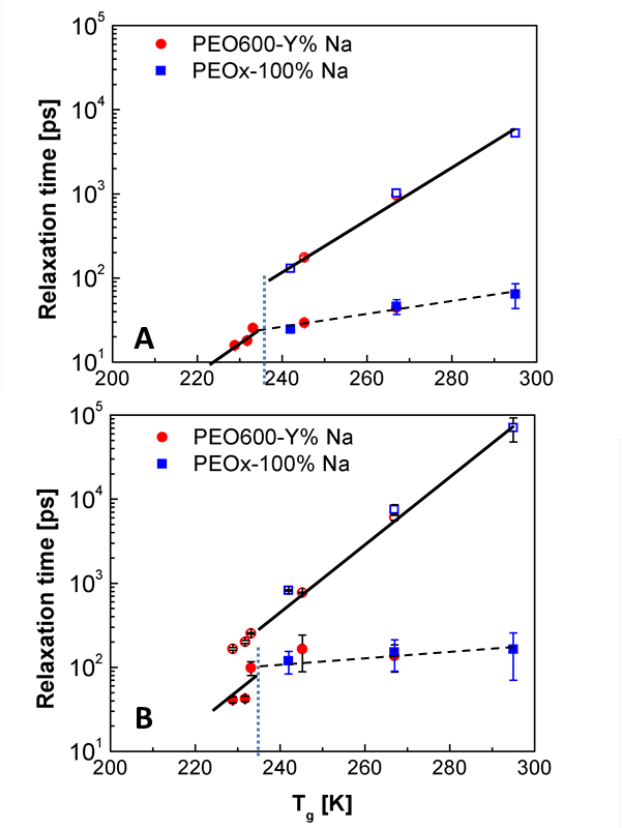

Figure 5.3. Correlation of bridge and anchor atom relaxation times with T_g[5] of the ionomers PEO600-Y%Na and PEOx-100%Na for (A) T = 348 K, Q = 1.35 Å^{-1}; and (B) T = 323 K, Q = 1.04 Å^{-1}.The solid lines in each part have the same slope.

ation times against ion content for PEO600-Y%Na and PEOx-100%Na. Changing the ion content in different ways does not affect trends in bridge and anchor relaxation times, suggesting that the dynamics depend on the total ion content, not on the way it was achieved. In Figure 5.4b we show the X_{BRIDGE} values for all three temperatures at Q = 1.35 Å^{-1}. At this Q value, the anchor atom relaxation is not observed below the cross-over ion content, except at low temperature (298 K). The dependence of conductivity on ion content is shown in Figure 5.4c for all three temperatures. Based on the fact that bridge relaxation times increase more rapidly below the cross-over ion content than above it, we hypothesize that below the ion content of 0.01, cations primarily add to the PEO spacers. Above this ion content, 3 or more ions are present per chain and cations begin preferentially populating the anchor regions, thus initiating cross linking, which increases relaxation times and

decreases conductivity. Our study includes two samples with the same ion content achieved in different ways: PEO600-49%Na and PEO1100-100%Na. If we examine these samples (marked with an arrow in the Figure), we see that the bridge and anchor atoms are slightly faster and the fraction X_{BRIDGE} higher for PEO1100-100%Na compared to PEO600-49%Na. This difference most likely arises because of the presence of unsulfonated isophthalate groups in PEO600-49%Na, which we know from data on the non-ionic polymer, lowers the mobility. This has a larger influence on conductivity than on relaxation times: at 298 K, the conductivity of PEO1100-100%Na is nearly an order of magnitude higher than PEO600-49%Na, with negligible differences in both bridge and anchor relaxation times.

These observations suggest that when given a choice, we should control ion content by varying the spacer length, rather than the degree of sulfonation. In Figure 5.4c, if we extrapolate the conductivity on the PEOx-100%Na series towards the crossover ion content (dotted line), we see that the predicted values of the conductivities (based on the trend) would be between $10^{-5} - 10^{-4}$ S/cm, which is 1-2 orders of magnitude higher than the maximum obtained by PEO600-Y% series. This is close to the ionic conductivity of 10^{-4} S/cm necessary for batteries to generate current densities of practical benefit.[20] The PEO salt system PEO/$LiClO_4$ with the same ion content (1:100) has conductivity of 10^{-4} S/cm near 348 K.[2] This similar value is misleading, because for the salt system it includes contributions from both anions and cations. For a fully sulfonated ionomer with the ion content of 0.01, we need a spacer length of 4400, which corresponds to 100 PEO repeat units. The disadvantage of increasing spacer length as opposed to reducing sulfonation is that crystallization is observed for spacers longer than 1100.[6] At realistic molecular weights, crystallization negatively impacts conductivity, the main reason that the conductivity of the PEO salt is low at 298K.

It is likely that differences in dynamics between PEO600-49%Na and PEO1100-100%Na are not the only cause for the difference in conductivity, as ionic aggregation of the two samples may not be the same. This observation highlights the need for understanding the structure of aggregates, their influence on dynamics of the polymer chain, and their impact on conductivity mechanism. It is possible that specific small aggregates increase conductivity and are more prevalent when all the isophthalate groups are sulfonated. Molecular dynamics simulations at 343 K[9]

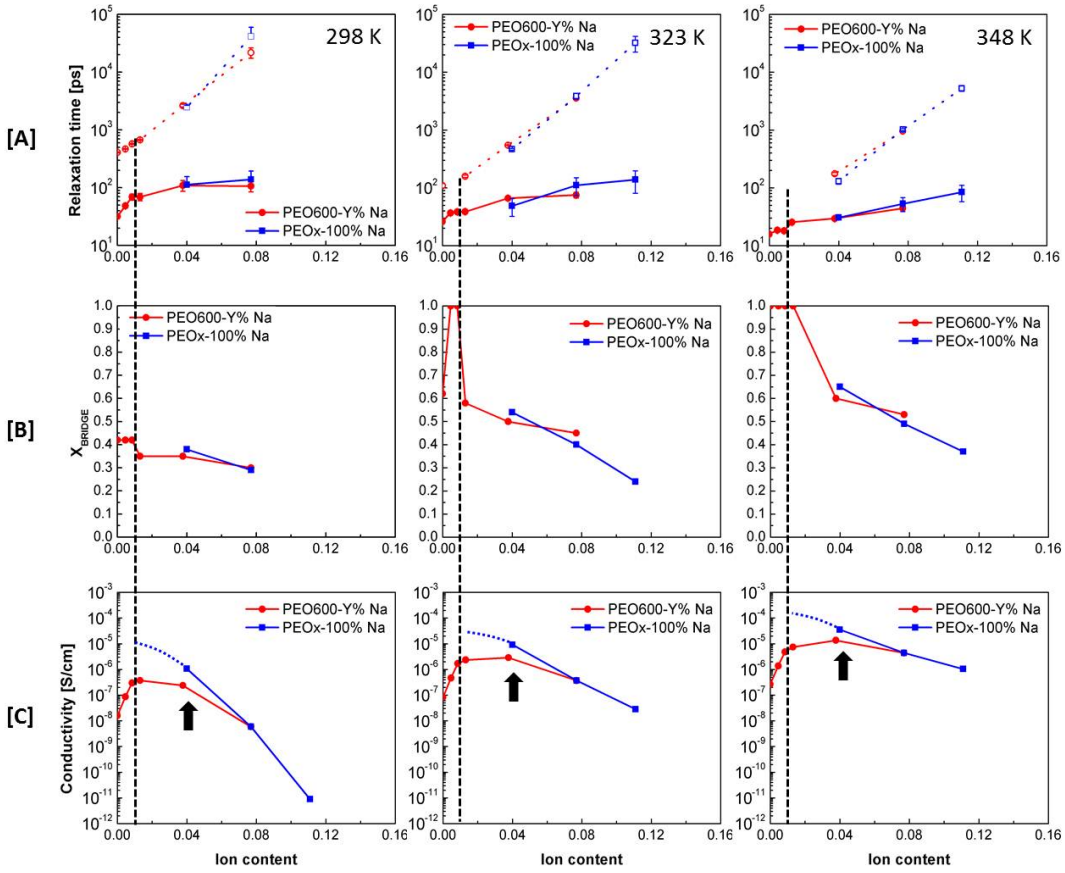

Figure 5.4. (A) Relaxation times, (B) X_{BRIDGE} and (C) conductivity[5] vs ion content for PEO600-Y%Na and PEOx-100%Na at 298 K, 323 K and 348 K. The dotted line in all the graphs denotes the crossover ion content of (0.01). Relaxation times and X_{BRIDGE} have been reported at Q = 1.35 $Å^{-1}$.

suggest that aggregates shaped like ion chains occur and facilitate charge transfer; one cation approaching the chain from one end causes another to leave from the other end, thus transferring charge over a larger distance than atom movement. While SAXS data for the degree of sulfonation series (PEO600-Y%Na) on which we previously reported are not available, SAXS data is available on the fully sulfonated ionomers (PEOx-100%Na) described in this paper.[6,7] These data show that ion states are varied and non-uniform, depend on spacer length and temperature, and are inconsistent with spherical aggregates. The aggregation state is important to conductivity: "free" ions are solvated by the polymer rather than their anion and proposed to be the main contributors to conductivity,[72] small

ion chains may influence conductivity as described above, whereas ion-pairing is considered detrimental to conductivity.[57,58,68,86,130]

5.3 Dynamic patterning of bridge and anchor regions

Because both polymer dynamics and ion aggregation states are important to conductivity, we now formulate a picture of the spatial organization of dynamically fast and slow regions of the polymer [bridge and anchor atoms] and cation aggregation, which is consistent with both QENS and SAXS data. The regions included are dynamically fast [bridge], dynamically slow [anchor atoms with ions; anchor atoms without ions], and primarily ionic [no polymer]. The reason for the two types of anchor atoms stem from SAXS observations of primarily ionic aggregations that form at high temperature.[6,7] In order for these to present a uniform feature in SAXS data, the boundary between ionic and non-ionic should be relatively sharp,[6,7] meaning that the ion content of the anchor regions of the spacer will decrease when sharp ionic boundaries are present. We cannot confirm this observation dynamically: although a decrease in ion content should lead to faster dynamics, the aggregation appears as the temperature is raised, which also leads to faster dynamics. However, we are able to estimate the ion content in the anchor region as a function of temperature. This estimate includes both ions that associate with the anchor regions, and ions in a purely ionic core. We make the distinction in our schematic based on the presence or absence of an ionomer peak in SAXS. To compile a schematic with spatial organization consistent with our data, we use the fraction of bridge atoms from QENS; the estimate of bridge and anchor atoms ion content [see below] from QENS; the total ion content of the sample; the existence, size and boundary definition of ionic aggregates from SAXS; and the distance between ionic aggregates from SAXS. We also use information from MD simulation that aggregates, regardless of size, tend to form string-like clusters.[9]

The fraction of bridge atoms is obtained directly as a fit parameter from QENS data. Because motion over larger length scales involves the entire spacer and the largest spatial scales probed by QENS are comparable to the spacer radius of

gyration, the fraction of bridge atoms is Q dependent, as illustrated in Figure 5.5. At spatial scales on the order of intermolecular chain spacing [Q $\sim$ 1.3 Å^{-1} or higher] the fraction of bridge atoms becomes Q independent, and we use this value for the bridge fraction of each sample.

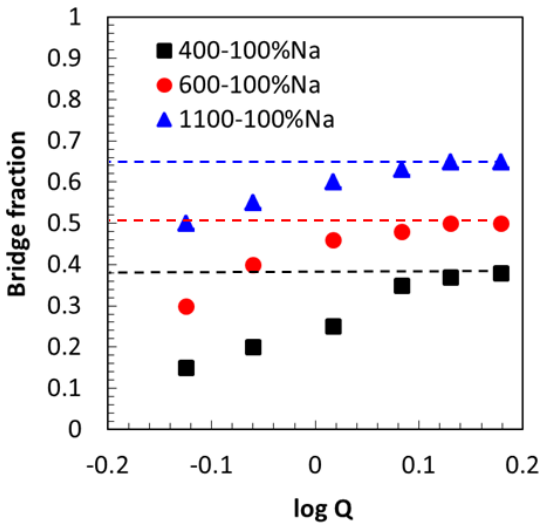

Figure 5.5. Q-dependence of X_{BRIDGE} for PEOx-100%Na at 298 K, 323 K and 348 K. The dotted lines are the values of the asymptotes at high Q.

To determine the ion concentration in bridge and anchor regions, we use the observation that bridge relaxation times are fairly insensitive to increasing ion content above 0.01. Because increasing ion content should cause a significant increase in relaxation times, which occurs only in the anchor region, we interpret these observations as the bridge region maintaining an ion content close to 0.01 while the ion content rises preferentially in the anchor region. This interpretation may be used to estimate the ion content in the anchor region. Consider the sample PEO1100-100%Na that has 25 EO atoms in each spacer, and a bridge fraction of 0.65. This means that there are approximately 16 bridge EO atoms and 9 anchor EO atoms for every cation. If the bridge ion content is 100:1, the 100 bridge EOs for each cation are provided by 100/16 $\sim$ 6 ionomer repeat units. It follows that from every 6 repeat units of PEO1100-100%Na (150 total EO atoms), 100 bridge EO atoms share 1 cation, and 50 anchor EO atoms share the remaining 5 cations. Therefore the ion content of the anchor atoms is 1:10, and the number of cations

in the anchor region is 10 times that of the bridge region. The calculations for the other two PEOx-100%Na samples are reported in Table 5.2. As expected, the ion content of the anchor atoms increases as the spacer length decreases. It also increases as temperature increases, consistent with increased aggregation as temperature is raised observed using SAXS.[6,7] It is interesting that the maximum conductivity occurs for an anchor region ion content of $\sim$ 1:10 [PEO1100-100%Na sample], as shown in Figure 5.6. This is different than the overall ion content of 1:25, but close to the ion content of maximum conductivity for PEO/salt systems [between 1:8 and 1:14].

Table 5.2. Distribution of cations in anchor atom region at T = 298 K, 323 K and 348 K (calculated values are approximate). Sample x-Na stands for PEOx-100%Na; *N* stands for the number of PEO spacer repeat units; *Br* and *An* stand for *Bridge* and *Anchor* respectively, X_{Br} stands for X_{BRIDGE}

Sample (N)	Ion content	Temp (K)	X_{Br}	Br | An EO atoms per spacer	Cation:EO ratio		Ratio of cations in anchor:bridge
					Bridge	Anchor	
600-Na (13)	0.08	298 K	0.3	4 | 9	1:100	1:9	11
1100-Na (25)	0.04		0.4	10 | 15	1:100	1:17	6
400-Na (9)	0.11	323 K	0.25	2 | 7	1:100	1:7	14
600-Na (13)	0.08		0.4	5 | 8	1:100	1:8	12
1100-Na (25)	0.04		0.55	14 | 11	1:100	1:13	8
400-Na (9)	0.11	348 K	0.36	3 | 6	1:100	1:6	16
600-Na (13)	0.08		0.5	6.5 | 6.5	1:100	1:7	14
1100-Na (25)	0.04		0.65	16 | 9	1:100	1:10	10

As discussed above, it is likely that bridge and anchor regions are spatially segregated and have different ion contents, in addition to different dynamic properties. We now consider SAXS data for this system.[6,7] These data shows the presence of multiplets, which scatter in the mid Q region, and ionic clusters, which scatter in the low Q region: see Figure 5.7 for the locations of these regions, and schematics of a multiplets and ionic clusters. We define a multiplet as a small aggregate, which could be a triple ion [charged], a quadrupole [neutral] or slightly larger charged or uncharged aggregates. Multiplets are distinct from pairs, which have their own scattering signature,[6,7] and are not uniform in spacing, number or size, because no distinct feature is observed in this region. Ionic clusters are larger and more

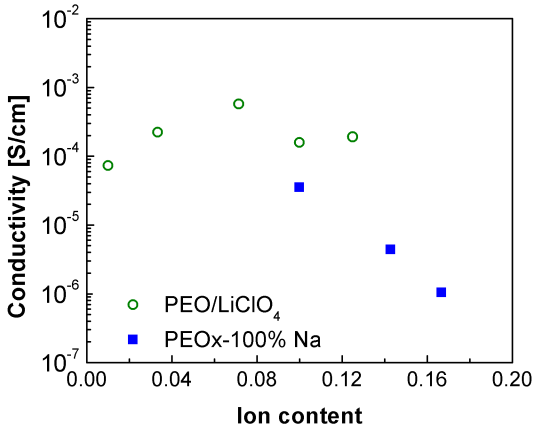

Figure 5.6. Conductivity (T = 348 K) vs. ion content for PEO/$LiClO_4$ system[2] (open, green circles) and conductivity[5] vs anchor ion content for PEOx-100%Na system (filled, blue squares)

regular in size, shape and definition than multiplets, giving rise to a well-formed peak. From this peak, we can determine the average distance between centers of ionic clusters: these distances (21 Å for PEO400, 24 Å for PEO 600 and 31 Å for PEO1100) are incorporated in our schematic at temperatures where the ionic peak is present. Also noticeable in Figure 5.7 is the chain-packing peak at high Q. This shows little to no variation between samples and is not discussed further.

Using the ideas discussed above, we present a schematic of the spatial organization of the bridge, anchor and ionic regions in Figure 5.8. This figure takes into account all of the data outlined above, drawing the fractions of each region to scale and depicting ionic clusters or aggregates as suggested by SAXS. Each of the nine combinations of spacer length and temperature is represented by an image. Differences in the same sample on increasing temperature are read from left to right, whereas differences from increasing spacer length at the same temperature are read from top to bottom. For example, the top row represents PEO400-100%Na as the temperature varies from 298K to 348K. At the end of the row, SAXS data for this sample at the three temperatures are plotted together. This data suggests the presence of multiplets at 298 K. As the temperature increases (to 323 K), the ions and anchor PEO atoms reorganize, bringing the multiplets closer. As we further increase the temperature to 348 K, large ionic aggregates separated by 21 Å are

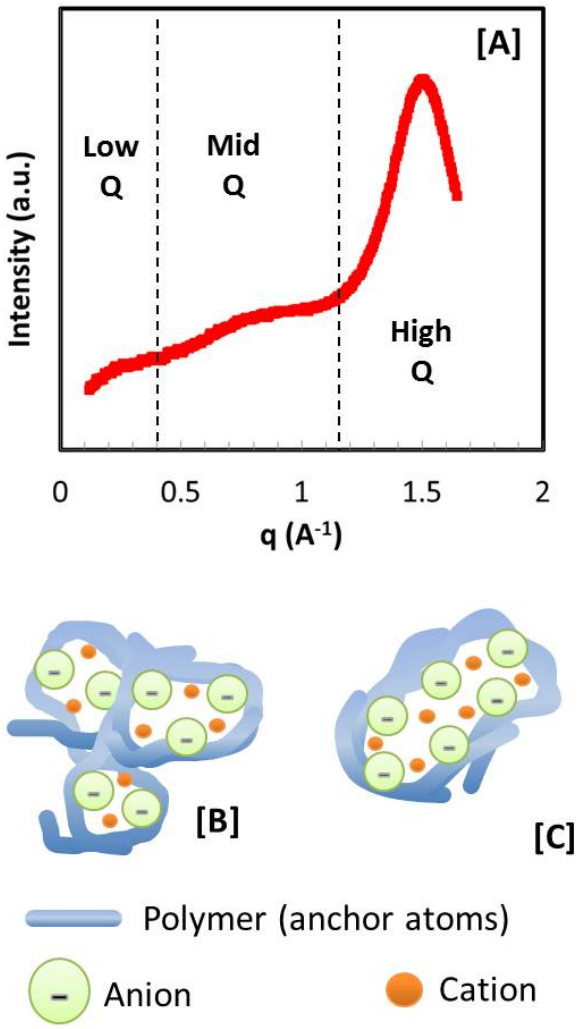

Figure 5.7. (A) SAXS data for PEO400-100%Na at 298 K illustrating the three Q regions, (B) multiplets and (C) large ionic aggregate

formed. Beginning with this sample, and reading down, the main differences are the decrease in overall ion content, which serves to increase the distance between ion aggregates and reduce their number compared to the samples with shorter spacer lengths. All three of these samples have ion aggregates, as illustrated by the ionomer peaks in the SAXS data shown at the bottom of the row.

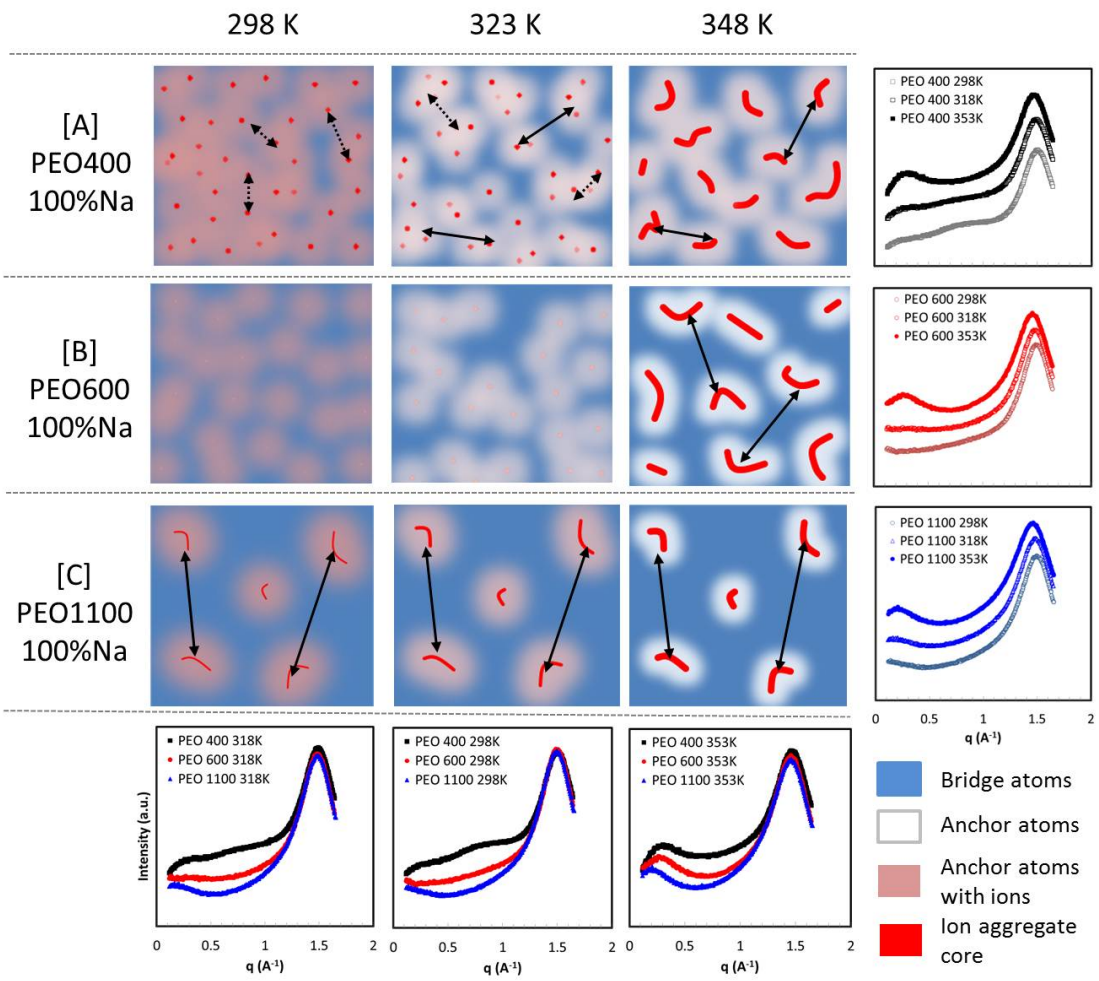

Figure 5.8. Dynamic patterning of bridge and anchor atoms for (A) PEO400-100%Na, (B) PEO600-100%Na, and (C) PEO1100-100%Na at 298 K, 323 K and 348 K, with corresponding SAXS data (298 K, 318 K and 353 K)[6,7]

5.4 Concluding remarks

Some interesting observations follow from these schematics. The samples are not homogeneous and it is not clear that ion transport occurs only through singly solvated ["free"] cations. The amounts of free cations in these ionomers are estimated at around 2% for the PEO600-100%Na sample, here we estimate around 12% for this sample [bridge cations], 22% for the 1100 spacer, and 8% for the 400 spacer, with little temperature dependence. The change in conductivity among this series [Figure 6.1] is larger than would be expected based on this increase in free ion

content. We speculate that the morphology of the samples, including the size and shape of ionic aggregates, and the extent of bridge and anchor regions contributes to conductivity. The sample with the highest conductivity at all three temperatures is the 1100 spacer, a sample that exhibits ion aggregation at all temperatures. The increasing ion aggregation as temperature increases does not negatively impact conductivity; although one expects some increase, conductivity increases by two orders of magnitude over 50 K [note that no crystallization occurs for these samples]. We also note that the spacer length dependence of conductivity at 348 K is much weaker than it is at 298 K or 323 K, the difference being the presence of ion aggregates at all spacer lengths at 348 K, whereas the 400 and 600 spacer lengths only show organized aggregation at 348 K. We thus suggest that ion aggregates play an as yet unknown role in ion conduction for single ion conductors.

Chapter 6

Favorable scenarios for conductivity in single ion conductors

6.1 Introduction

The previous two chapters on the PEOx-Y%Na samples were based on observing dynamics as a function of ion content. We chose sodium (Na+) as the cation because the Na-based ionomers are amorphous, single phase materials and have a smaller extent of microphase separation (than Li-based ionomers) in the temperature range of our study.[5–7] We varied the ion content in two ways - by changing the degree of sulfonation and by changing the spacer length. In PEO600-0%Na, i.e. the non-ionic polymer, we observed that the presence of the isophthalate group introduced a slower segmental relaxation in addition to the segmental relaxation typically observed in pure PEO. The faster fraction is composed of "bridge atoms" and the slower fraction is composed of "anchor atoms," as shown in Figure 6.1a. The relaxation times of the anchor atoms, unlike the bridge atoms, increase significantly (1-2 orders of magnitude) with increasing ion content (see Figure 6.1b). Regardless of how the ion content is changed, the trends for bridge and anchor atom relaxation times are the same. Above the ion content of 0.01 (vertical dashed line), the bridge relaxation times are almost constant, and the anchor atom relaxation time starts increasing rapidly. Below the crossover ion content, the glass transition temperatures (T_g) of the samples depend on the bridge relaxation times,

and above the crossover ion content they depend on the anchor atom relaxation times. The maximum conductivity of these ionomers is also observed at the ion content of 0.01. Below this value, there aren't enough ions to contribute to conductivity and above this value, the slow anchor atoms reduce the overall mobility drastically. SAXS results show the existence of ionic aggregates of several cations and anions that is characteristic of these ionomers.[5–7] These aggregates crosslink the isophthalate groups and thereby reduce the mobility of the adjoining anchor atoms. By comparing dynamics and conductivity of samples with similar ion content (PEO600-49%Na and PEO1100-100%Na), we learned that to achieve higher conductivity it is better to have a completely sulfonated sample with a long spacer, rather than an unsulfonated sample with a short spacer. The unsulfonated isophthalates appear to prevent the formation of certain string like aggregates which assist in ion conduction, as seen by MD simulations[9] on PEO600-100%Na. With the help of QENS we also quantified the ion content in the anchor and bridge regions. The high ion content of anchor atoms is detected in the form of ionic aggregates and multiplets in SAXS. Combining the observations from QENS and temperature dependence of morphology from SAXS, we proposed the spatial organization of bridge and anchor atoms as a function with the help of SAXS data (see Figure 6.1c).

In this chapter we investigate the effect of ion identity on the dynamics of PEOx-100%M ionomers where x = 400/600/1100 and M = Li/Na/Cs (see Table 6.1). Studies show that a larger cation has smaller surface charge density and therefore interacts weakly with both the anion and polymer host, resulting in low dissociation energy, faster dynamics and higher conductivity.[20,41,73–77] The radii of the cations in this study increases in the order $Li^+ < Na^+ < Cs^+$, causing the binding energies (to the anion and EO atoms) to decrease in the order $Li^+ > Na^+ > Cs^+$. Although we expect the ionomer T_g to follow the trend established by binding energies of the cations, we observe deviations which imply that the dynamics are not a function of binding energies alone. While *ab initio* calculations can help identify these factors,[6] a lack of knowledge of the exact environment (number of surrounding ions, ether oxygen atoms, PEO segments etc.) poses a challenge for accurate calculation. QENS offers the advantage of studying how variations in binding energy and cation size affect the anchor atom dynamics. An

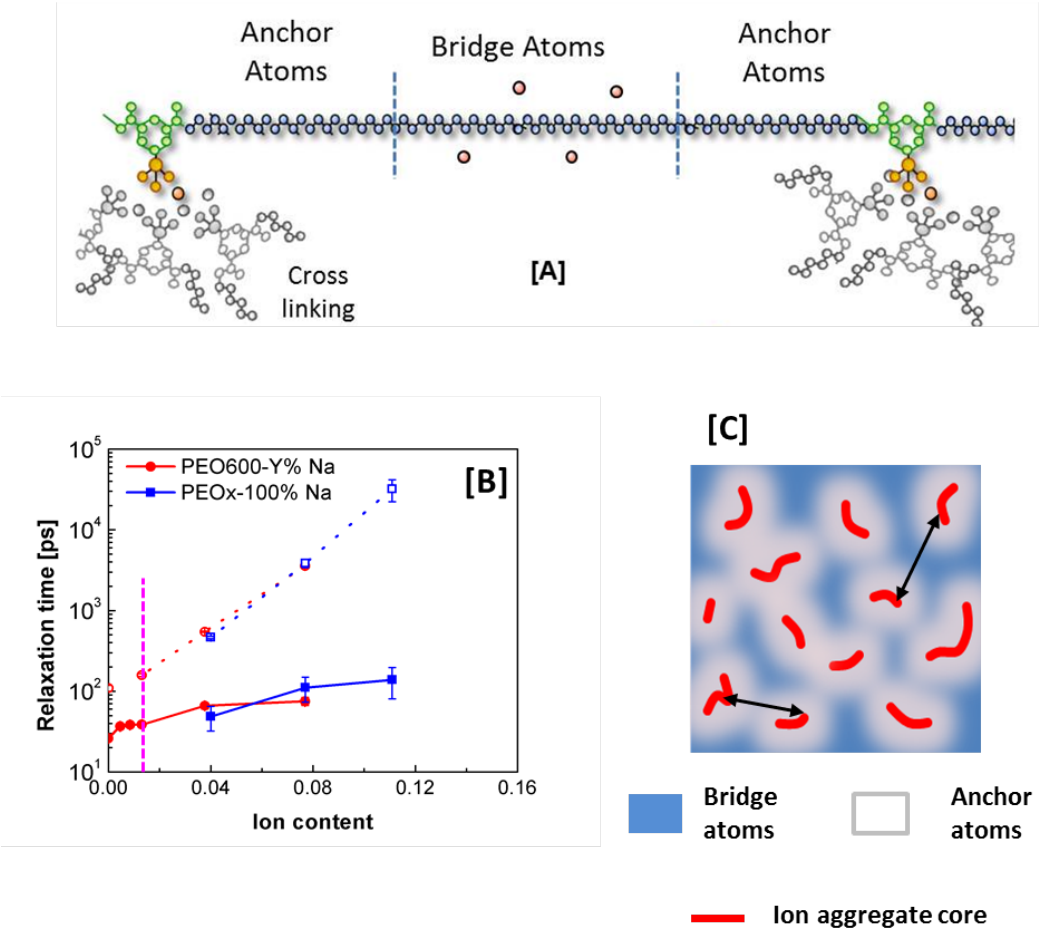

Figure 6.1. (A) Schematic illustrating the location of bridge and anchor atoms along the PEO spacer, (B) Relaxation times vs ion content for bridge (filled symbols connected by solid line) and anchor (open symbols connected by dashed line) for PEO600-Y%Na (red) and PEOx-100%Na (blue) [x = 400, 600, 1100]. The dotted line at ion content 0.01 represents the crossover ion content. (C) Spatial organization of bridge and anchor atoms (arrows denote the distance between aggregates as detected by SAXS[6,7])

MD simulation study of the effect of cation-anion binding energies in PEO600-100%Na observes a variety of cation coordination states[9] that affect the anchor atoms differently. Morphological features observed in SAXS[6,7] are dependent on the cation identity and affect the nature of interaction between cations and the polymer. In this chapter we identify the parameters that govern dynamics at different temperatures. The temperature dependence of conductivity[8,131] and anchor atom dynamics for PEOx-100%M throw light on how cation coordination with the anchor atoms plays a critical role in determining ion transport. We thereby

identify favorable conditions that can contribute to high ionic conductivity in single ion conductors. We conclude that while amorphous regions of high mobility are required from the ionomer for high conductivity, we need to focus on creating beneficial cation coordination states, which assist in charge transfer and/or ion transport. We finally propose a model system which has the potential to achieve high conductivity in single ion conductors by partially decoupling ion transport and polymer mobility.

Table 6.1. Properties of PEOx-100%M samples (where x = 400/600/1100, Y ∈ [0,100] and M = Li/Na/Cs)

Sample	Cation:EO ratio	Ion content	T_g (K)	Molecular Weight (g/mol)
PEO400-100%Li	1:09	0.111	285	3300
PEO400-100%Na	1:09	0.111	295	3300
PEO400-100%Cs	1:09	0.111	294	3300
PEO600-100%Li	1:13	0.077	258	4600
PEO600-100%Na	1:13	0.077	267	4600
PEO600-100%Cs	1:13	0.077	270	4600
PEO1100-100%Li	1:25	0.04	236	4500
PEO1100-100%Na	1:25	0.04	236	4500
PEO1100-100%Cs	1:25	0.04	238	4500

6.2 Effect of ion identity on ionomer dynamics

As seen in the previous chapters, for ion content values over 0.01, the bridge atoms are saturated and report similar relaxation times, whereas the anchor atoms have a strong dependence on ion content. In Figure 6.2 we report the relaxation times of the (a) bridge and (b) anchor atoms for PEO600-100%M where M = Li^+, Na^+, Cs^+. For the sake of brevity, we refer to these samples as 600-Li, 600-Na and 600-Cs respectively. As expected, the bridge atom relaxation times are similar in value, but the anchor atom relaxation times show deviation from expected behavior. Since the binding energies of the cations follow the order $Li^+ > Na^+ > Cs^+$, we expect the anchor atom dynamics for 600-Li to be the slowest, 600-Cs to be the fastest. Since the anchor atom dynamics directly affect T_g at this ion content, we

expect the T_g for 600-Li to be the highest, and 600-Cs to be the lowest. However, the glass transition temperatures follow the trend $T_{g,Li} < T_{g,Na} < T_{g,Cs}$. This is reflected in the anchor atom dynamics at 298 K and 323 K, where the anchor atom relaxation times (τ_{ANCHOR}) follow the order $\tau_{600-Li} < \tau_{600-Na} < \tau_{600-Cs}$. We further observe that the difference between τ_{ANCHOR} for 600-Na and 600-Cs reduces as the temperature increases, and at 348 K, 600-Cs has faster anchor atom dynamics than 600-Na.

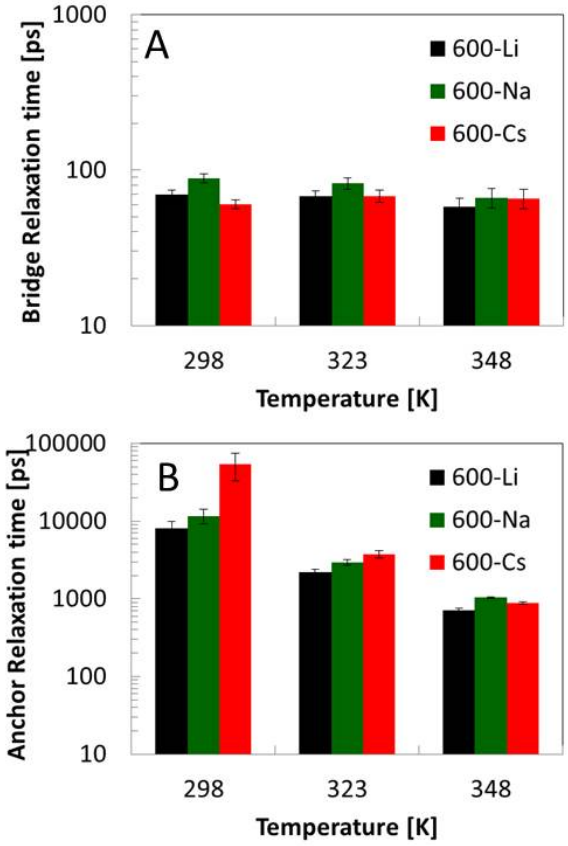

Figure 6.2. (A) Bridge atom relaxation times; (B) Anchor atom relaxation times; and (C) Anchor atom fractions for PEO600-100%M where M = Li (black), Na (green), Cs (red) for 298 K, 323 K and 348 K, Q = 1.55 Å^{-1}.

Since the ion content of all these samples is the same, we attribute the variation in behavior of τ_{ANCHOR} to the nature of interaction between the cation and anchor EO atoms. This interaction depends on the formation of ionic aggregates which is observed in several ionomers[52–56,59,132] and in the ionomers in this study.[6,7] The

high ion content of the anchor atoms in the PEOx-100%M ionomers makes it possible for SAXS to detect different ionic moieties, as shown in the previous chapter. SAXS measurements show the existence of different aggregates and ionic moieties which depend on ion identity as well as temperature.[6,7] SAXS data for 600-M (M = Li, Na, Cs) is shown in Figure 6.3.[7] The temperatures of SAXS measurement are at 298 K, 318 K and 353 K (in contrast to 298 K, 323 K and 348 K for QENS), but we do not expect significant effects due to the difference in measurement temperatures. There are two features observed in the SAXS measurements that can affect the anchor atom mobility - (i) a low Q "ionomer peak" between 0.2 and 0.3 $Å^{-1}$, and (ii) mid-Q features between 0.5 and 1.1 $Å^{-1}$. The ionomer peak corresponds to the spacing between ionic aggregates, which is uniform because of the monodisperse PEO spacers that separate ions along the polymer molecule. The mid-Q intensity corresponds to shorter distances between ionic moieties suggesting the presence of smaller aggregates like ion pairs, triple ions, quadrupoles etc., which we refer to as multiplets. As the temperature increases, the ions and polymer segments in multiplets undergo a rearrangement such that the anchor atoms surround an ionic core. This corresponds to a gradual reduction in mid-Q intensity and a rise in low-Q with increasing temperature. The aggregates are thermally stable at higher temperatures (measured up to 393 K).[6,7] The "amorphous halo" at high Q (1.5 $Å^{-1}$) corresponds to the interchain packing distance of PEO and is observed for all samples in this study.

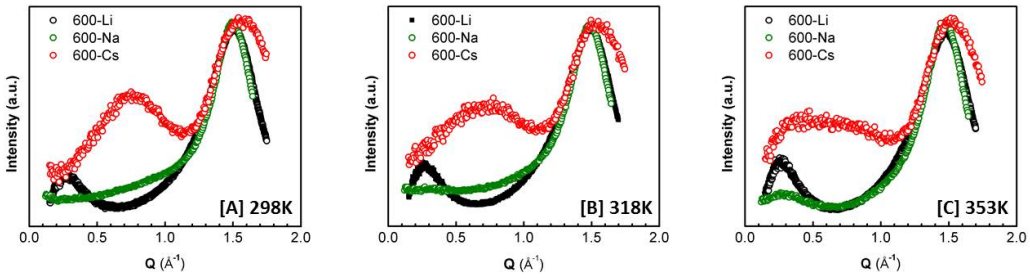

Figure 6.3. SAXS data for PEO600-100%M at 298 K, 318 K and 353 K, where M = Li (black), Na (green), Cs (red)[7]

The high intensity of the ionomer peak and lack of mid-Q features for 600-Li suggest the presence of large ionic aggregates that are microphase separated. A graphical depiction of the same is shown in Figure 6.4a where an ion core is

surrounded by anchor atom segments. Comparatively, 600-Na and 600-Cs have a distribution of coordination states (multiplets) which reports shorter ion-ion distances, as shown in Figure 6.4b. 600-Li has the fastest anchor atom dynamics despite having the largest aggregates. This suggests that aggregates affect the anchor atoms differently from multiplets. The multiplet formation in 600-Na and 600-Cs offer a greater surface area of ions interacting with the anchor atoms as compared to Li based samples, which are more microphase separated. Additionally, the partial charges on Li^+ ions are shared mostly by the SO_3^- groups and the periphery is formed by the anchor atoms, thereby resulting in reduced interaction between the Li^+ ions and anchor EO atoms. Therefore, for the same number of ions, the anchor atoms associated with aggregates are faster than those associated with multiplets. This results in 600-Li anchor atoms having the fastest dynamics, despite having the largest aggregates.

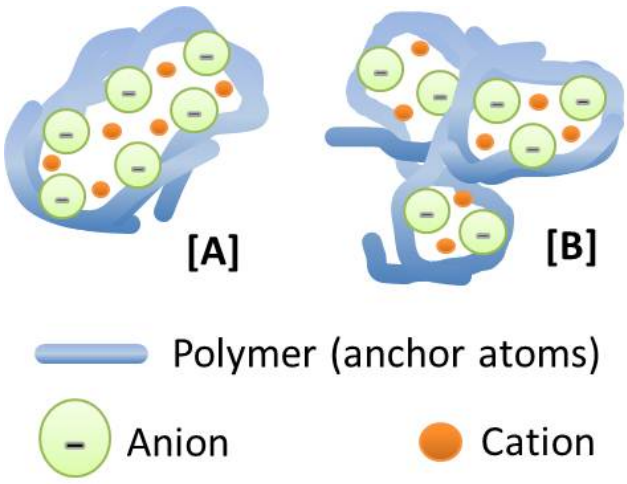

Figure 6.4. Cation coordination states that reduce anchor atom mobility (A) Large aggregate (B) Multiplets

We now address the anchor atom relaxation times for 600-Na and 600-Cs. 600-Cs has mostly ion pairs at 298 K and 318 K, but still has slower anchor atoms compared to 600-Na. The anchor atom relaxation for 600-Cs is 400% higher than that of 600-Na at 298 K, and is 50% higher at 323 K. This is surprising because we expect that pairs cannot slow the anchor atoms as much as multiplets do, because an ion pair does not crosslink one part of the chain to another. Furthermore,

the comparison shows that the difference between τ_{ANCHOR} of 600-Na and 600-Cs decreases when we increase the temperature. When the temperature approaches 348 K, the order is reversed and the anchor atoms of 600-Na are about 15% slower than those of 600-Cs. By comparing the anchor atom relaxation times at reduced temperature [T - T_g (see Figure 6.5), we see that the realxation times crossover at [T - T_g] $\sim$ 60°C (shown by the dashed line).

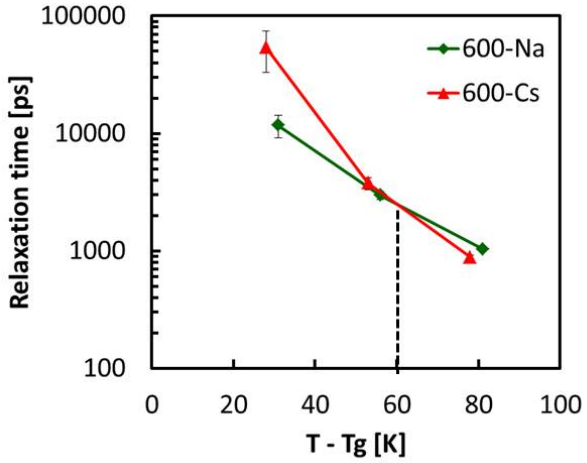

Figure 6.5. Anchor atom relaxation times vs. reduced temperature [T - T_g] for 600-Na and 600-Cs at Q = 1.55 $Å^{-1}$

To explain this behavior we identify two aspects that control the mobility of anchor atoms. The first aspect is the strength of coordination between the anchor EO atoms and the cation, which depends on the size of the cation; Cs^+ has a larger radius and weaker binding energy compared to Na^+. A larger cation also has a higher coordination number with the EO atoms (e.g. the cation coordination numbers of PEO for LiSCN, NaSCN, KSCN and CsSCN are 3, 4, 5 and 9, respectively[20]). The second aspect that controls the anchor atom dynamics is the temperature, which determines the segmental mobility (thermal energy) of the anchor atoms. Based on the observation in Figure 6.5, it is reasonable to assume that the dominating factor that govern anchor atom dynamics (coordination number vs. binding energy) is affected by the thermal energy of the polymer backbone, and is different on either side of the [T - T_g] = 60°C. We thereby propose a hypothesis - when [T - T_g] < 60°C, the thermal energy of the anchor atoms is low, and the dynamics are controlled by the *number* of EO atoms coordinating with the cation

(i.e. coordination number); when [T - T_g] > 60°C, the polymer has sufficient thermal energy to move and the dominating factor of the anchor atom dynamics is the cation-EO *binding energy*. For the remainder of this study, we refer to the reduced temperature [T - T_g] = 60°C as the ΔT_c (crossover temperature).

With regards to 600-M, it follows that at 298 K and 323 K (T - T_g < 60°C), 600-Cs has slower anchor atom dynamics than 600-Na due to the higher coordination number of Cs. At 348 K (T - T_g > 60°C), 600-Na has slower anchor atom dynamics than 600-Cs due to the higher binding energy of Na. Note that in the first case (T - T_g < ΔT_c), the reduction in anchor atom mobility is due to coordination of EO atoms with the cation in ion pairs, as opposed to being crosslinked by multiplets/aggregates in the second case (T - T_g < ΔT_c). Note that this hypothesis applies to systems where the cation-EO interaction is substantial. It does not apply to 600-Li because microphase separation of its aggregates at all temperatures of measurement results in little or no interaction between the cations and the anchor EO atoms.

In the above discussion, we studied the 600-M series which has a T_g range of 258 - 270 K. Since all our measurements have been made at 298 K, 323 K and 348 K, we now study samples with T_gs that are lower, and higher than the 600-M series. We start with samples with longer spacer length (PEO1100-100%M), which have T_gs (236 - 238 K) that are lower than PEO600-100%M (see Table 6.1). The low ion content of these samples results in a smaller number of aggregates/multiplets and a lower fraction of anchor atoms, which in turn lowers the T_g. As before, we refer to the samples as 1100-Li, 1100-Na and 1100-Cs for brevity. The bridge and anchor atom dynamics are for 1100-M are shown in Figure 6.6.

Since the ion content of all these samples is greater than 0.01, we expect the bridge atom relaxations to be similar, as shown in Figure 6.6a. Based on our previous observation that anchor atom relaxations determine T_g, we expect that the relaxation times of the anchor atoms should be similar. In contrast to 600-M, the anchor atom relaxation of 1100-Na is slower than 1100-Cs at all temperatures of measurement, as shown in Figure 6.6b. At 298 K, the value of [T - T_g] is ∼ 60 °C, which is very close to ΔT_c defined above. At this temperature, we observe that the anchor atom relaxation of 1100-Cs is only 5% faster than 1100-Na. The difference increases to 100 % at 348 K [T - T_g ∼ 110 °C]. Since Na^+ binds more strongly to the

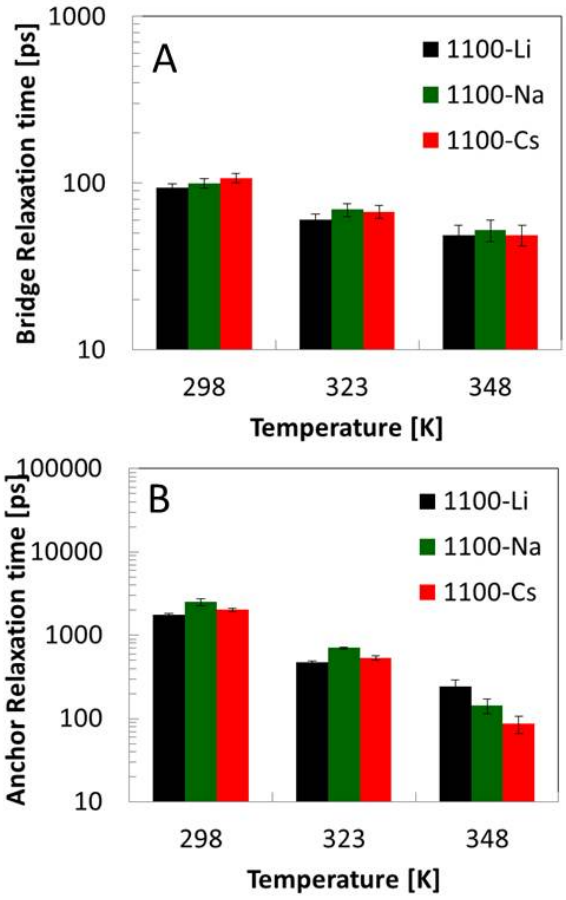

Figure 6.6. (A) Bridge atom relaxation times; (B) Anchor atom relaxation times for PEO1100-100%M where M = Li (black), Na (green), Cs (red) for 298 K, 323 K and 348 K, Q = 1.55 $Å^{-1}$.

anchor EO atoms than Cs^+, this observation supports our hypothesis that when [T - T_g] is greater than ΔT_c, the cation-EO binding energy dominates the anchor atom dynamics. This is summarized in a graph of 1100-M anchor atom relaxation time vs. reduced temperature (see Figure 6.7). The dotted line represents ΔT_c = 60°C.

We also observe that 1100-Li has the fastest anchor atom relaxation (compared to 1100-Na/1100-Cs) at 298 K and 323 K but the slowest at 348 K. This is in contrast to 600-Li, which is faster than 600-Na/600-Cs at all temperatures. This behavior suggests two things - firstly, the differences in extent of aggregation and microphase separation in 1100-Li compared to 1100-Na and 1100-Cs results

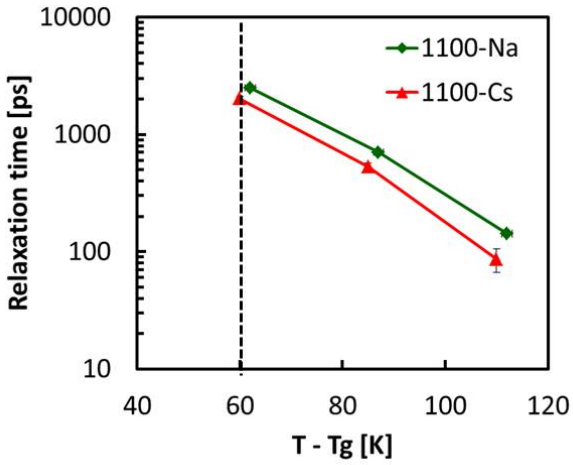

Figure 6.7. Anchor atom relaxation times vs. reduced temperature [T - T_g] for 1100-Na and 1100-Cs at Q = 1.55 $Å^{-1}$

in a different temperature dependence. Secondly, this effect is prominent in 1100-Li but not in 600-Li. The difference in temperature behavior between 1100-Li and 1100-Na/1100-Cs is attributed to the morphology of the three samples; SAXS measurements of PEO1100-100%M are shown in Figure 6.8. The strong ionomer peak for 1100-Li at all temperatures of measurement shows a high extent of microphase separation, as shown in Figure 6.4a. Comparatively, the weak ionomer peak for 1100-Na and the presence of mid-Q features for 1100-Cs suggests the existence of fuzzy boundaries between the ion cores and the polymer, as shown in Figure 6.4b. As discussed before, for microphase separated aggregates, there is less cation-EO interaction, and the anchor atoms have reduced mobility because of being crosslinked by the aggregates. Comparatively, for multiplets, there is a substantial cation-EO interaction in addition to the anchor atoms being crosslinked. This difference in interaction can potentially result in different temperature behavior for anchor atoms of 1100-Li compared to 1100-Na/1100-Cs.

This observation raises a question - why is different temperature behavior compared to the Na and Cs counterparts observed in 1100-Li but not 600-Li? The difference between 1100-Li and 600-Li requires an understanding of the effect of spacer length. The presence of aggregates is prominent in both the samples at all temperatures, but it is possible that the extent of microphase separation is higher for 1100-Li, which results in reduced interaction between the anchor EO atoms

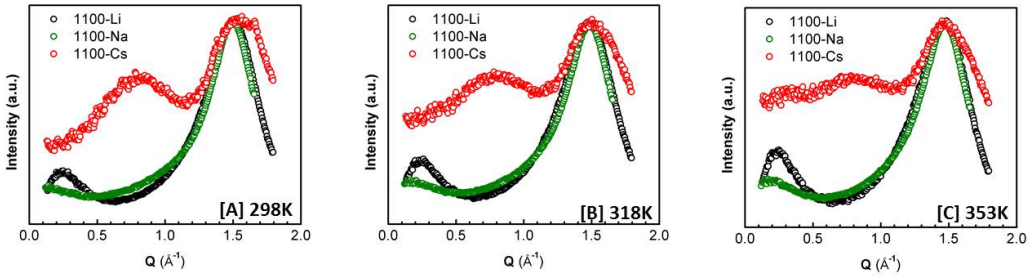

Figure 6.8. SAXS data for PEO1100-100%M at 298 K, 318 K and 353 K where M = Li (black), Na (green), Cs (red)[7]

and the cations. This possibility the question - does the extent of microphase separation increase when the spacer length increases? Microphase separated ionic aggregates in ionomers have been shown to be analogous to microphase separated block copolymers.[60] Studies have shown that longer segments in block copolymers with immiscible blocks tend to facilitate phase separation.[60–62] Long PEO molecules tend to crystallize readily, implying that a long spacer has a natural tendency to establish long range order as is seen with PEO3300-100%Na.[6] This idea is also supported by SAXS measurements on the 1100-Na sample (see Figure 6.8). In contrast to the 600-Na sample in Figure 6.3, 1100-Na has an ionomer peak at all three temperatures of measurement. 600-Na develops an ionomer peak only at 353 K, suggesting that the long spacer of 1100-Na allows microphase separation more easily than 600-Na. Similarly, at 353 K, 1100-Cs shows a clear difference between the mid-Q ion pair peak and the low Q ionomer peak. This implies that there is a coexistence of segregated ionic aggregates and ion pairs for 1100-Cs. In contrast, 600-Cs has a distribution of cation coordination states spanning both the mid-Q and low-Q regions, implying that the sample with a longer spacer allows easier segregation between ionic aggregates and the polymer. QENS measurements show that when compared to a long spacer, a short spacer is more restricted in mobility because a greater fraction of the spacer coordinates with cations in aggregates. This is shown in Figure 6.9 where the anchor atom relaxation time (τ_{ANCHOR}) and the anchor atom fraction (X_{ANCHOR}), both increase as we decrease the spacer length. A schematic showing this difference is illustrated in Figure 6.10. Most of the short spacer is forced to interact with the cations (see Figure 6.10a), whereas a long spacer has greater freedom to rearrange and allow the system to microphase

separate and creates a sharp boundary between the polymer and the cations (see Figure 6.10b). The anchor atoms in longer spacers are therefore faster than those in short spacers.

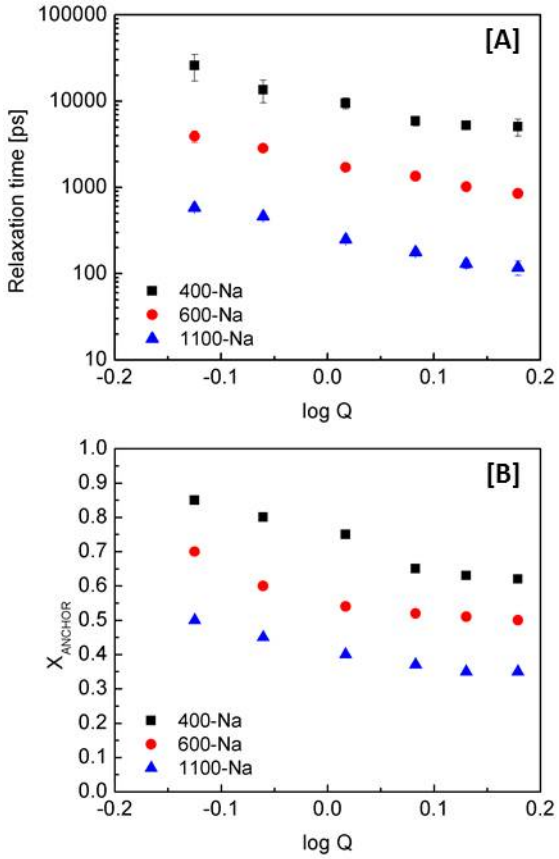

Figure 6.9. Q dependence of [A] relaxation times and [B] fraction of anchor atoms for PEOx-100%Na at T = 348 K, Q = 1.35 $Å^{-1}$.

We therefore recognize that a long spacer assists aggregate formation and microphase separation in our system. Yet, there is no clear explanation as to why at 348 K, the dynamics of 1100-Li are slower than 1100-Na/Cs. It is possible that at 348 K, the extent of microphase separation is so high that the anchor atom segments are expelled from the ion core and forced to lie on the periphery. One possible theory is that this results in local pockets of highly entangled PEO segments (anchor atoms) which have lower mobility.

We now investigate the dynamics of the PEO400-100%M samples, which have

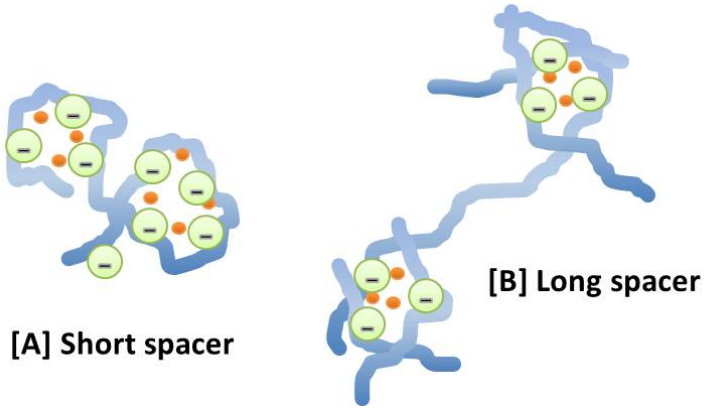

Figure 6.10. Polymer rearrangement and aggregate formation for [A] short spacer, and [B] long spacer

higher ion content and higher T_g than the PEO600-100%M samples (see Table 6.1). As before, we refer to the samples as 400-Li, 400-Na and 400-Cs. The bridge and anchor atom dynamics for 400-Na and 400-Cs are shown in Figure 6.11. We do not have QENS data for 400-Li. The bridge atom relaxations are almost the same (see Figure 6.11a), which is expected because the ion content is more than 0.01. Since the temperatures of measurement are close to T_gs (294 - 295 K) of the 400-M system ([T - T_g] $<$ 60°C), we expect that the sample with a higher cation coordination number (400-Cs) will have slower anchor atom dynamics. However, we do not see a significant difference in the anchor atom relaxations (see Figure 6.11b).

Due to the short length of the spacer, we expect that most of it coordinates with the cations. Correspondingly, the anchor atoms have high ion content (about 16 times higher than the bridge atoms at 348 K, as seen for PEO400-100%Na in Table 5.2). SAXS observes high intensity low-Q and mid-Q features corresponding to multiplets and aggregates, as shown in Figure 6.12. As is the case with 600-Li and 1100-Li, high extent of microphase separation is observed for 400-Li. At 353 K, there is a marked difference between 400-Cs and 400-Na. Note that Cs has more electrons than Na, which is why features in 400-Cs will be more pronounced than 400-Na. Regardless, the relative intensities of the mid-Q and low-Q features in 400-Cs is different from 400-Na. While the low-Q and mid-Q intensities are similar for 400-Na, the low-Q intensity for 400-Cs is much higher than its mid-Q intensity. This suggests that 400-Cs has high aggregate formation (as opposed to multiplets) compared to 400-Na. The reason for this behavior is not well understood, but

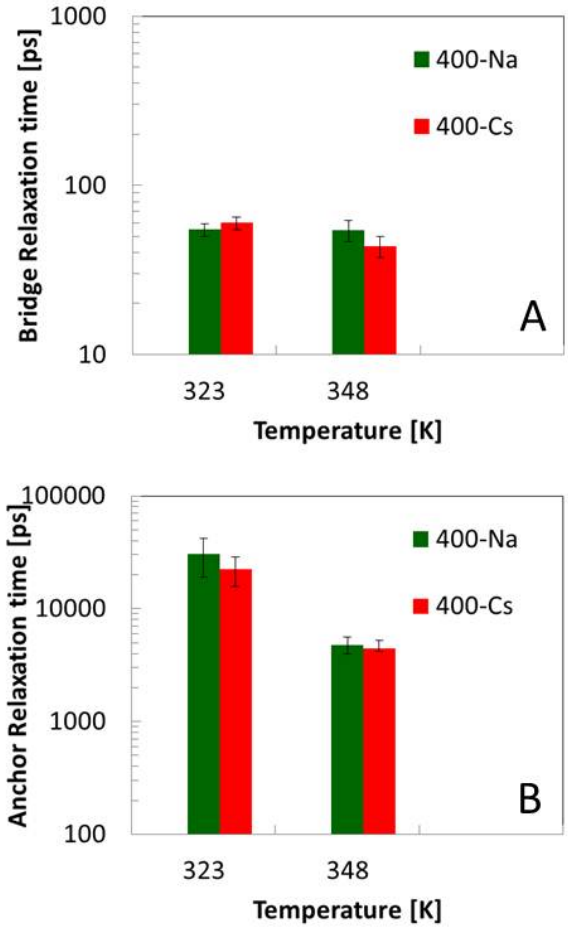

Figure 6.11. Relaxation times of (a) bridge and (b) anchor atoms for PEO400-100%M where M = Na, Cs at 323 K and 348 K, Q = 1.55 $Å^{-1}$.

it could arise from the large radius of Cs^+, combined with low mobility of the spacer (due to high T_g). Since the spacer is short, a 'loopback' of the spacer is possible that results in consecutive isophthalate groups being part of the same aggregate. This could lead to the formation of large ionic aggregates especially for large cations (like Cs), resulting in high intensity of the low-Q peak. Though the aggregates in 400-Cs (at 353 K) are large, we do not expect sharp boundaries between the ions and the anchor EO atoms due to the short spacer.

To summarize, we learned that when the reduced temperature [T - T_g] is less than 60°C (defined as the crossover reduced temperature ΔT_c), the cation coordination number dominates the anchor atom dynamics. When the reduced tempera-

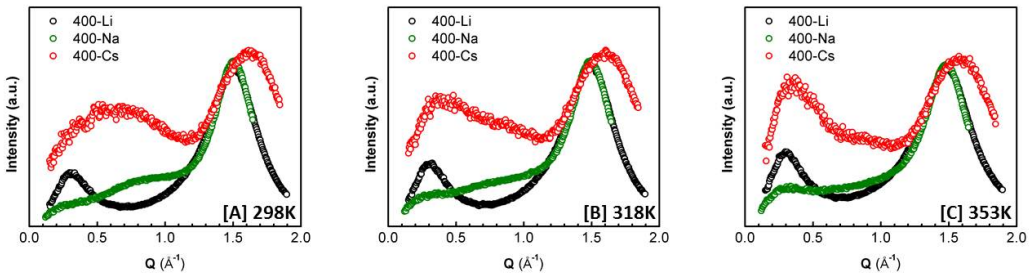

Figure 6.12. SAXS data for PEO400-100%Na at 298 K, 318 K and 353 K. Li (black), Na (green), Cs (red)[7]

ture is above ΔT_c, cation-EO binding energy dominates the anchor atom dynamics. It is interesting to observe that both these factors depend on the cation radius, but the factor that controls the dynamics depends on the temperature. We further compare a short spacer vs. a long spacer; the latter rearranges more easily to enable microphase separation compared to the former.

6.3 Ionomer dynamics and conductivity - Favorable scenarios

To identify the species with the best conductivity for a given relaxation time, we plot the conductivity of PEO600-Y%Na and PEOx-100%M against the anchor atom relaxation times in Figure 6.13. We choose the anchor atom relaxation because it determines the overall dynamics of the ionomer samples. We observe that for all temperatures, at a given relaxation time, the conductivity for the Cs series is the highest. This highlights the importance of weak binding energies (to the anion and EO atoms) that is required for high conductivity.

The temperature dependence of conductivity of PEOx-100%M systems is shown in Figure 6.14 for x = 400, 600 and 1100.[8] In each case, there is a crossover of conductivity curves that occurs between 298 K and 348 K. At high temperatures, the trend of conductivity follows the trend $\sigma_{Cs} > \sigma_{Na} > \sigma_{Li}$, which is expected based on the cation binding energies. At low temperatures, though insufficient for practical application, Li based samples have the highest conductivity. The exception is PEO1100-100%Li, which had crystallized.[8] If this sample had not

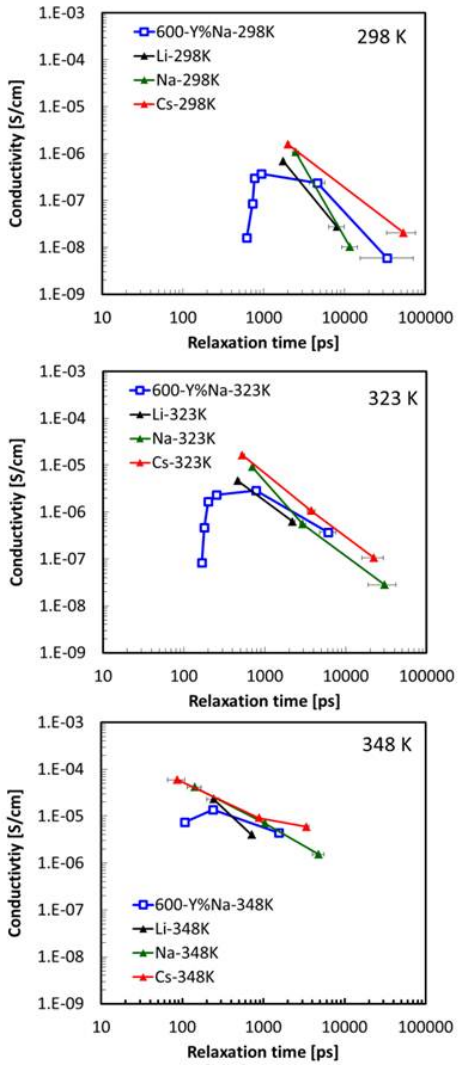

Figure 6.13. Conductivity[5,8] vs anchor atom relaxation time (Q = 1 Å^{-1}) for PEO600-Y%Na, PEOx-100%Li (black), PEOx-100%Na (green) and PEOx-100%Cs (red) where x = 400, 600, 1100 at (a) 298 K, (b) 323 K and (c) 348 K. The format Li-323K stands for PEOx-100%Na at 323 K.

crystallized, we expect that the conductivity curve would have been the highest at low temperatures. Note that the PEOx-100%Li systems show the formation of large aggregates even at low temperatures, as discussed earlier in this chapter. This suggests that the presence of certain ionic aggregates might assist in charge transfer, which Na and Cs based systems cannot offer. SAXS data can shed light on the shapes of these aggregates; however, we are unable to fit the data

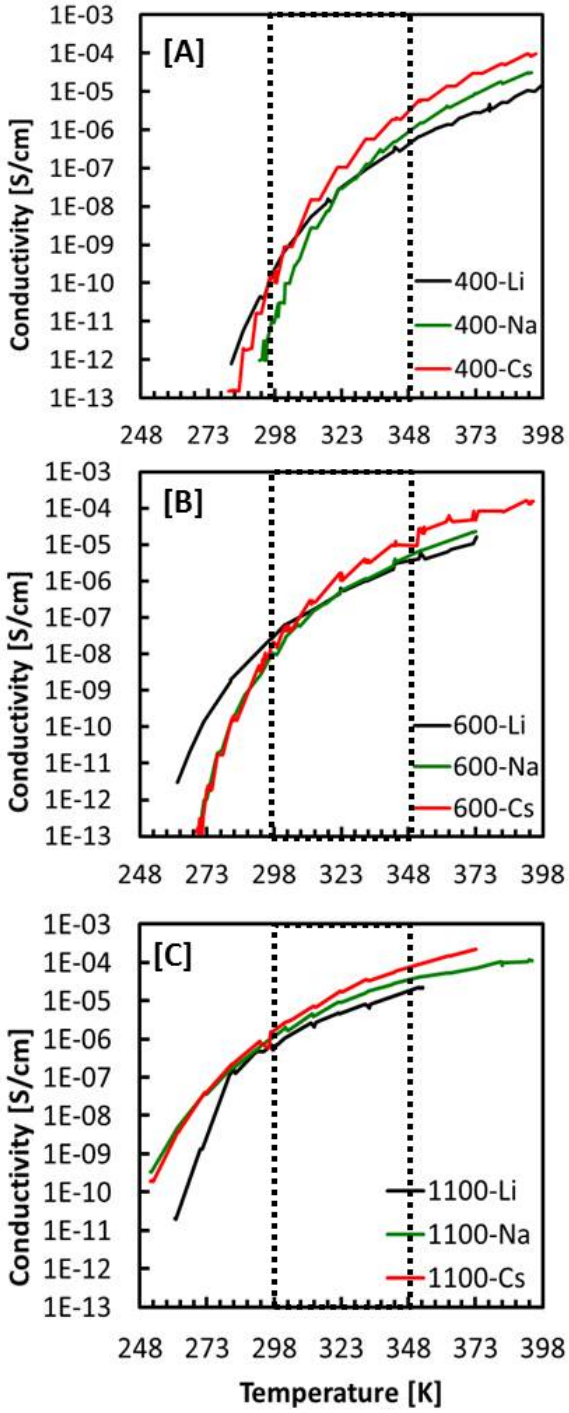

Figure 6.14. Temperature dependence of conductivity for (a) PEO400-100%M, (b) PEO600-100%M, and (c) PEO1100-100%M where M = Li, Na, Cs. The format 1100-Li stands for PEO1100-100%Li. The data points for these graphs were not available in the raw form; so they were extracted from a previous publication[8] using a graph-reading software.

to models which have spherical aggregates. MD simulations on PEO600-100%Na at 343 K reveal the existence of string like aggregates,[9] as shown in Figure 6.15. These structures allow charge transfer across the aggregate, thereby serving as a favorable cation coordination state. Here a cation attaches itself to one end of the chain, causing a cation from the other end to leave the aggregate, resulting in a net charge transfer (see arrows in Figure 6.15). This presents a decoupled mechanism, where the charge transport does not require the polymer mobility. This simulation also registered a higher conductivity than experimental values at 343 K, suggesting that the real PEO600-100%Na system may not contain as many string like aggregates as generated by the MD simulation. Therefore, with careful experimental manipulation, we may be able to achieve systems that have several of the string like aggregates. Note that though the actual transport of charge is decoupled from polymer motion, it is important to have high mobility in the peripheral anchor atoms that can allow cation motion from one aggregate to another.

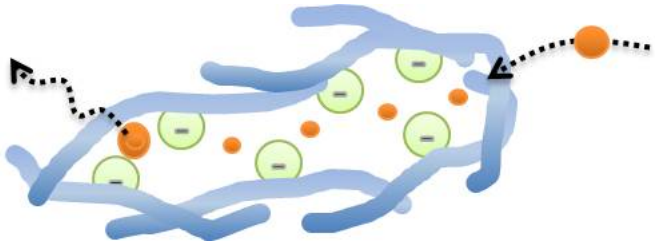

Figure 6.15. Chain like ionic aggregate that helps in charge transfer, based on MD simulations.[9] The larger cations (orange) represent the entering and exiting cations.

Using the ideas discussed in this chapter, we identify favorable scenarios for high conductivity in ionomers. We recognize that ion transport in solid polymer electrolytes is limited by the segmental mobility of host polymers. As discussed in Chapter 1, ionic conductivity is decoupled from polymer mobility in certain specific crystalline structures of PEO/Li-salt systems and have reported high values of conductivity.[73,80,87–93] Here, helical structures of PEO are surrounded by anions; the Li^+ cation uses these as pathways for conduction. However, these crystalline structures occur under very specific conditions and are cumbersome to maintain in practical situations. A recent study on conductivity and dynamics of PEO/$LiClO_4$ revealed that at temperatures above T_m of PEO, the amorphous host contained remnants of the helical crystalline structure that helped achieve high conductivity.[2]

This implies that the presence of certain local structures can serve to be useful in boosting conductivity. *We therefore need to make a departure from solely relying on segmental relaxation, and focus on favorable cation coordination states which can assist in improving conductivity.*

In this study we have identified the following requirements for high conductivity - (a) the presence of cation coordination states (such as string like aggregates) that are favorable for conductivity, (b) the presence of a low binding cation, which allows easy dissociation, and (c) a highly mobile polymer backbone. Consider a system that is populated enough with string like aggregates, where we can create a percolated network of aggregates. A weakly binding cation combined with such conducting pathways can potentially give rise to high conductivity. With regards to the ionomers in this study, we can conceivably create percolated string like aggregates by using short spacer lengths and large cations (such as Cs) (e.g. 400-Cs shows high aggregation in SAXS measurements). Proton conduction in NAFION occurs through such percolated networks.[104–107] This mechanism of conductivity decouples ion transport and polymer mobility because the ion motion/charge transport takes place through the percolating channels of ion aggregates, and not with the help of segmental motion of the polymer host. To create such a percolated network with a short spacer, the ion content increases significantly, thereby reducing T_g. This can serve to be a disadvantage for building flexible electrolytes at room temperature.

We should therefore try to achieve a healthy ratio of cation coordination states that increase conductivity and amorphous regions that allow cation transport from one coordination state to another. This poses an important question - what should the concentration of string like aggregates be in the system that allows both, a low T_g, and high number of favorable cation coordination states? To answer this question, we utilize the idea we should have control over the number, shape etc. of string like aggregates in the system. As shown in Figure 6.16 string like shape of aggregates can be achieved by using a number of comonomer anion "containers" adjacent to each other. This potentially allows a partial decoupling of ion transport and cation mobility, wherein charge transfer takes place through the string like aggregate (decoupled), and the cation motion from one aggregate to another depends on the polymer mobility (coupled). It is important to lower the

binding energy of the cation to the anion. This can be done by choosing a large cation which can also move faster in the amorphous regions through fast exchange between sites. Alkali metal ions (e.g. Cs^+) are preferred over organic cations (e.g. tetraalkyl ammonium) because the surface charge density of the latter is not fully delocalized. The binding energy can also be reduced by altering the anion group. By choosing a long spacer, we can maintain high mobility of the peripheral anchor atoms and lower the T_g of the ionomer. Since long spacers run the risk of getting crystallized at low temperatures (like PEO1100-100%Li), introducing random irregularities (like $-CH_2O-$ instead of $-CH_2CH_2O-$) in the spacer can prevent this from happening. One big advantage of this design over those investigated in this work (PEOx-Y%M) is that the spacer length and ions per spacer can be changed independently. This means that we can compare systems of different spacer lengths but the same ion content, and not worry about unsulfonated isophthalate groups (which reduce mobility). This sample can potentially answer several questions about the practical feasibility of ionomers with such string like aggregates. In the next chapter (section 7.5), we discuss some of these aspects as the future direction that can be taken by this study.

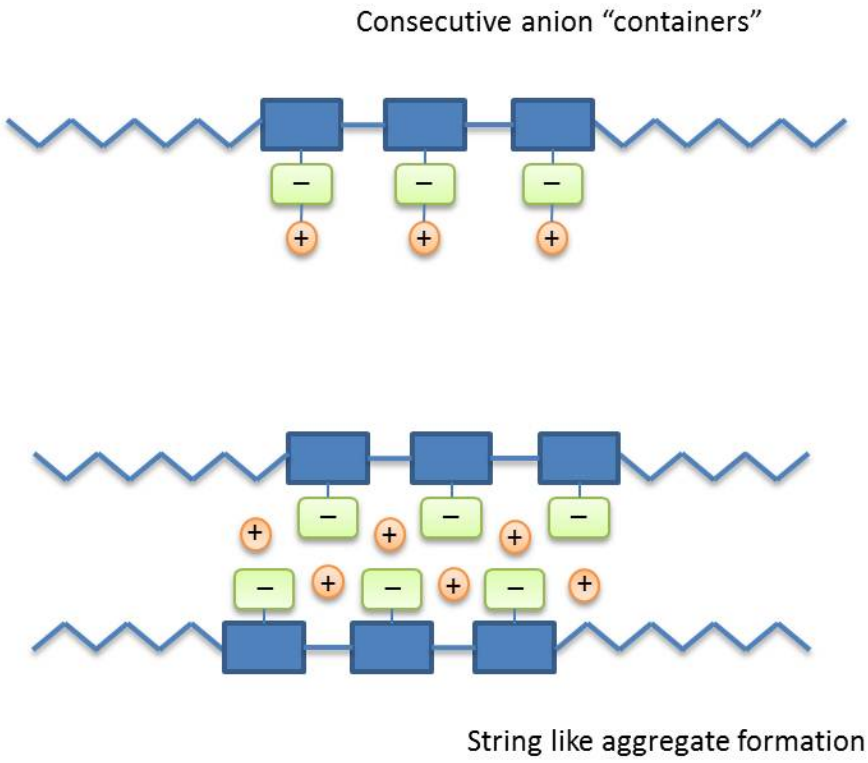

Figure 6.16. Proposed ionomer design featuring adjacent anion “containers” to favor string like aggregate formation

Chapter 7

Summary and Future Direction

In this study, we investigate the dynamics of the polymer backbone in PEO based single ion conductors. The anion in single ion conductors is chemically bonded to the polymer backbone so that only the cation is the conducting element. The samples we study have a sulfonate (SO_3^-) anion covalently bonded to a PEO backbone (of fixed length) through an isophthalate comonomer unit as shown in Figure 7.1. We use the nomenclature PEOx-Y%M (e.g. PEO600-50%Na). We vary three features in this sample - (1) the degree of sulfonation (Y%), which is the percentage of sulfonated isophthalate groups in the entire molecule; (2) the spacer length x, which is the MW weight of the spacer (400/600/1100 g/mol) corresponding to the number of repeat units N (9/13/25); and (3) the identity of the cation M (Li/Na/Cs).

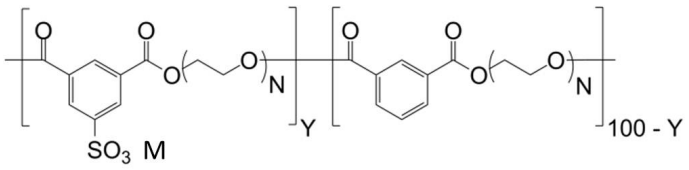

Figure 7.1. Chemical structure of PEOx-Y%Na

Ion conduction in amorphous polymers is strongly coupled to the segmental mobility of the polymer. The cation is solvated by ether oxygen (EO) atoms in the PEO matrix by weak electrostatic coordination. The cation migrates by hopping to these EO rich sites, and the hopping is facilitated by the segmental motion of the polymer. In this study we investigate the backbone dynamics of the ionomer using

quasi-elastic neutron scattering (QENS), which allows us to isolate the hydrogen atom motion. We first identify the impact of the isophthalate group, and then understand the effect of adding ions to the system. We define the ion content of these samples by the molar ratio of cations to ether oxygen (EO) atoms. We study the effect of ions on the dynamics by changing the ion content in two ways - by varying the degree of sulfonation, and by changing the spacer length. We further compare the dynamics of the ionomers with PEO/$LiClO_4$ samples[2] and identify the differences in ion-polymer interaction between them. We also change the ion identity to understand the interplay between cation binding energies and polymer dynamics. The properties of the samples studied in this dissertation are listed in Table 7.1.

We conduct QENS experiments on the Disk Chopper Spectrometer and High Flux Backscattering Spectrometer (NIST) and on the Backscattering Spectrometer (ORNL). Data obtained in the energy domain is inverse Fourier transformed to the time domain to give the self intermediate scattering function, S(Q,t) (see Figure 7.2), which is a function of Q (representative of the spatial scale). A higher the deviation of S(Q,t) from 1 represents a more mobile polymer. The data is fit to combinations of the KWW equation

$$S(Q,t) = exp\left[-\left(\frac{t}{\tau(Q)}\right)^{\beta(Q)}\right] \tag{7.1}$$

which gives us the characteristic relaxation time (τ) of the constituent relaxation processes. The details of the data treatment for the three instruments is discussed in Chapter 3.

7.1 Identifying component dynamics in ionomers

We first identify the impact of the isophthalate group on the backbone dynamics without the presence of ions, by comparing PEO600-0% to pure PEO. We observe that while pure PEO has only one segmental relaxation, the ionomer has two fractions undergoing two different segmental relaxations. We identify that the isophthalate group in the non-ionic polymer introduces the slower segmental relaxation. This is based on similar behavior that is seen in block-copolymers where

Table 7.1. Properties of PEOx-Y%M samples (where x = 400/600/1100, Y ∈ [0,100] and M = Li/Na/Cs) and PEO/$LiClO_4$

Sample	Cation:EO ratio	Ion content	T_g (K)	Molecular Weight (g/mol)
PEO600-0%Na	0	0	229	5800
PEO600-6%Na	1:217	0.005	230	5800
PEO600-11%Na	1:118	0.008	232	5800
PEO600-17%Na	1:76	0.013	233	8700
PEO600-49%Na	1:26	0.038	245	4700
PEO600-100%Na	1:13	0.077	267	6300
PEO400-100%Li	1:09	0.111	285	3300
PEO600-100%Li	1:13	0.077	258	4600
PEO1100-100%Li	1:25	0.04	236	4500
PEO400-100%Na	1:09	0.111	295	3300
PEO600-100%Na	1:13	0.077	267	4600
PEO1100-100%Na	1:25	0.04	236	4500
PEO400-100%Cs	1:09	0.111	294	3300
PEO600-100%Cs	1:13	0.077	270	4600
PEO1100-100%Cs	1:25	0.04	238	4500
PEO/$LiClO_4$	1:30	0.033	251	500000
PEO/$LiClO_4$	1:14	0.071	257	500000
PEO/$LiClO_4$	1:10	0.01	246	500000
PEO/$LiClO_4$	1:8	0.125	256	500000
PEO/$LiClO_4$	1:4	0.25	264	500000

the polymer block with higher T_g (slower block) reduces the mobility of the neighboring atoms of the faster block, as shown in Figure 7.3a. We thereby identify the physical location of the slow fraction as the atoms neighboring the isophthalate group. We refer to these atoms as *anchor atoms*, and the fast fraction as *bridge atoms*.

We then study the dynamics in the presence of ions by increasing the degree of sulfonation (Y%) in PEO600-Y%Na. We choose Na^+ as the cation because SAXS measurements on the samples shows that the Na-based samples do not undergo microphase separation of ion rich phases. As seen with PEO/Li-salt systems,

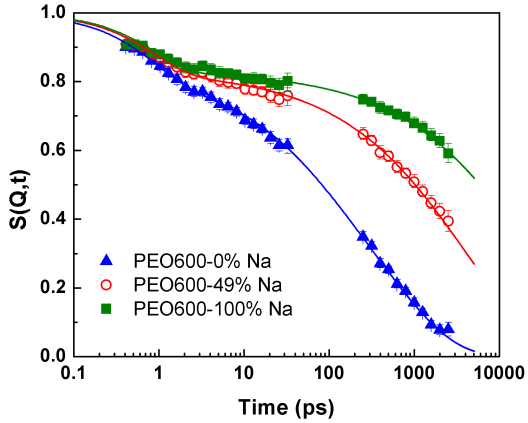

Figure 7.2. DCS data, shifted HFBS data and the corresponding fitting lines for PEO400-100%Na, PEO600-100%Na, and PEO1100-100%Na at T = 298 K, Q = 1.04 $Å^{-1}$

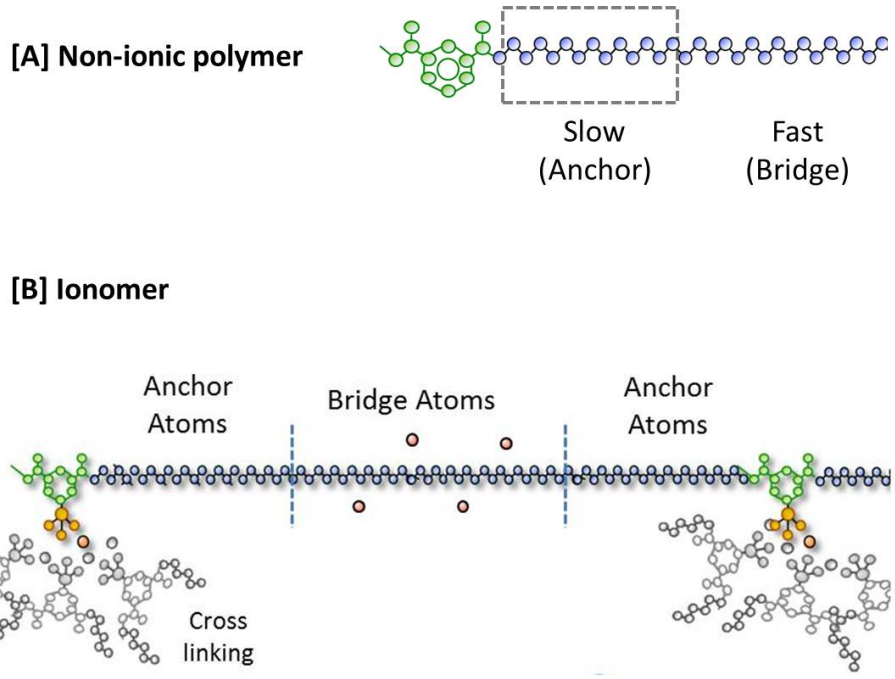

Figure 7.3. [A] Location of the slow fraction of atoms (anchor atoms) for the non-ionic polymer; [B] Bridge and anchor atoms in the presence of ions

ionomer samples with greater ion content are less mobile than those with low ion content. No new processes arise on the addition of ions, but we observed that the presence of ions affects the two fractions differently. The bridge atoms appear to saturate at the ion content of 0.01, whereas the relaxation times of anchor atoms increase drastically as the ion content increases (see Figure 7.4). The glass transition temperature (T_g) of samples follows the trend of anchor atom relaxation times, as shown by the triangles in Figure 7.4a.

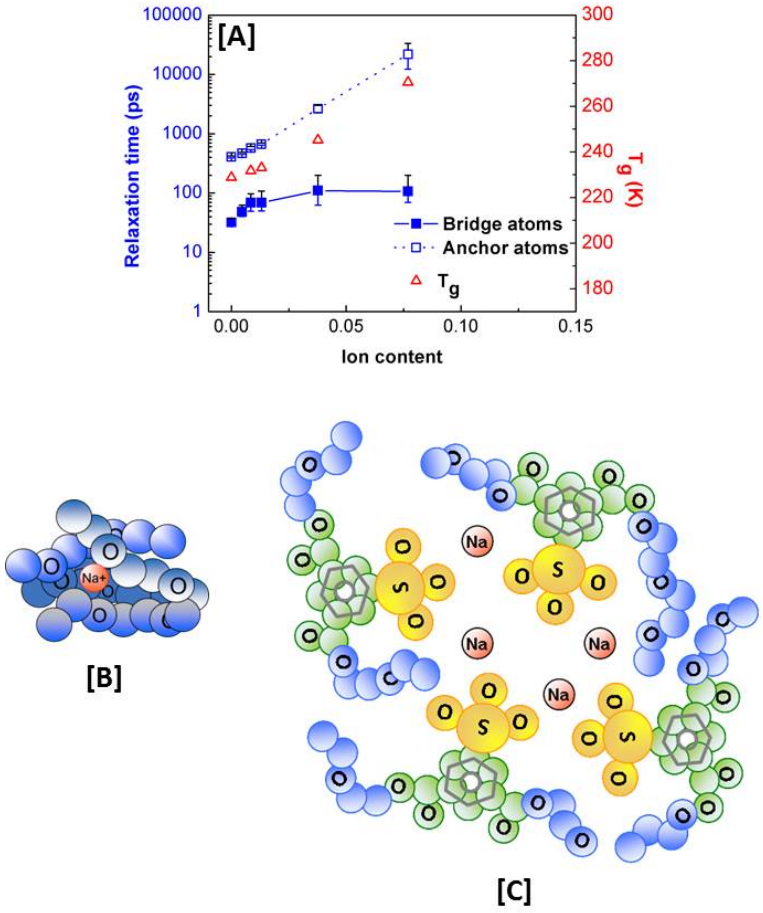

Figure 7.4. [A] Relaxation times of bridge and anchor atoms for PEO600-Y%Na T = 298 K, Q = 1.35 $Å^{-1}$ and T_g vs ion content; [B] Single cation coordinating with bridge atoms; [C] Group of cations and anions crosslinking anchor atoms

Bridge atoms are slowed by the coordination of single (or free) cations with the ether oxygen atoms, as shown in Figure 7.4b, as seen in PEO/Li-salt systems. Comparatively, the Q dependence of relaxation times of the slower process

is very different from that of PEO/$LiClO_4$, which observes rotational motion of helical crystalline remnants. Since the PEO600-Y%Na samples do not crystallize, we cannot expect the origin of the slower relaxation to be the same. However, interaction between two aions and a cation can form physical crosslinks via ionic clusters (See Figure 7.4c). We know that these clusters are not well-defined, large or of consistent size because ionic aggregation is not evident in the SAXS data for PEO600-100%Na below 353 K. However, it is reasonable to assume that small, polydisperse clusters with weak boundaries are present, which greatly reduce the anchor atom mobility because the anion is chemically bonded to the polymer backbone. On comparing the conductivities of PEO600-Y%Na with PEO/$LiClO_4$ in the same ion content range, we observe that the maximum conductivity of PEO600-Y%Na occurs at lower ion content than PEO/$LiClO_4$. This is attributed to the fact that clustering of ions in PEO/Li-salt systems do not involve the polymer, whereas in ionomers, the clustering automatically reduces the polymer mobility because the anion is bonded to the polymer backbone. The details of these findings are discussed in Chapter 4.

7.2 Dynamic patterning of bridge and anchor regions

We then study the effects of changing ion content by varying the spacer length (x = 400/600/1100) at 100% sulfonation, in contrast to our previous study where we changed the ion content by varying the degree of sulfonation. We observe that changing the ion content in either way does not change the overall trends of anchor and bridge relaxation times with ion content, as shown in Figure 7.5a. We identify a crossover ion content (0.01), above which the T_g is no longer controlled by the bridge relaxation, but by the anchor relaxation. Above the crossover ion content, the bridge relaxation times are almost constant, whereas the anchor atom relaxation times increase drastically. The slope of relaxation times vs. ion content for anchor atom relaxation above 0.01 is the same as that for the bridge atom relaxation below 0.01, as shown by the solid line in Figure 7.5b.

When we compare two samples with similar ion content (PEO600-49%Na and

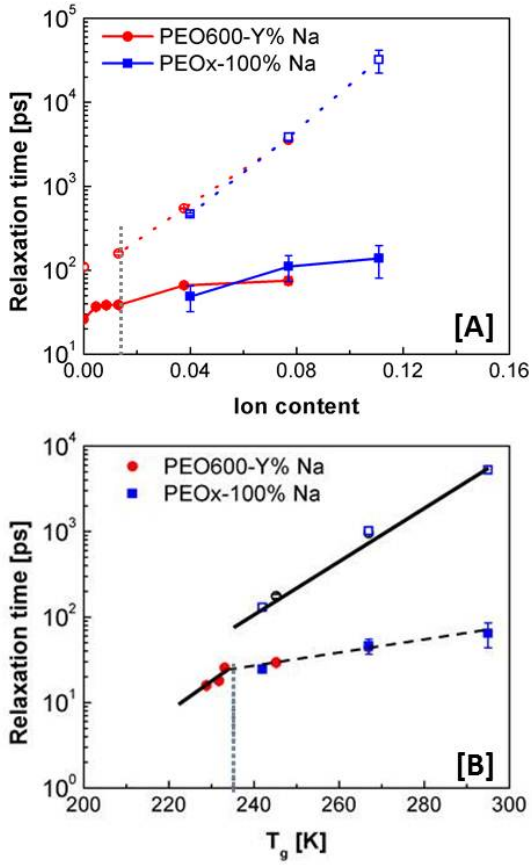

Figure 7.5. Bridge and anchor atom relaxation times vs (A) ion content; and (B) T_g for PEO600-Y%Na and PEOx-100%Na. The dotted line denotes the crossover ion content of (0.01). Relaxation times and X_{BRIDGE} have been reported at Q = 1.35 $Å^{-1}$ and T = 323 K.

PEO1100-100%Na), the fully sulfonated sample has faster dynamics than the partially sulfonated sample. PEO1100-100%Na also has higher conductivity, but the difference in dynamics are not sufficient to explain an order of magnitude difference in the conductivity. MD simulations show the existence of certain string like aggregates that assist in charge transfer, suggesting that that the unsulfonated isophthalate groups prevent the formation such favorable cation coordination states. We conclude that for higher conductivity, it is better to have a completely sulfonated ionomer rather than a partially sulfonated one.

Using the fractions of bridge and anchor atoms obtained from QENS, and the observation that bridge atoms saturate at an ion content ∼0.01, we can evaluate

the ion contents of the two fractions. This is as summarized in Table 7.2. Based on these calculations and our knowledge of two different relaxations, we propose that the anchor and bridge atoms are spatially segregated. Such a situation would be visible using small angle scattering, if the difference in cation:EO ratio provides sufficient contrast. We thus examine SAXS data for PEOx-100%Na samples, using this as a guide to propose the spatial segregation of bridge and anchor atoms.

Table 7.2. Distribution of cations in anchor atom region at T = 348 K (calculated values are approximate). Sample x-Na stands for PEOx-100%Na; X_{Br} stands for X_{BRIDGE}

Sample	Spacer repeat units	X_{Br}	Number of bridge | anchor atoms per spacer	Cation:EO ratio		Ratio of cations in anchor:bridge
				Bridge	Anchor	
400-Na	9	0.36	3 | 6	1:100	1:6	16
600-Na	13	0.5	6.5 | 6.5	1:100	1:7	14
1100-Na	25	0.65	9 | 9	1:100	1:10	10

The dynamic patterning for PEOx-100%Na is shown in Figure 7.6 for 348 K. The distance between ion cores (red) correspond to SAXS measurements of the inter-aggregate distance (black arrows), which increases with spacer length (shown by shifting of ionomer peak to lower Q values). The relative fraction of anchor atom (white) to bridge atoms (blue) corresponds to QENS calculations. The details of the QENS calculations, SAXS measurements, along with a comprehensive depiction of the spatial arrangement for all temperatures of measurement are in Chapter 5.

7.3 Effect of ion identity

The final part of this work (Chapter 6) is to understand the effect of cation identity on the backbone dynamics of PEOx-100%M where we vary both, the spacer length x (400/600/1100) and M (Li/Na/Cs). We discuss the interplay of polymer dynamics with conductivity, binding energy, cation radius and the corresponding morphology. Large cations have low binding energies because of which they interact weakly with anions and EO atoms, resulting in faster polymer dynamics. Since the ionic size of the cations in this study follow the order Li < Na < Cs, we expect Li based samples to have the slowest dynamics, and Cs based samples to

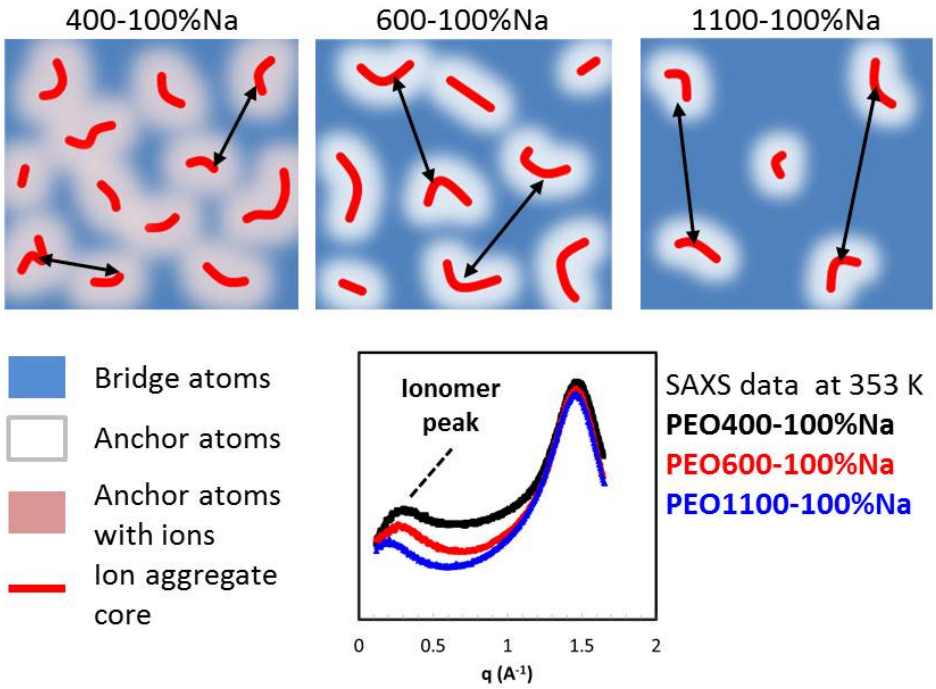

Figure 7.6. Spatial arrangement of bridge and anchor regions in PEOx-100%Na (x = 400/600/1100) at 348 K; and SAXS data at 353 K[6]

have the fastest dynamics. However, the strong interdependence of dynamics and morphology shows deviations from this expected trend. In general, since the ion content values of these samples is greater than 0.01, the bridge atom relaxation times for these samples are similar, as expected. However, differences are observed in the anchor atom relaxation times.

We begin our investigation with PEO600-100%M samples, where we observe that Li based samples have the fastest anchor atom dynamics at all temperatures. This is despite the fact that Li has the strongest binding energy and SAXS observes the highest extent of aggregation in PEO600-100%Li compared to the Na and Cs couterparts. We attribute this reason to the nature of aggregate formation, as detected by SAXS measurements. The high aggregate formation of PEO600-100%Li corresponds to a sharp boundary between the ion-rich core and peripheral anchor atoms; the corresponding fast anchor atom dynamics suggest that the cations in large aggregates interact less with the EO atoms and more with the anions, as shown in Figure 7.7a. Comparatively, smaller aggregates (called multiplets) of Na and Cs based samples have more interaction between the cation and EO atoms, as

depicted in Figure 7.7b. This difference in structures results in PEO600-100%Li having faster dynamics.

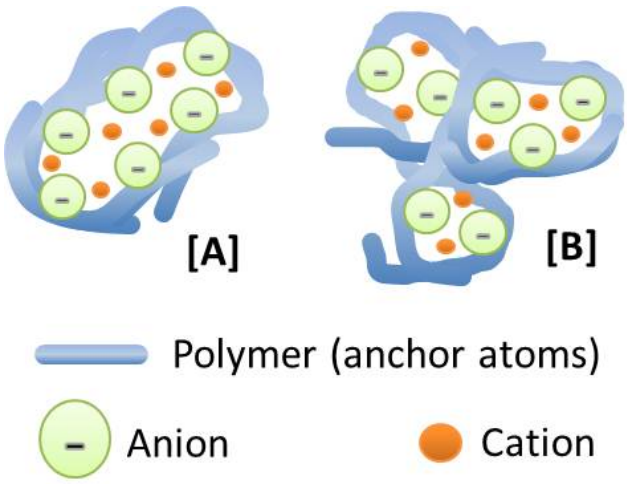

Figure 7.7. Cation coordination states that reduce anchor atom mobility (A) Large aggregate (B) Multiplets

We further observe that PEO600-100%Na has faster anchor atom dynamics than PEO600-100%Cs at 298 K and 323 K, though the former has a distribution of multiplets and the latter has mostly ion pairs (according to SAXS measurements). This is surprising because ion pairs do not crosslink the polymer chain and are not expected to reduce the mobility drastically. The difference between relaxation times is the largest at 298 K and gradually diminishes till they reverse at 348 K. To explain this behavior we propose a hypothesis that defines the factors determining anchor atom dynamics based on the proximity to T_g: when the reduced temperature [T - T_g] is less than 60 °C, the cation coordination number is the dominating factor affecting anchor atom dynamics. When the reduced temperature exceeds 60 °C, the anchor atom dynamics depend on the binding energy of the cation. With regards to the PEO600-100%M samples, when [T - T_g] < 60 °C a larger cation (like Cs^+) which interacts with a greater number of EO atoms will reduce the polymer mobility more than a smaller cation (like Na^+). When [T - T_g] > 60 °C, the cation with higher binding energy (Na^+) will reduce the polymer mobility more than a cation with lower binding energy (Cs^+). We verify this hypothesis with PEO1100-100%M (low T_g) and PEO400-100%M (high T_g).

For PEO1100-100%M samples, the temperature dependence of relaxation times for the Li based sample is different from Cs and Na. This is not seen for PEO600-100%M, which has a shorter spacer. Based on several observations in literature, we infer the possibility that the long spacer allows for a greater extent of microphase separation compared to short spacers, thereby reducing the cation-EO interaction in the former case (see Figure 7.8).

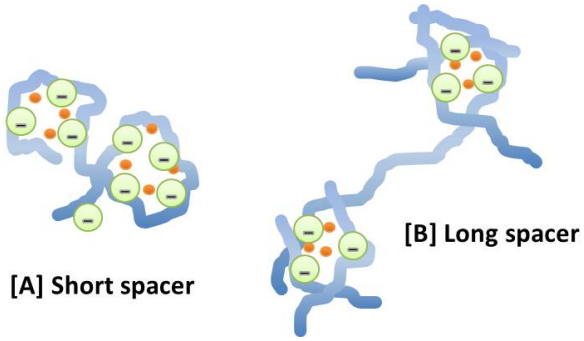

Figure 7.8. Polymer rearrangement and aggregate formation for [A] short spacer, and [B] long spacer

7.4 Favorable conditions for conductivity

We compare the conductivity vs. anchor atom relaxation times for all samples in this study as shown in Figure 7.9a and observe that Cs based samples have the highest conductivity for a given relaxation time. This highlights the importance of having a weakly binding cation for high conduction. At low temperatures, Li based samples have higher conductivity than Na and Cs based samples, as shown in the conductivity vs. temperature plot shown in Figure 7.9b. The Li based samples show aggregation even at lower temperatures, suggesting that some of the aggregates might be serving as favorable cation coordination states for ion/charge transport. MD simulations on PEO600-100%Na at 343 K report the existence of string like aggregates (see Figure 7.10) which assist in charge transfer. The conductivity obtained from MD simulation is also higher than that measured experimentally; it is possible that the number of these helpful local structures are not present in high number in reality. With careful experimental manipulation we can design samples which allow the formation of string like aggregates.

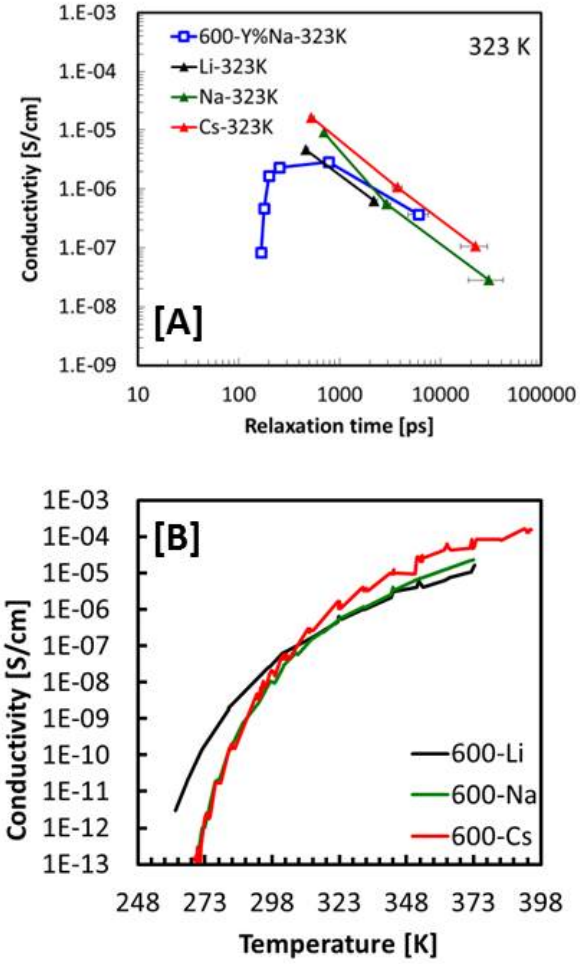

Figure 7.9. [A] Conductivity vs. anchor atom relaxation times (Q = 1.35 $Å^{-1}$) for PEO600-Y%Na (blue), PEOx-100%Li (black), PEOx-100%Na (green) and PEOx-100%Cs (red) at 323 K; [B] Conductivty vs. temperature for PEO600-100%M where M = Li, Na, Cs. The dotted line represents temperatures from 298 K to 348 K.

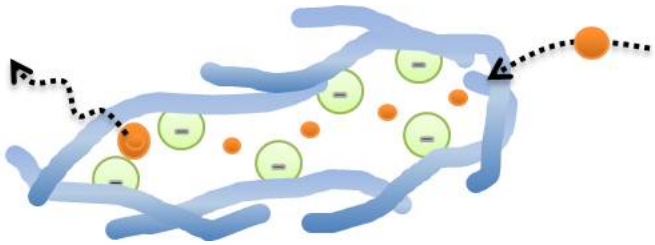

Figure 7.10. String like aggregates that help in charge transfer

One such proposed design is shown in Figure 7.11. Based on our identification of three features that assist in conduction in ionomers - a low binding energy cation which dissociates easily from the anion or EO atoms, the presence of favored coordination states that allows easy charge transport to take place, a highly mobile polymer host that allows cation migration from one coordination state to another. The consecutive anion "containers" allow for string like aggregates to form, which can allow charge migration from one end to the other. A low binding energy cation can facilitate this. Additionally, the structure is such that the cations are forced to interact more with the anions, thereby resulting in a highly mobile periphery of anchor atoms that have low T_g, and allow cation hopping from one site to another. Long spacers between the anion groups assists in microphase separation (and therefore higher polymer mobility) but run the risk of getting crystallized. This can be prevented by introducing random "errors" in the PEO backbone (like a methoxy group). This sample allows us to partially decouple ion transport and polymer dynamics. By using a healthy ratio of string like aggregates and amorphous polymer, we can potentially achieve high conductivity.

7.5 Recommendations for future direction

One of the shortcomings of this study was that we made QENS measurements at only three temperatures. This was not sufficient to draw concrete conclusions about the temperature behavior of bridge and anchor relaxation times. In the future, I recommend that QENS experiments made on such ionomers should include a larger range of temperatures. If need be, instruments with better resolution and energy windows from around the world should be included in our studies.

The variation of dynamics and conductivity with chain length has not been studied for the PEOx-Y%M systems. The chain length, as well as the number of ions per chain can potentially play a role in determining the extent of entanglement, aggregation, and the corresponding conductivity of single ion conductors. The critical molecular weight for entanglement in PEO is about 4000; the MWs used for our systems range between 3000-6000 (see Table 7.1). The presence of ionic aggregates greatly impacts the entanglement of the spacer units, and by varying the ionomer MW to values that are higher and lower than 4000, we can study the

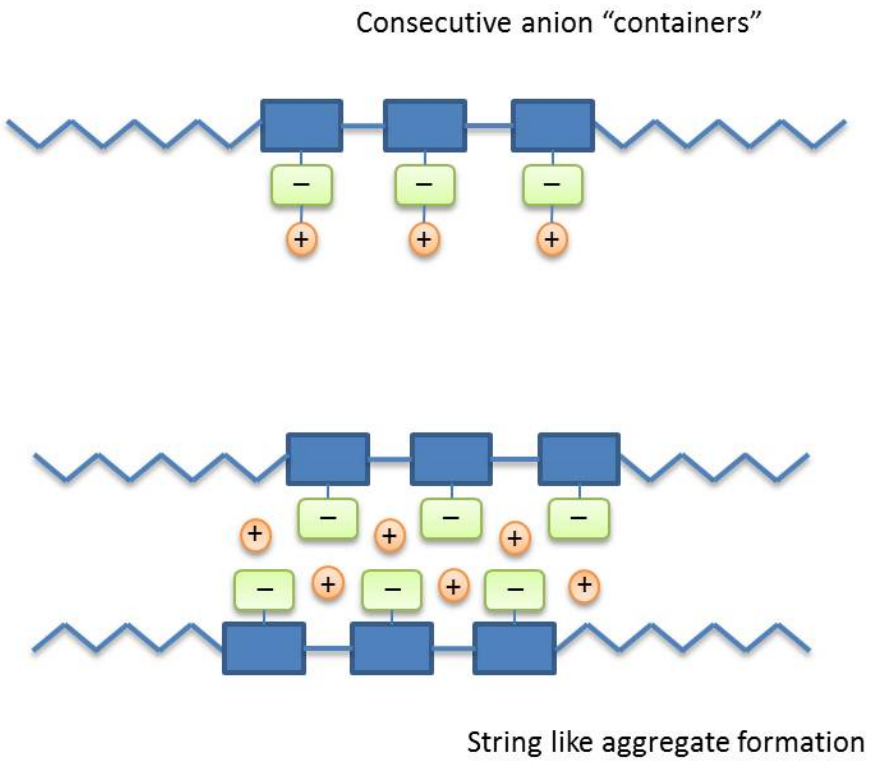

Figure 7.11. Proposed ionomer design featuring adjacent anion "containers" to favor formation of string like aggregates

differences in dynamics and conductivity.

It will be of immense scientific interest to study how the PEO based ionomers compare with PEO/benzenesulfonate-M salts (M = Li, Na, Cs). MD simulations on the latter show the formation of aggregates.[101] It will be immensely useful to complement these observations with QENS measurements of these PEO/salt systems, and study the measurements as a function of temperature, MW of PEO, cation, anion etc.

The room temperature conductivity in single ion conductors (and polymers in general) cannot reach practical values if we rely on segmental dynamics alone. While the alternative is to have systems with decoupled conductivity mechanism, they have their own set of disadvantages pertaining to preparation and maintenance of structure. The dependence of conductivity on reduced temperature (defined as T/T_g)is shown in Figure 7.12 for coupled and decoupled systems of conductivity. The two dashed lines correspond to conduction mechanisms that

are coupled and decoupled with polymer mobility (approximately, based on prior studies.[10–14]) Sample design should aim to achieve conductivity that lies in between the two dashed lines, corresponding to partial decoupling. MD simulations of PEO600-100%Na show higher conductivity than experimentally measured values, which lie on the conductivity curve of coupled mechanisms. We suspect that the MD simulations have a higher number of string like aggregates, which result in higher conductivity due to the partially decoupled mode of conduction. Several questions arise with regards to the role played by string like aggregates, which pave the path for future studies on these single ion conductors. As discussed in Chapter 6, a high number of such aggregates can potentially create a percolated network; however, this kind of system can have high T_g which prevents it from being flexible. If we were to build a system with a non-percolating network (partially decoupled), there arises an important question. While string like aggregates can be useful for conductivity, is there a limit on the number we can have for high conductivity? Additionally, how does the number, shape etc. of such aggregates depend on the total chain length of the ionomer? This will help us answer the question if it is better to have one long chain or several short ones. We can further evaluate the optimized number of string like aggregates which allow high conductivity while the ionomer has low T_g. By manipulating the sample design in Figure 7.11, we can not only achieve partial decoupling of ion transport and polymer mobility, but we can also answer several of the questions discussed above. For example, the number of anion containers adjacent to each other determines the length of the string like aggregate. By varying the length of the spacer units, we can control both, the number of aggregates as well as the T_g. Another big advantage of this sample over those investigated in this work (PEOx-Y%M) is that the spacer length and ions per spacer can be changed independently. This means that we can compare systems of different spacer lengths but the same ion content. We can also investigate the effect of the chain MW on the number of aggregates being formed and the corresponding polymer dynamics and conductivity.

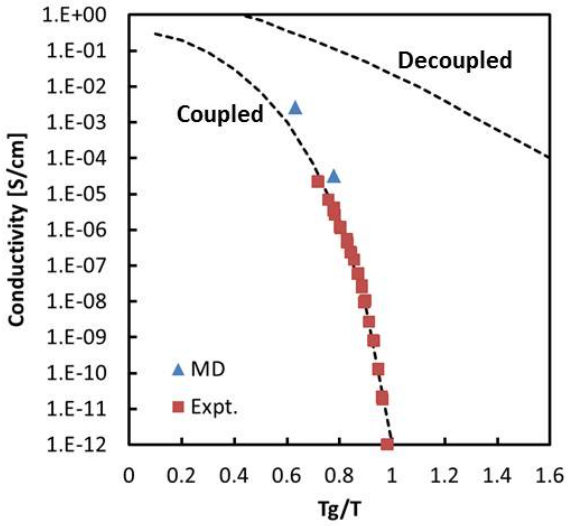

Figure 7.12. Conductivity vs. T_g/T curves[10–14] (approximate) showing limits for conductivity mechanisms that are coupled and decoupled with polymer mobility. The data points correspond to conductivity values of PEO600-100%Na obtained experimentally[5] (red) and via MD simulation[9] (blue).

Appendix A

Inverse Fourier Transformation

A.1 General algorithm for Inverse Fourier Transformation (IFT)

The basic concept of the Inverse Fourier transformation is to transform the intensity in energy/frequency domain $I(Q,\omega)$ to the self-intermediate scattering function $S(Q,t)$. For the sake of brevity, we will refer to these variables as $I(\omega)$ and $S(t)$. The generic IFT equation for transforming a function $X(\omega)$ to $X(t)$ is given by

$$X(t) = \frac{1}{2\pi}\int_{-\pi}^{\pi} X(\omega)\ e^{i\omega t}\ \mathrm{d}\omega \tag{A.1}$$

In the case of QENS data, we first evaluate

$$\begin{aligned} I(t) &= \frac{1}{2\pi}\int I(\omega)\ e^{i\omega t}\ \mathrm{d}\omega \\ &= \frac{1}{2\pi}\int I(\omega)\left[\cos\omega t + i\sin\omega t\right]\mathrm{d}\omega \end{aligned} \tag{A.2}$$

Converting the integral to a summation over all frequencies ω,

$$I(t) = \frac{1}{2\pi}\sum_{n=0}^{N-1}\ \left[I(\omega_n)\left[\cos\omega_n t + i\sin\omega_n t\right]\left[\omega_{n+1}-\omega_n\right]\right] \tag{A.3}$$

The magnitude of the above expression for $I(t)$ is

$$I(t) = \frac{1}{2\pi}\left[\left(\sum_{n=0}^{N-1}\left[I(\omega_n).\cos\omega_n t.\,(\omega_{n+1}-\omega_n)\right]\right)^2 + \left(\sum_{n=0}^{N-1}\left[I(\omega_n).\sin\omega_n t.\,(\omega_{n+1}-\omega_n)\right]\right)^2\right]^{\frac{1}{2}} \tag{A.4}$$

We normalize this equation by dividing by the value of $I(t)$ at $t = 0$.

$$I^{norm}(t) = \frac{I(t)}{I(0)} \tag{A.5}$$

We perform the above calculations for sample (I_S) data as well as resolution (I_R) data, and define the self-intermediate scattering function $S(t)$ as

$$\begin{aligned} S(t) &= \frac{I_S^{norm}(t)}{I_R^{norm}(t)} \\ &= \frac{[I_S(t)/I_S(0)]}{[I_R(t)/I_R(0)]} \end{aligned} \tag{A.6}$$

The $I(\omega)$ from the instrument has error for both, sample and resolution data. This error gets propagated through the IFT algorithm. Since the error bar calculation is not trivial, we adopt a bootstrap algorithm to evaluate the error. We generate 500 datasets of $I(\omega)$ within the error bar for each data point. For each of the data sets, we generate $I^{norm}(t)$ using Eq (A.5) for both, sample and resolution. By comparing the data sets, we obtain $I^{norm}_{S,max}(t)$, $I^{norm}_{S,min}(t)$, $I^{norm}_{R,max}(t)$, $I^{norm}_{R,min}(t)$. The maximum value of $S(t)$ is given by

$$S_{max}(t) = \frac{I^{norm}_{S,max}(t)}{I^{norm}_{R,min}(t)} \tag{A.7}$$

whereas, the minimum value of $S(t)$ is given by

$$S_{min}(t) = \frac{I^{norm}_{S,min}(t)}{I^{norm}_{R,max}(t)} \tag{A.8}$$

Finally, we report $S(t)$ with a (+,-) error bar given by $([S_{max}(t) - S(t)], [S(t) - S_{min}(t)])$

A.2 Updated DCS energy window

Prior to 2008, we have used FORTRAN code written by Victoria Garcia Sakai (Vicky) to perform inverse Fourier transformation of DCS and HFBS frequency domain data. Over time, changes were made to the DCS instrument which altered the behavior of the instrument slightly. Some of these changes propagated into the data, and because of the way Vicky's code is written, it was not handled appropriately. In Figure A.1, we see the S(Q,t) outputs from the inverse Fourier transformation codes for PEO600-100%Na at 298 K from February 2008 and December 2009, if Vicky's code was used for both. Clearly, there is a difference in

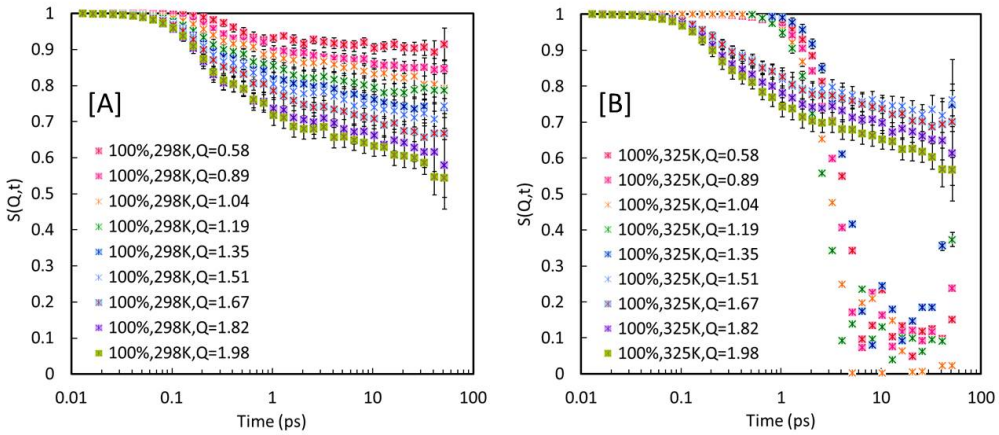

Figure A.1. $S(Q,t)$ for PEO600-100%Na at 298 K, inverse Fourier transformed using Vicky's code. (A) Sample measured in 2008 (using resolution from February 2008) and (B) sample measured in 2009 (using resolution from December 2009)

the data treatment which is causing this issue. Numerous tests in the time domain do not reveal the origin of this problem. So we consider the data in the energy domain, and compare two files of the same sample (PEO600-100%Na): one from 2008 and the other from 2009 for a low Q value, where the issue was more severe. We realized that the error in the energy window corresponding to this Q was higher in 2009 compared to 2008, as shown by the shaded region in Figure A.2

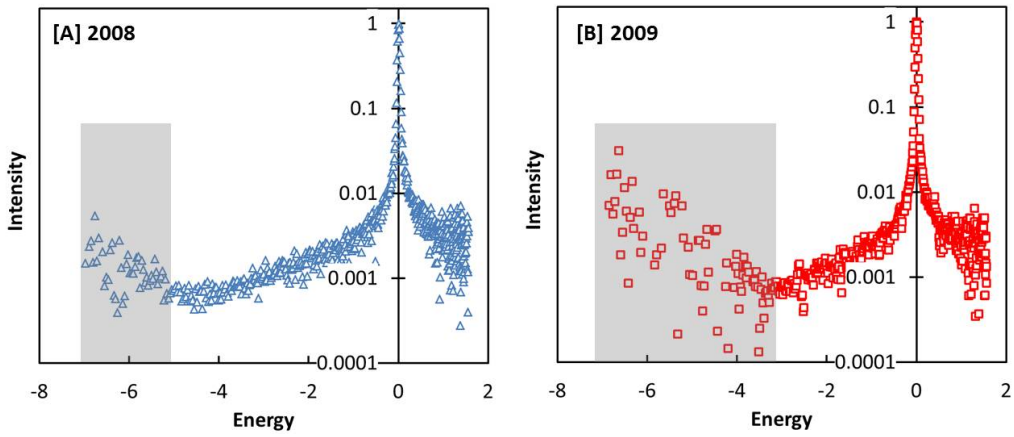

Figure A.2. I vs. E data for PEO600-100%Na, T = 348 K, Q = 0.89 Å^{-1} from (A) 2008 and (B) 2009

This shows that the quality of data in the energy window (from 2008 to 2009) has degraded. To get a better idea of this change, we compare the percentage error in intensity for different Q values for data from 2008 and 2009. We perform this comparison for vanadium resolution to remove any effects of the sample, as shown in Figure A.3. Here we see that the error in the shaded region in the 2009 data is significantly higher than that for 2008. This chance in instrumental error contributes to an erroneous intensity in the calculation of the area under the curve required for inverse Fourier transformation. We therefore update Vicky's code to neglect the data points corresponding to the erroneous intensity. Vicky's code is designed to reject data points up to the number obtained from the kinematically allowed region (see Figure 2.6). The updated code removes the erroneous data points as well, and is summarized in Table A.1. Prior to 2008, we used the data set corresponding to Q = 0.57 Å^{-1}; however, after this analysis, we believe it should not be included as a good data set any more (in post-2008 analyses). Similar calculations are made for the higher Q values, which have excessive error on the energy loss side.

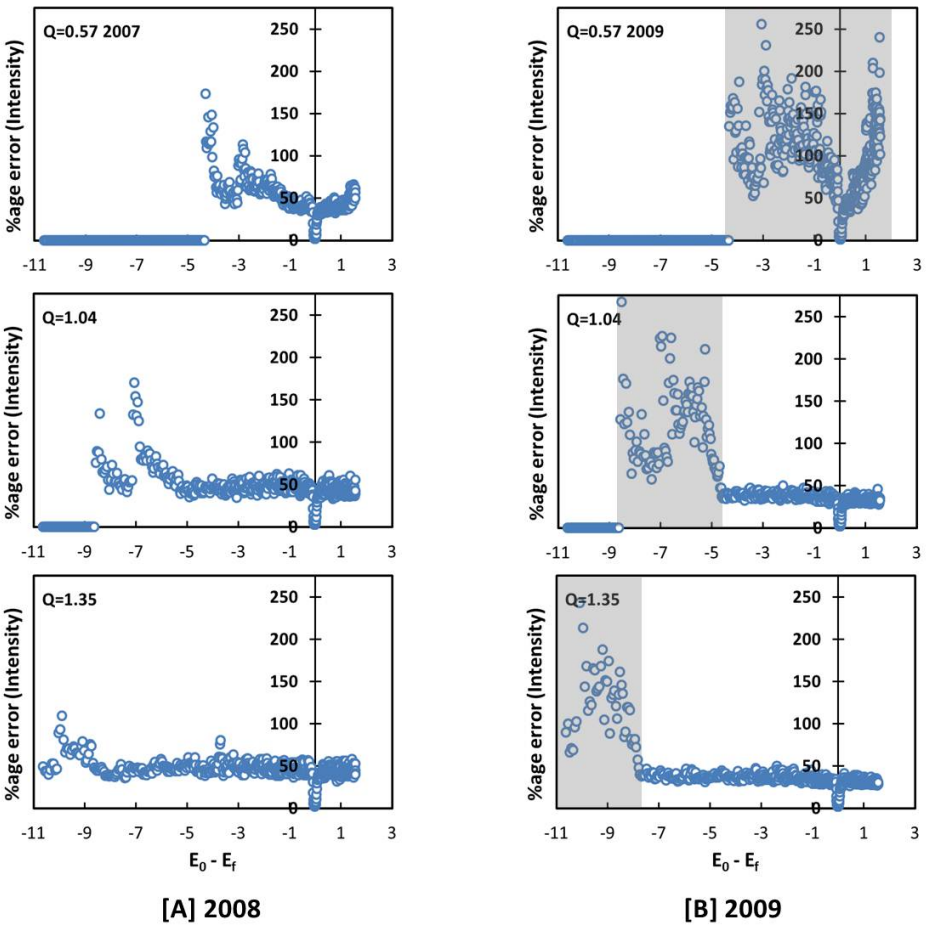

Figure A.3. Comparison of percentage error in intensity vs energy for the vanadium resolution data (Q = 0.57, 1.04 and 1.35 $Å^{-1}$) for (A) 2008 and (B) 2009.

Table A.1. Updated number of data points to consider for each Q value in DCS. The theoretical and current values of ΔE_{min} are obtained from the kinematically allowed region (see Figure 2.6). The total number of energy values for each Q is 678. DNU stands for "Do Not Use"

	Value of ΔE_{min} (meV)			Exclude up to		Exclude after	
Q	Theoretical	2008	2009	2008	2009	2008	2009
0.16	DNU	DNU	DNU	DNU	DNU	DNU	DNU
0.29	DNU	DNU	DNU	DNU	DNU	DNU	DNU
0.42	DNU	DNU	DNU	DNU	DNU	DNU	DNU
0.57	-3.7	-3.56	DNU	168	DNU	-	DNU
0.75	-4.9	-4.7	-2	125	244	-	-
0.89	-6.3	-6.2	-3.3	83	178	-	-
1.04	-7.7	-7.7	-4.7	49	127	-	-
1.2	-9.38	-9.38	-6.2	19	84	-	-
1.35	-10.66	-10.66	-7.8	0	49	-	-
1.51	-10.66	-10.66	-9.5	0	18	-	-
1.67	-10.66	-10.66	-10.66	0	0	-	-
1.82	-10.66	-10.66	-10.66	0	0	-	-
1.98	-10.66	-10.66	-10.66	0	0	678	622
2.13	-10.66	-10.66	-10.66	0	0	DNU	474
2.28	-10.66	-10.66	-10.66	0	0	DNU	438
2.38	-10.66	-10.66	-10.66	0	0	DNU	432

A.3 FORTRAN Code for IFT - BASIS

Unlike the DCS and HFBS inverse Fourier transform codes (programmed by Vicky), the BASIS code has been written with a single subroutine that performs the data transformation. The subroutine is then called multiple times for sample, resolution and error bar calculations.

```
PROGRAM basis
IMPLICIT NONE
!-----------------
!1. MUST CHECK THE FOLLOWING VALUES BEFORE REDUCTION
!2. MUST MATCH THEM IN THE SUBROUTINE AS WELL
integer, parameter :: DATAPTS=550 !Number of datapoints per Q group
integer, parameter :: FTM=41 !Number of fourier transform times
integer, parameter :: IT=500 !Number of iterations for error calculation
integer, parameter :: DET=10 !Number of detectors
!-----------------
character*256 filein, vanfile, fileout
character*256 filenormvan, filenormsample
character*256 iftinter, viftinter, iftforerror, viftforerror
real*8 q(DET), tm(FTM), Sqtr(DET,FTM), Sqte(IT,DET,FTM)
real*8 vSqtr(DET,FTM), vSqte(IT,DET,FTM)
real*8 Sqtnorm(IT,DET,FTM), vSqtnorm(IT,DET,FTM)
real*8 Sqtmax(DET,FTM), vSqtmax(DET,FTM)
real*8 Sqtmin(DET,FTM), vSqtmin(DET,FTM)
real*8 Sqt(DET,FTM), plus(DET,FTM), minus(DET,FTM), time(FTM)
integer d,ft,i,iter

filein="ReducedData_10Q/ROIgt500/Samples/PEG400-50Na323K"
vanfile="ReducedData_10Q/ROIgt500/Vanadium.yNTI.txt"
fileout="IFTfiles_10Q/ROIgt500/PEG400-50Na323K.xls"

!Ignore these unless you know what you are doing
filenormsample="ignore.txt"
filenormvan="ignore.txt"

!Intermediate files that help with error calculation
iftinter="tempfiles/iftintermediate.txt"
viftinter="tempfiles/viftintermediate.txt"
```

```
    iftforerror="tempfiles/iftiter.txt"
    viftforerror="tempfiles/viftiter.txt"

    !Q values
    do d=1,DET
           q(d)=0.2+(1.8/DET)*(2*d-1)/2
    end do

    !Perform sample IFT
    print*, 'Working on sample data...'
    call doift(filein, iftinter, filenormsample, 0)
    open(21,FILE=iftinter)
    do d=1,DET
           read(21,*)
           do ft=1,FTM
                  read(21,*) tm(ft), Sqtr(d,ft)
           end do
           read(21,*)
    end do
    close(21)

!Perform sample error calculation
    !Use an error flag (0 or 1) to notify the subroutine whether this
    !is part of the main IFT or for evaluating error bars. The difference
    !is that for the latter, where there is an additional index
    !called 'iter'. This will be used later for max and min values
    print*, 'Working on sample error calculation...'
    do iter=1,IT
           call doift(filein, iftforerror, filenormsample, 1)
           open(22,FILE=iftforerror)
           do d=1,DET
                  read(22,*)
                  do ft=1,FTM
                         read(22,*) tm(ft), Sqte(iter,d,ft)
                  end do
                  read(22,*)
           end do
           close(22)
    end do
```

```
    !Perform Vanadium IFT
    print*, 'Working on Vanadium file...'
    call doift(vanfile, viftinter, filenormvan, 0)
    open(23,FILE=viftinter)
    do d=1,DET
           read(23,*)
           do ft=1,FTM
                  read(23,*) tm(ft), vSqtr(d,ft)
           end do
           read(23,*)
    end do
    close(23)

!Perform Vanadium error calculation
    print*, 'Working on error from Vanadium data...'
    do iter=1,IT
           call doift(vanfile, viftforerror, filenormvan, 1)
           open(24,FILE=viftforerror)
           do d=1,DET
                  read(24,*)
                  do ft=1,FTM
                         read(24,*) tm(ft), vSqte(iter,d,ft)
                  end do
                  read(24,*)
           end do
           close(24)
    end do

    print*, 'Processing data and normalizing...'

    !Evaluating max and min of computed values
    do d=1,DET
           do ft=1,FTM
                  vSqtmax(d,ft) = maxval(vSqte(1:IT,d,ft))
                  vSqtmin(d,ft) = minval(vSqte(1:IT,d,ft))
                  Sqtmax(d,ft) = maxval(Sqte(1:IT,d,ft))
                  Sqtmin(d,ft) = minval(Sqte(1:IT,d,ft))
           end do
    end do
```

```
       !Final calculations and normalizations
       do d=1,DET
              do ft=1,FTM
                     Sqt(d,ft) = Sqtr(d,ft)/vSqtr(d,ft)
                     plus(d,ft) = Sqtmax(d,ft)/vSqtmin(d,ft) - Sqt(d,ft)
                     minus(d,ft) = Sqt(d,ft) - Sqtmin(d,ft)/vSqtmax(d,ft)
              end do
       end do

       print*, 'Writing to output file...', fileout
       time(1) = 1.0387d0
       do ft=1,FTM
              time(ft+1) = time(ft)*(10.d0**0.10d0)
       end do

       open(25,FILE=fileout)
       write(25,300) fileout
       do d=1,DET
              write(25,*) "q=",q(d)," ","Det=",d
              write(25,*) "time(ps) S(q,t) Error+ Error-"
              do ft=1,FTM
                     write(25,200) time(ft),Sqt(d,ft),plus(d,ft),minus(d,ft)
              end do
       end do
       print*, 'Done!'

200 format(F8.2,1X,F12.10,1X,F12.10,1X,F12.10)
300 format(A60)
   END PROGRAM
!--------------------
       SUBROUTINE doift(inputfile,outputfile,normfile,ErrorFlag)
       IMPLICIT NONE
       integer, parameter :: DATAPTS=550 !TOtal number of datapoints per Q
           group
       integer, parameter :: FTM=41 !Number of fourier transform times
       integer, parameter :: IT=500 !NUmber of iterations for error calculation
       integer, parameter :: DET=10 !Number of detectors
       character*256 inputfile, outputfile, normfile
       integer ErrorFlag
       real*8 energy(DATAPTS), q(DET), rndm(DATAPTS), omega(DATAPTS)
```

```
      real*8 Iqw(DET,DATAPTS), Iqw_u(DET,DATAPTS), Iqw_l(DET,DATAPTS)
      real*8 error(DET,DATAPTS), ErrorSize(DET,DATAPTS), tzero
      real*8 h*16, t(FTM), Iqtzero(DET), Iqtraw(DET,FTM), Iqt(DET,FTM)
      integer i,d,ft
      real*8 fxcos, fxsin, sumvalsin, sumvalcos, dw, valcos, valsin

                           open(11,FILE=inputfile)
      !Reading the file and assigning variables
      do i=1,5
         read(11,*)
      end do
      do i=1,DATAPTS
                    read(11,*) energy(i)
      end do
      read (11,*)
      do d=1,DET
                    read(11,*) q(d)
      end do
      do d=1,DET
                    read(11,*)
                    do i=1,DATAPTS
                           read(11,*) Iqw(d,i), error(d,i)
                           Iqw_u(d,i) = Iqw(d,i) + error(d,i)
                           Iqw_l(d,i) = Iqw(d,i) - error(d,i)
                           ErrorSize(d,i) = Iqw_u(d,i) - Iqw_l(d,i)
                    end do
      end do
      close(11)
      !Checking ERRORFLAG to see if this is part of error calculation
      !If yes, then calculate Iqw(d,i) between error bars
      if (ErrorFlag .EQ. 1) then
             do d=1,DET
                    do i=1,DATAPTS
                           call random_number(rndm(i))
                           Iqw(d,i) = Iqw_l(d,i) + rndm(i)*ErrorSize(d,i)
                    end do
             end do
      end if
   !Calculating omega from energy values
   do d=1,DET
```

```
        do i=1,DATAPTS
                h=6.582D-10 !Technically, this is h_bar, in ueV.s
                omega(i)=energy(i)/(h*1.d12) !Converted to 1/ps
        end do
end do

!Performing Inverse Fourier Transform
open(17,FILE=normfile) !For writing I(q,0) values
do d=1,DET
        t(1)=1.0387d0
        do ft=1,FTM
                t(ft+1)=t(ft)*(10.d0**0.1d0)
                sumvalsin = 0.0D0
                sumvalcos = 0.0D0
                do i=1,DATAPTS-1
                        fxcos = Iqw(d,i)*cos(omega(i)*t(ft))
                        fxsin = Iqw(d,i)*sin(omega(i)*t(ft))
                        dw = omega(i+1) - omega(i)
                        valcos = fxcos*dw
                        valsin = fxsin*dw
                        sumvalsin = sumvalsin + valsin
                        sumvalcos = sumvalcos + valcos
                end do
                Iqtraw(d,ft)=SQRT(sumvalsin**2 + sumvalcos**2)
                tzero = 0.0D0
                Iqtzero(d) = 0.0D0
                sumvalsin = 0.0D0
                sumvalcos = 0.0D0
                do i=1,DATAPTS-1
                        fxcos = Iqw(d,i)*cos(omega(i)*tzero)
                        fxsin = Iqw(d,i)*sin(omega(i)*tzero)
                        dw = omega(i+1) - omega(i)
                        valcos = fxcos*dw
                        valsin = fxsin*dw
                        sumvalsin = sumvalsin + valsin
                        sumvalcos = sumvalcos + valcos
                end do
                Iqtzero(d) = SQRT(sumvalsin**2 + sumvalcos**2)
                Iqt(d,ft) = Iqtraw(d,ft)/Iqtzero(d)
        end do
```

```
              write(17,*) "Detector",d,Iqtzero(d)
       end do
       close(17)

   !Writing to outputfile
   open(12,FILE=outputfile)
       do d=1,DET
              write(12,*) "Detector",d
              do ft=1,FTM
                            write(12,100) t(ft), Iqt(d,ft)
              end do
              write(12,*)
       end do
       close(12)

100 format(F8.2,1x,F12.10)
   END SUBROUTINE
```

A.3.1 Verification of BASIS IFT code

To verify the correctness of the BASIS inverse Fourier transforming code, I compared it to Vicky's HFBS code. Both the instruments have different ASCII output formats, but essentially contain intensity vs. energy data. We modified the HFBS version of $I(Q,\omega)$ vs E (frequency) data of PEO600-100%Na (298 K) to look like an output from BASIS. The two formats are shown in Figure A.4. We adjusted the BASIS code to handle the time scale of HFBS. The resulting $S(Q,t)$ curves when superimposed, were within error bars of each other, as shown in Figure A.5.

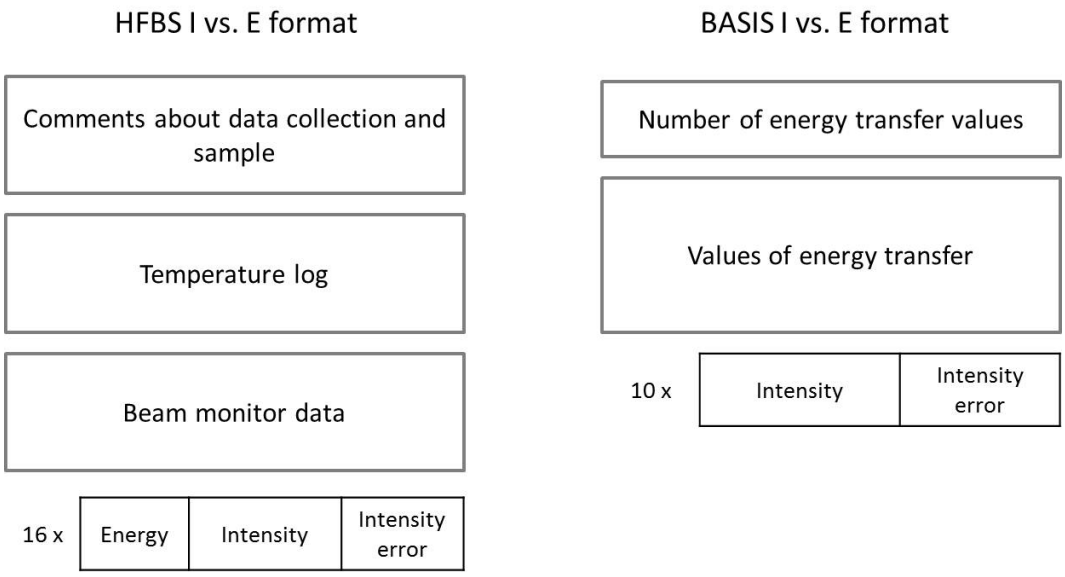

Figure A.4. Formats for HFBS and BASIS intensity vs. energy files, as obtained from the instruments after data reduction. Each block represents a set of data points pertaining to the text inside the block.

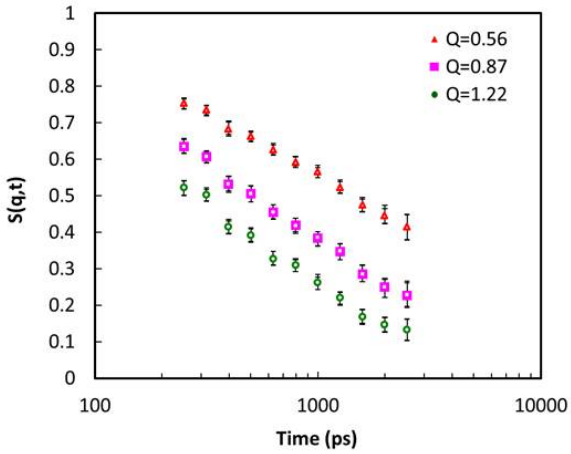

Figure A.5. Superimposition of S(Q,t) for PEO600-100%Na (298 K) obtained by using Vicky's code (open symbols) and my BASIS code (filled symbols) for three Q values - 0.56 $Å^{-1}$, 0.87 $Å^{-1}$, and 1.22 $Å^{-1}$. The data points lie on top of each other.

Appendix B

BASIS Data Treatment

B.1 Resolving BASIS data to two processes

As discussed in Chapter 3, it is challenging to resolve the BASIS data to the two constituent bridge and anchor atom relaxations because the time range accessible by BASIS is small. We identify that a range of relaxation time (τ) and EISF (ϵ) values can fit the S(Q,t) data (see Figure 3.7). We extract a parameter τ_0 from the loci, which helps us connect the parent processes (τ_{ANCHOR} and τ_{ANCHOR}) to τ and ϵ. In this section, we discuss the derivation of Eq (3.15) (reproduced below) in Chapter 3 for BASIS data treatment.

$$\tau_0 = [\tau_{BRIDGE}]^{X_{BRIDGE}} [\tau_{ANCHOR}]^{1-X_{BRIDGE}} \tag{B.1}$$

The above expression is derived by comparing the area under the S(Q,t) curve obtained from two equations (Eq 3.14 and Eq 3.12). Since KWW expressions involve stretched exponentials, it is not possible to obtain an analytical expression for the integral (which provides the area under the curve). We therefore performed a numerical analysis for the same. To fully understand the impact of τ_{ANCHOR} and τ_{ANCHOR} on the range of τ and ϵ that fit this data, we studied the parameters for *generated* data sets. We generated S(t) data sets of two fractions undergoing a

slow and fast relaxation

$$S(t) = x \exp\left[-\left(\frac{t}{\tau_1}\right)^{\beta_1}\right] + (1-x)\exp\left[-\left(\frac{t}{\tau_2}\right)^{\beta_2}\right] \tag{B.2}$$

where τ_1 = (50, 75, 100, 125, 150, 175, 200 ps), with $\beta_1 = 0.6$, and τ_2 = (500, 750, 1000, 2000 and so on), with $\beta_2 = 0.45$. We varied the fraction of fast process x from 0 to 1. Understandably, the subscripts 1 and 2 correspond to bridge and anchor atoms respectively. We choose these values of β because they are similar to the values obtained from bridge and anchor atom relaxations (measured in DCS/HFBS). The values of τ_1 are consistent with bridge atom relaxations which range between 30 and 250 ps. The only constraint on the values of τ_2 values are that they are greater than τ_1. To emulate the BASIS instrument, we spliced data points from time = 40 to 800 ps, as shown by the unshaded region in Figure B.1. We then fit the spliced data to a single stretched relaxation, thereby obtaining a range of $[\tau,\ \epsilon]$ that fit the dataset.

$$S(t) = \epsilon + (1-\epsilon)\exp\left[-\left(\frac{t}{\tau}\right)^{\beta}\right] \tag{B.3}$$

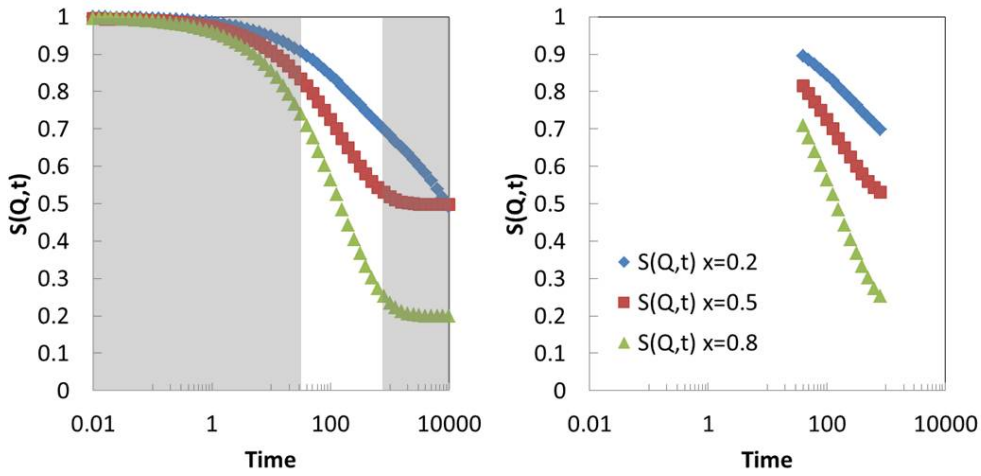

Figure B.1. Splicing generated datasets to lie within limits of BASIS instrument. The figure on the right is the portion of the generated data that is fit to Eq (B.1). These curves were generated using $\tau_1 = 150$ ps, $\tau_2 = 50000$ ps, and the fast fraction x corresponding to the values in the legend.

In order to examine the relationship between τ and ϵ, we plot relaxation time (τ) vs. EISF (ϵ) as shown in Figure B.2. We observe that an exponential relation

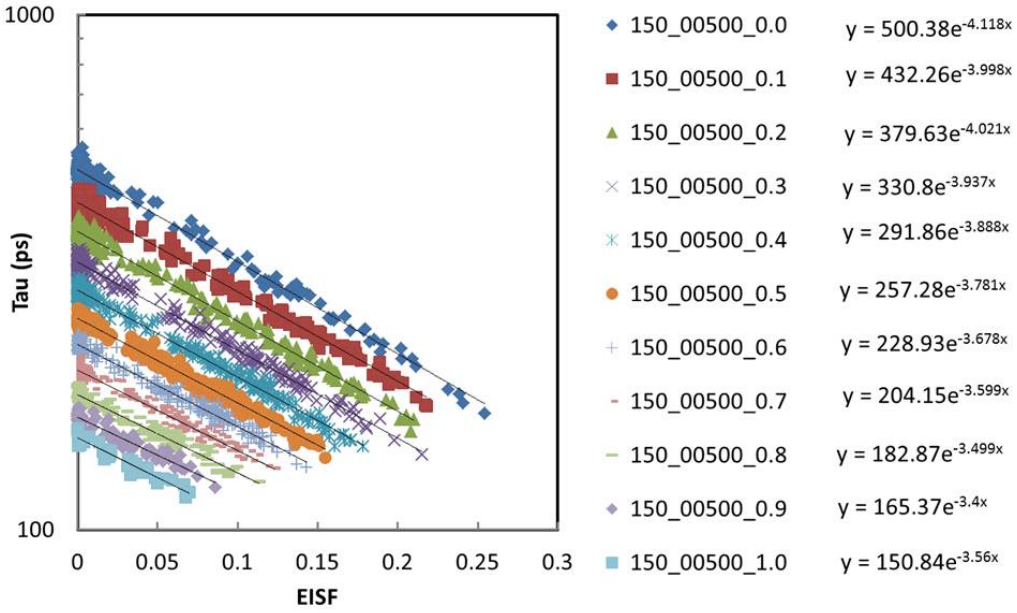

Figure B.2. Relaxation time vs. EISF for generated data, with the corresponding fitting equations for $\tau_1 = 150$ ps, $\tau_2 = 500$ ps and x ranging from 0 to 1.

of the form

$$\tau = \tau_0 \exp\left[-B\epsilon\right] \tag{B.4}$$

can fit the data, where τ_0 is the value of τ when $\epsilon \rightarrow 0$. We observe that $\tau_0 = \tau_2$ when $x = 0$ (i.e. slow process only) and $\tau_0 = \tau_1$ when $x = 1$ (i.e. fast process only). This suggests that the value of τ_0 is affected by τ_1, τ_2 and the fraction x.

To understand the relationship better, we plot τ_0 vs τ_2 (see Figure B.3a) while τ_1 and x are constant and observe that there is a linear dependence between the logarithmic values of τ_0 and τ_2.

Therefore,

$$\begin{aligned} \log \tau_0 &= m_2 \ \log \tau_2 + \text{constant} \\ \text{or} \quad \tau_0 &\propto \tau_2^{m_2} \quad \text{when } \tau_1 \text{ and } x \text{ are constant} \end{aligned} \tag{B.5}$$

The value τ_0 is symmetric for τ_1 and τ_2, i.e it varies with τ_2 the same way as it varies with τ_2. This is because $[\tau_1, \beta_1]$ and $[\tau_2, \beta_2]$ can be interchanged in Eq B.3.

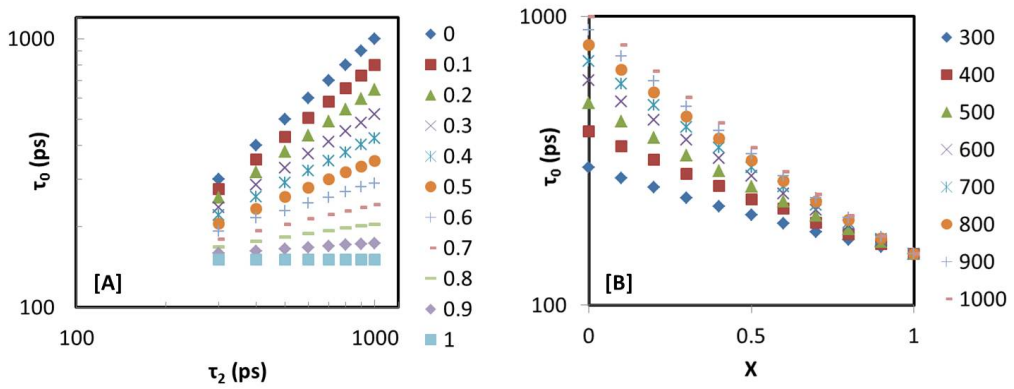

Figure B.3. (A) Parameter τ_0 vs τ_2, for different x (see legend); (B) Parameter τ_0 vs x for different τ_2 (see legend). The value of τ_1 for both these graphs is 150.

Therefore, if follows that

$$\begin{aligned} \log \tau_0 &= m_1 \ \log \tau_1 + \text{constant} \\ \text{or} \quad \tau_0 &\propto \tau_1^{m_1} \quad \text{when } \tau_2 \text{ and } x \text{ are constant} \end{aligned} \tag{B.6}$$

The dependence of the logarithm of τ_0 with x (at constant τ_1 and τ_2) is also linear, as shown in Figure B.3b. Therefore,

$$\log \tau_0 = m_3 \ x + \text{constant} \quad \text{when } \tau_1 \text{ and } \tau_2 \text{ are constant} \tag{B.7}$$

with the constraints (as seen in Figure B.2)

$$\tau_0 = \begin{cases} \tau_1 & \text{if } x = 1 \\ \tau_2 & \text{if } x = 0 \end{cases}$$

Combining Eq B.7 with the constraints above, we obtain

$$\begin{aligned} \log \tau_0 &= x \log \frac{\tau_2}{\tau_1} + \log \tau_2 \\ \text{or} \quad \tau_0 &= \tau_2 \left[\frac{\tau_1}{\tau_2} \right]^x \end{aligned}$$

which simplifies to

$$\tau_0 = \tau_1^x \ \tau_2^{(1-x)} \tag{B.8}$$

This equation is similar to Eq (B.2) (i.e. Eq (3.15)), where τ_1 is τ_{BRIDGE}, τ_2 is τ_{ANCHOR}, and x is X_{BRIDGE}. Eq (B.8) satisfies the requirement of symmetry with τ_1 and τ_2. To test this equation, we varied τ_1 and τ_2 over a large range (150 to 80000 ps) and plotted the estimated value of τ_0 (from Eq (B.8)) with that obtained by fitting the generated data to Eq (B.3) (for $\epsilon \rightarrow 0$) by plotting them against each other, as shown in Figure B.4. The red line has a slope of 1, denoting equality of the X and Y axes.

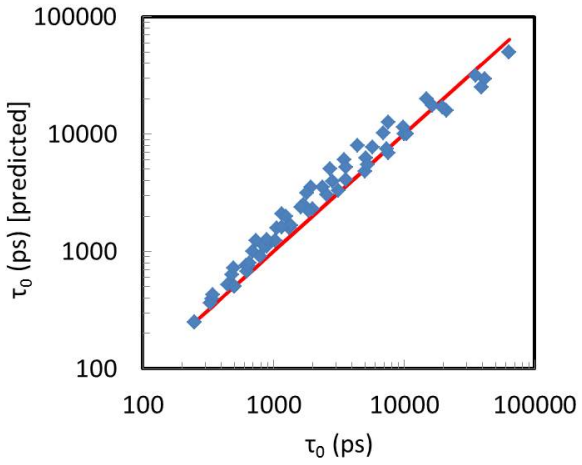

Figure B.4. Predicted τ_0 ($\tau_1^x \tau_2^{(1-x)}$) vs τ_0 obtained from fitting. The red line has a slope of 1 (denoting equality between predicted and actual τ_0)

B.2 Comparison of fitting parameters - BASIS and DCS/HFBS

The above technique proved to be successful in providing the bridge and anchor relaxation times obtained from DCS/HFBS for samples that were measured on all three instruments. The comparison of τ_{BRIDGE}, τ_{ANCHOR} and X_{BRIDGE} obtained from BASIS and DCS/HFBS for PEOx-100%Na (x = 400,600,1100) and PEO600-100%Li are shown in Figure B.5 and Figure B.6.

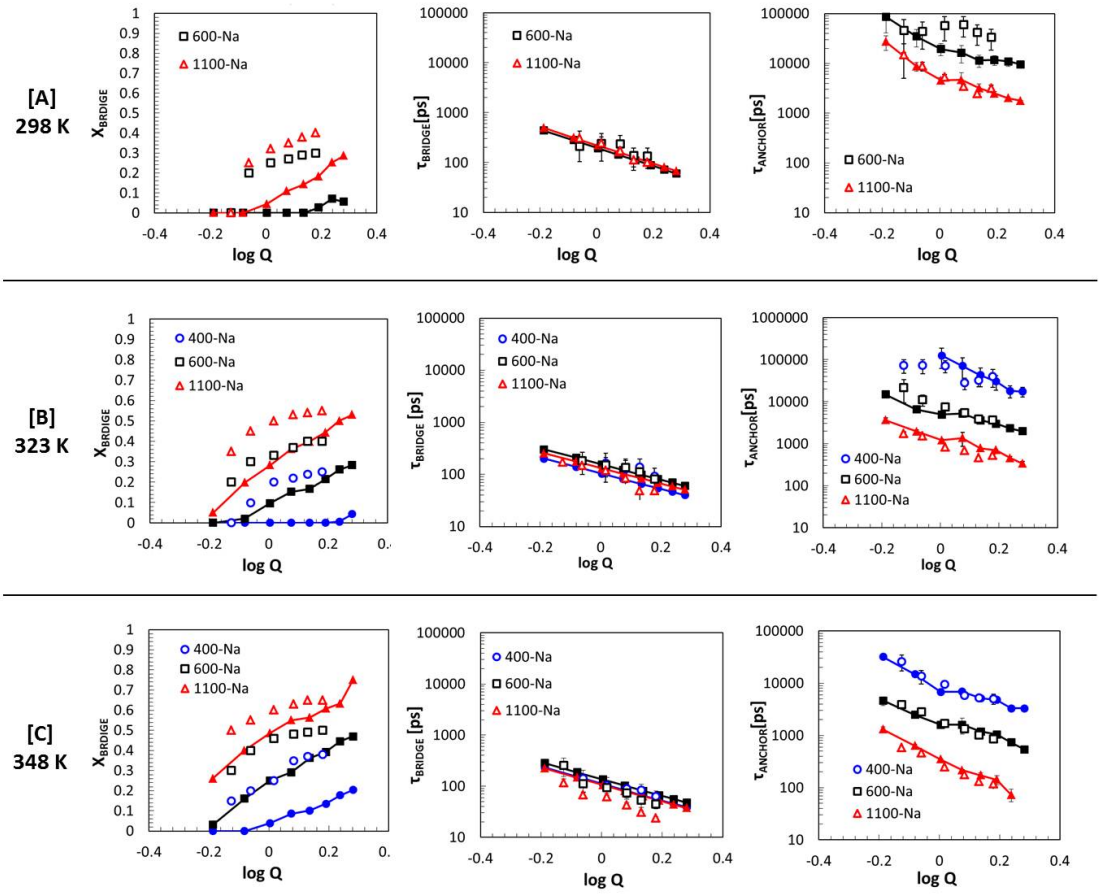

Figure B.5. Q dependence of X_{BRIDGE}, τ_{BRIDGE} and τ_{ANCHOR} for PEOx-100%Na (x = 400, 600, 1100) at [A] 298 K, [B] 323 K, [C] 348 K. Open symbols - Fitting parameters obtained from DCS/HFBS; Filled connected symbols - Fitting parameters obtained from BASIS

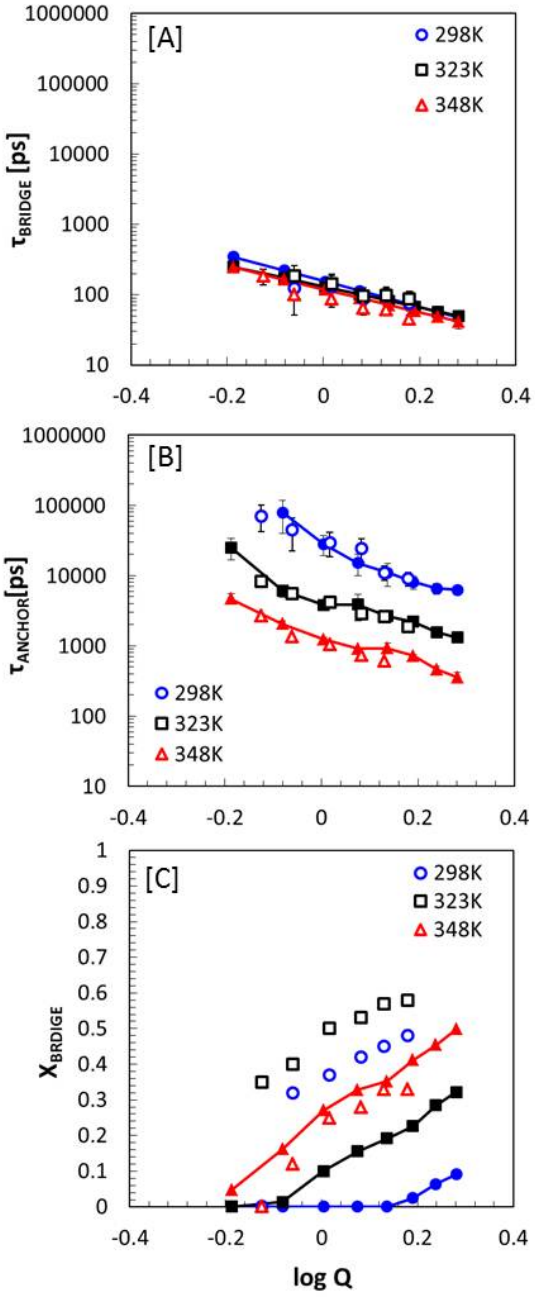

Figure B.6. Q dependence of [A] τ_{BRIDGE}, [B] τ_{ANCHOR}, and [C] X_{BRIDGE} for PEO600-100%Li for 298 K, 323 K and 348 K. Open symbols - Fitting parameters obtained from DCS/HFBS; Filled connected symbols - Fitting parameters obtained from BASIS

Appendix C

Range of fitting parameters

This appendix discusses how different programs are used to obtain the error bars (ranges) on fitting parameters from DCS, HFBS and BASIS. The curve fitting is done using the software **XMgrace** (available on LionXO, LionXH etc.). There are several steps involved for obtaining the range of fitting parameters, and differs for DCS/HFBS and BASIS.

C.1 Using XMgrace

XMgrace (also known as **grace**) stands for "GRaphing, Advanced Computation and Exploration of data" and uses the X Window System and Motif for its GUI. It is a very powerful tool for non-linear curve fitting. It uses the Levenberg-Marquardt non-linear least squares fitting program. **XMgrace** has a command line interface which offers the advantage that it be executed from shell scripts or from a command prompt. It requires a data file [data.txt] which has two columns in the form (x,y) as shown below

```
 41.35 0.8700640660
 52.06 0.8566128715
 65.54 0.8296022583
 82.51 0.8264609317
103.87 0.7999248536
130.76 0.7864872068
164.62 0.7735087996
207.25 0.7520059854
```

and uses a batch file [gracefit.bat] for reading the equation, initial guesses and tolerance, as shown below.

```
fit formula "y = Exp(-1*(x/a0)^a1)"
fit with 2 parameters
fit prec 0.001
a0 = 506.30
a0 constraints on
a0min = 1
a0max = 10000000
a1 = 0.9802
a1 constraints on
a1min = 0
a1max = 1
nonlfit (s0,500)
```

To run **XMgrace** and print the output to output.txt, we execute the command

```
gracebat data.txt -batch gracefit.bat > output.txt
```

and the output is of the form

```
Fitting with formula: y = Exp(-1*(x/a2)^a3)
Initial guesses:
       a0 = 506.3
       a1 = 0.9802
Tolerance = 0.0001
Relative error in the sum of squares is at most tol.
Computed values:
       a0 = 3854.58
       a1 = 0.425733

Chi-square: 0.000202182
Correlation coefficient: 0.991385
RMS per cent error: 0.0061155
Theil U coefficent: 0.00618551
```

We parse the fitting parameters and use the "Chi-square" (ξ^2-error) and "RMS per cent error" [which in reality is (RMS percent error)/100] as criteria for selecting good fits. The outline of obtaining the error bars on the fitting parameters is summarized in the form of flowcharts in the next two sections.

C.2 Finding error bars for fitting - DCS/HFBS

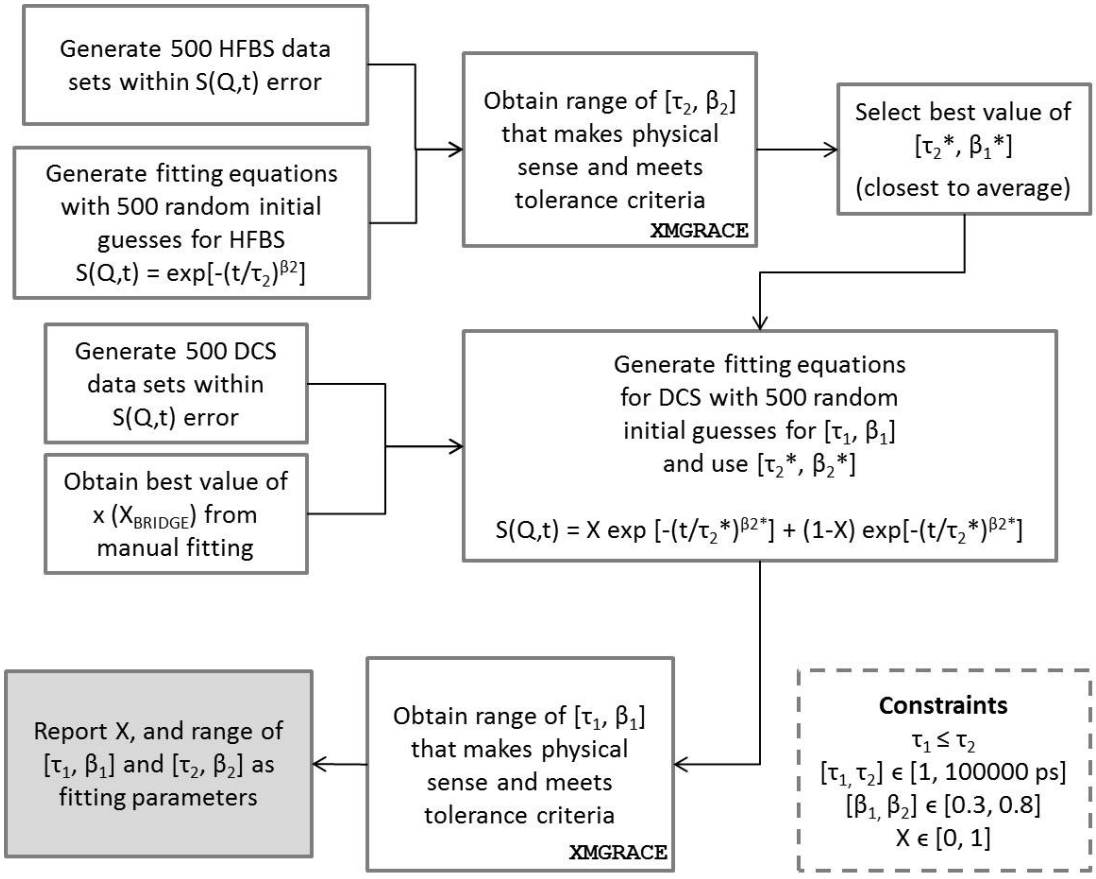

Figure C.1. Overview of fitting DCS/HFBS data

C.3 Finding error bars for fitting - BASIS

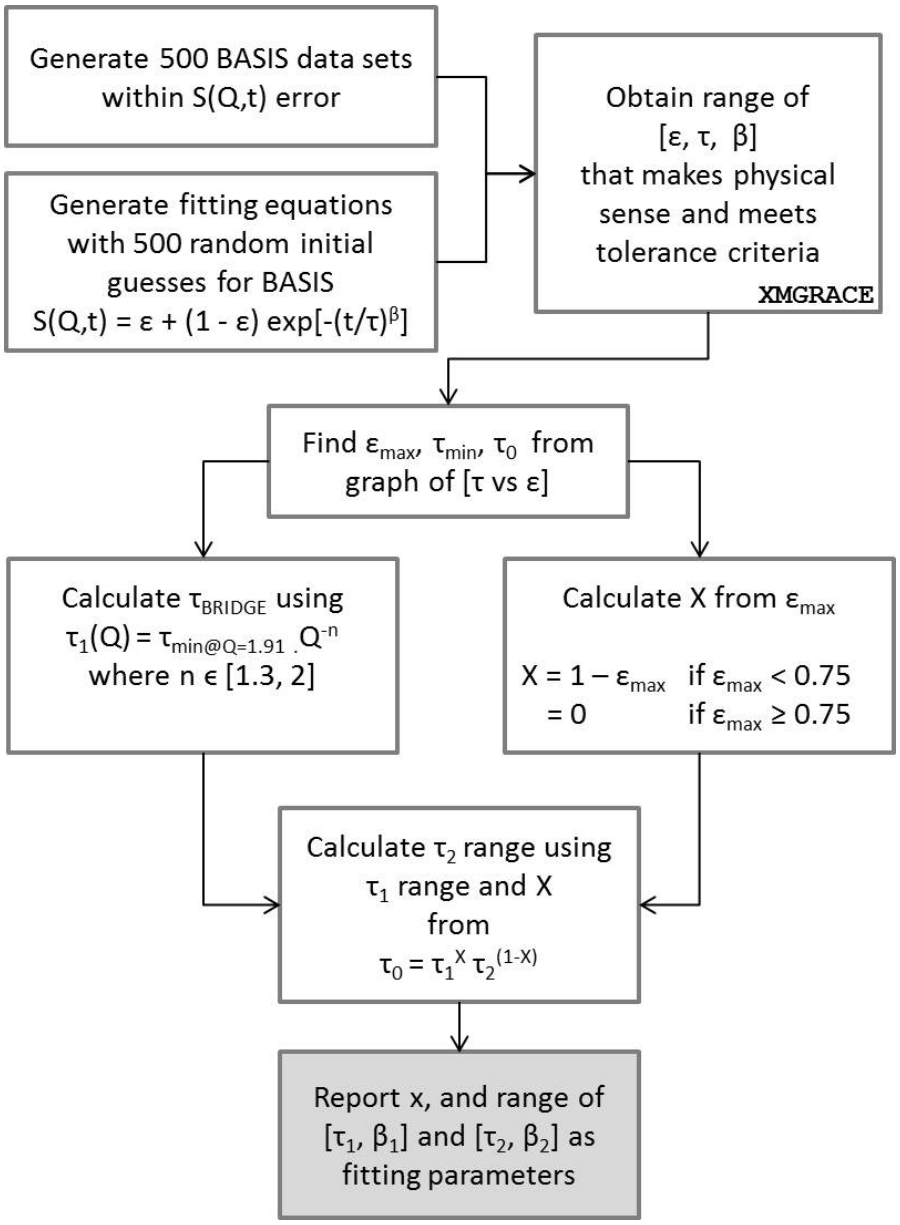

Figure C.2. Overview of fitting BASIS data

C.4 Summary of programs/scripts

The FORTRAN programs and BASH scripts written for the above processes follow a simple structure as shown in Figure C.3, and exist for DCS, HFBS and BASIS separately.

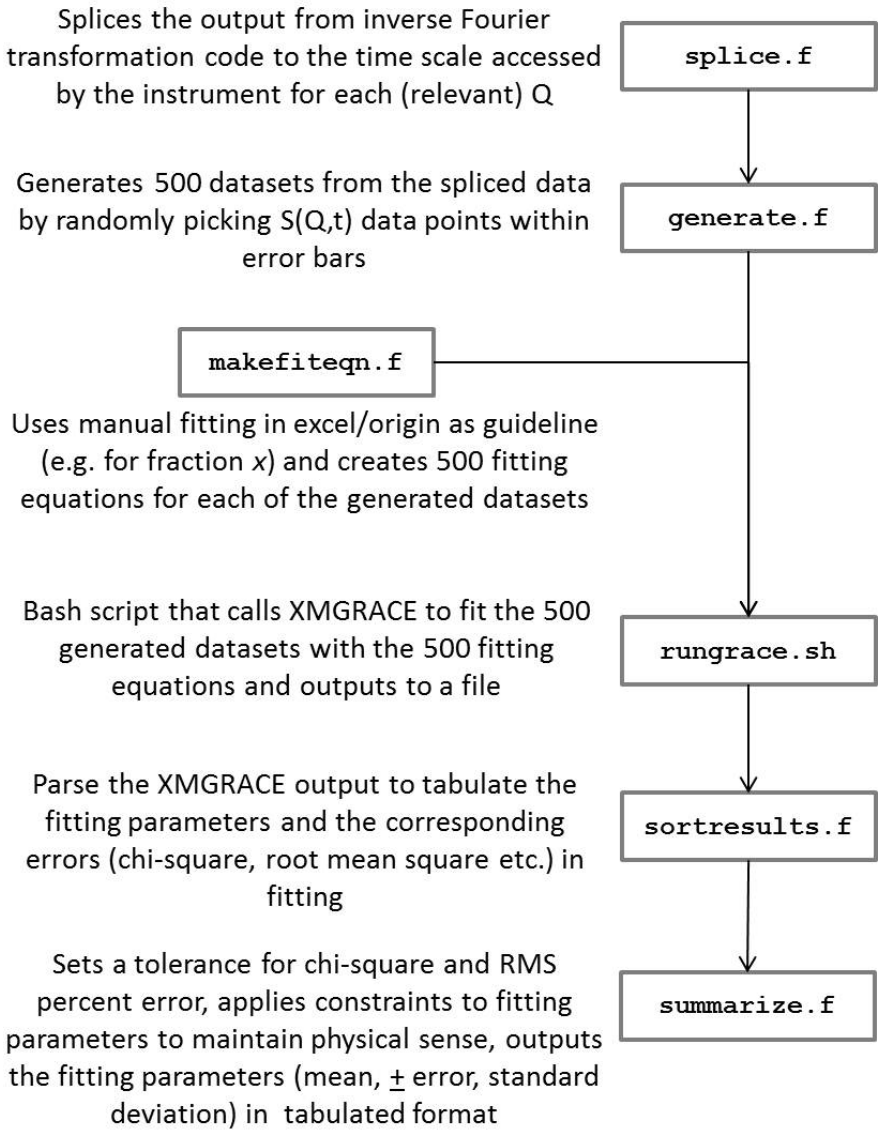

Figure C.3. Overview of programs written for finding error bars (ranges) on fitting parameters

Appendix D

S(Q,t) curves from DCS/HFBS

In this chapter we compare the S(Q,t) curves of several samples based on the fitting algorithm for DCS/HFBS discussed in Chapter 3, section 3.3.2.1. These curves are a depiction of how the S(Q,t) data would look like if a single instrument were capable of measuring the entire energy window of DCS and HFBS.

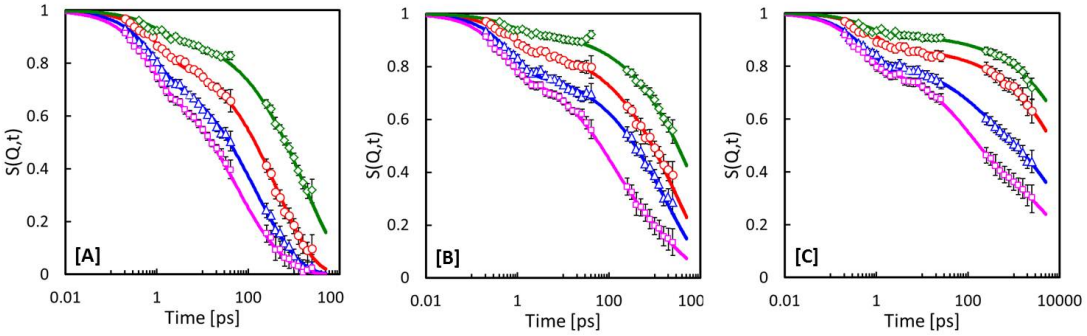

Figure D.1. S(Q,t) curves for [A] PEO600-0%, [B] PEO600-49%Na, [C] PEO600-100%Na at 298 K for Q = 0.57 Å^{-1} (green), 0.89 Å^{-1} (red), 1.21 Å^{-1} (blue), and 1.51 Å^{-1}(magenta)

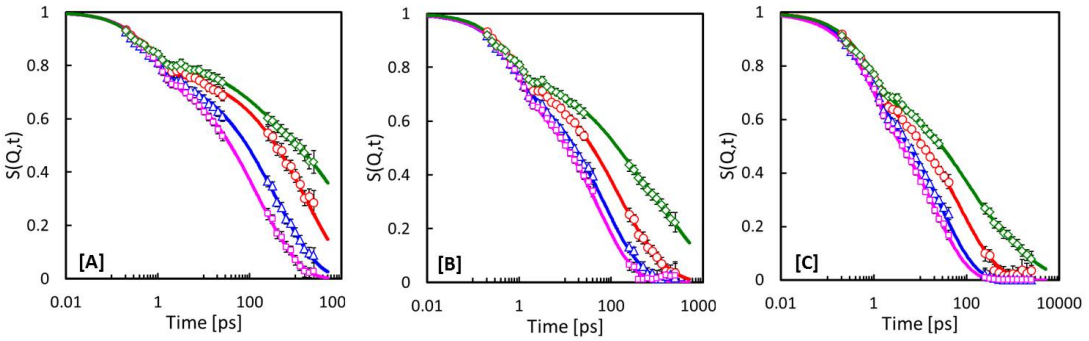

Figure D.2. S(Q,t) curves for PEO600-0% (magenta), PEO600-17%Na (blue), PEO600-49%Na (red), and PEO600-100%Na (green) at [A] 298 K, [B] 323 K, and [C] 348 K for Q = 1.2 Å^{-1}

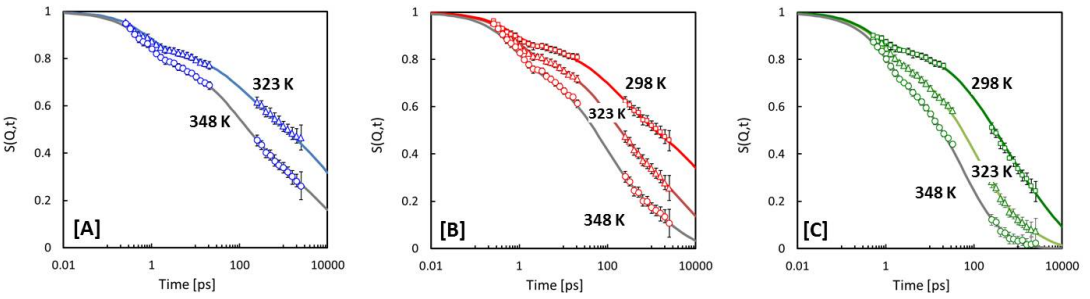

Figure D.3. S(Q,t) curves for [A] PEO400-100%Na, [B] PEO600-100%Na, [C] PEO1100-100%Na at Q = 1.21 Å^{-1} for different temperatures

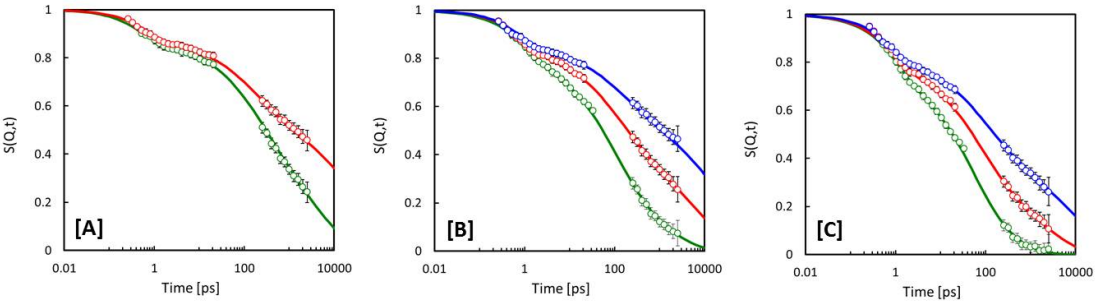

Figure D.4. S(Q,t) curves comparing PEO400-100%Na (blue), PEO600-100%Na (red) and PEO1100-100%Na (green) for [A] 298 K, [B] 323 K, and [C] 348 K at Q = 1.21 Å^{-1}

Bibliography

[1] Roger Pynn. Neutron Scattering - A Primer. *Los Alamos Science*, 19, 1990.

[2] S K Fullerton-Shirey and J K Maranas. Effect of LiClO4 on the Structure and Mobility of PEO-Based Solid Polymer Electrolytes. *Macromolecules*, 42(6):2142–2156, 2009.

[3] D Fragiadakis, S Dou, R H Colby, and J Runt. Molecular mobility and Li+ conduction in polyester copolymer ionomers based on poly(ethylene oxide). *Journal of Chemical Physics*, 130(6), 2009.

[4] Xing Jin, Shihai Zhang, and James Runt. Broadband Dielectric Investigation of Amorphous Poly(methyl methacrylate)/Poly(ethylene oxide) Blends. *Macromolecules*, 37(21):8110–8115, October 2004.

[5] G J Tudryn, D R King, M OReilly, K I Winey, and R H Colby. Molecular mobility and cation conduction in sulfonated polyester copolymer ionomers. *Manuscript in preparation.*

[6] W Q Wang, W J Liu, G J Tudryn, R H Colby, and K I Winey. Multi-Length Scale Morphology of Poly(ethylene oxide)-Based Sulfonate Ionomers with Alkali Cations at Room Temperature. *Macromolecules*, 43(9):4223–4229, 2010.

[7] W Wang, G Tudryn, R Colby, and K Winey. Thermally Driven Ionic Aggregation in Poly(ethylene oxide)-Based Sulfonate Ionomers. *Journal of the American Chemical Society*, 133(28):10826–10831, 2011.

[8] S C Dou, S H Zhang, R J Klein, J Runt, and R H Colby. Synthesis and characterization of poly(ethylene glycol)-based single-ion conductors. *Chemistry of Materials*, 18(18):4288–4295, 2006.

[9] K-J Lin and J K Maranas. A molecular dynamics study of cation coordination and motion in a poly(ethylene oxide)-based ionomer. *Manuscript in preparation.*

[10] M. McLin and C. A. Angell. Contrasting conductance/viscosity relations in liquid states of vitreous and polymer solid electrolytes. *The Journal of Physical Chemistry*, 92(8):2083–2086, April 1988.

[11] C Angell. Fast ion motion in glassy and amorphous materials. *Solid State Ionics*, 9-10:3–16, December 1983.

[12] C Angell. Recent developments in fast ion transport in glassy and amorphous materials. *Solid State Ionics*, 18-19:72–88, January 1986.

[13] C Angell. Mobile Ions in Amorphous Solids. *Annual review of physical chemistry (0066-426X)*, 43(1):693, 1992.

[14] P B Macedo. Role of ionic diffusion in polarization in vitreous ionic conductors. *Physics and chemistry of glasses*, 13(6):171, 1972.

[15] J M Tarascon and M Armand. Issues and challenges facing rechargeable lithium batteries. *Nature*, 414(6861):359–67, November 2001.

[16] Peter V. Wright. Electrical conductivity in ionic complexes of poly(ethylene oxide). *British Polymer Journal*, 7(5):319–327, September 1975.

[17] M B Armand, J M Chabagno, M J Duclot, J N Mundy, and G K Shonoy. *Fast Ion Transport in Solids*. North-Holland, Amsterdam, 1979.

[18] M Minier, C Berthier, and W Gorecki. Differntial scanning calometry of sodium iodide poly(ethylene oxyde) complexes. *Solid State Ionics*, 9-10:1125–1127, December 1983.

[19] C Berthier, W Gorecki, M Minier, M Armand, J Chabagno, and P Rigaud. Microscopic investigation of ionic conductivity in alkali metal salts-poly(ethylene oxide) adducts. *Solid State Ionics*, 11(1):91–95, September 1983.

[20] Shinji Takeoka, Hiroyuki Ohno, and Eishun Tsuchida. Recent advancement of ion-conductive polymers. *Polymers for Advanced Technologies*, 4(2-3):53–73, 1993.

[21] Peter V. Wright. Developments in Polymer Electrolytes for Lithium Batteries. *MRS Bulletin*, 27(08):597–602, August 2002.

[22] Ping-Lin Kuo, Sheng-Shu Hou, Chung-Yie Lin, Chi-Chang Chen, and Ten-Chin Wen. Solid polymer electrolytes I, preparation, characterization, and ionic conductivity of gelled polymer electrolytes based on novel crosslinked siloxane/poly(ethylene glycol) polymers. *Journal of Polymer Science Part A: Polymer Chemistry*, 42(9):2051–2059, May 2004.

[23] A Bouridah. Poly(dimethylsiloxane)-poly(ethylene oxide) based polyurethane networks used as electrolytes in lithium electrochemical solid state batteries. *Solid State Ionics*, 15(3):233–240, April 1985.

[24] Dan Luo, Yang Li, Weili Li, and Mujie Yang. Synthesis and characterization of novel semi-interpenetrating polymer network electrolyte based on crosslinked P(GMA-co-AN)/PEO. *Journal of Applied Polymer Science*, 108(4):2095–2100, May 2008.

[25] D Golodnitsky. Effect of plasticizers on the CPE conductivity and on the Li-CPE interface. *Solid State Ionics*, 85(1-4):231–238, May 1996.

[26] M.S Michael, M.M.E Jacob, S.R.S Prabaharan, and S Radhakrishna. Enhanced lithium ion transport in PEO-based solid polymer electrolytes employing a novel class of plasticizers. *Solid State Ionics*, 98(3-4):167–174, June 1997.

[27] H S Lee, X Q Yang, J McBreen, Z S Xu, T A Skotheim, and Y Okamoto. Ionic Conductivity of a Polymer Electrolyte with Modified Carbonate as a Plasticizer for Poly(ethylene oxide). *Journal of The Electrochemical Society*, 141(4):886–889, April 1994.

[28] R Frech. Effect of propylene carbonate as a plasticizer in high molecular weight PEO_LiCF3SO3 electrolytes. *Solid State Ionics*, 85(1-4):61–66, May 1996.

[29] F M Gray. *Polymer Electrolytes*. The Royal Society of Chemistry, Letchworth, UK, 1997.

[30] F. Croce, G. B. Appetecchi, L. Persi, and B. Scrosati. Nanocomposite polymer electrolytes for lithium batteries. *Nature*, 394(6692):456–458, July 1998.

[31] Duncan W. Bruce, Dermot O'Hare, and Richard I. Walton, editors. *Energy Materials*. John Wiley & Sons, Ltd, Chichester, UK, February 2011.

[32] K Xu. Nonaqueous liquid electrolytes for lithium-based rechargeable batteries. *Chemical Reviews*, 104(10):4303–4417, 2004.

[33] T Hamaide and C Le Deore. Cationic conductivity and relaxation processes in solid polymer electrolytes with lithium perfluoroalkyl sulfonate or sulfonato end-capped poly(ethylene oxide). *Polymer*, 34(5):1038–1046, March 1993.

[34] G C Rawsky, T Fujinami, and D F Shriver. Aluminosilicate Poly(Ethylene Glycol) Copolymers - a New Class of Polyelectrolytes. *Chemistry of Materials*, 6(12):2208–2209, 1994.

[35] Xiao-Guang Sun and John B Kerr. Synthesis and Characterization of Network Single Ion Conductors Based on Comb-Branched Polyepoxide Ethers and Lithium Bis(allylmalonato)borate. *Macromolecules*, 39(1):362–372, 2005.

[36] Xiao-Guang Sun, John B Kerr, Craig L Reeder, Gao Liu, and Yongbong Han. Network Single Ion Conductors Based on Comb-Branched Polyepoxide Ethers and Lithium Bis(allylmalonato)borate. *Macromolecules*, 37(14):5133–5135, 2004.

[37] Kaori Ito and Hiroyuki Ohno. Ionic conductivity of poly(ethylene oxide) having charges on the chain end. *Solid State Ionics*, 79:300–305, 1995.

[38] L M Bronstein, R L Karlinsey, B Stein, Z Yi, J Carini, and J W Zwanziger. Solid polymer single-ion conductors: Synthesis and properties. *Chemistry of Materials*, 18(3):708–715, 2006.

[39] K Ito, N Nishina, Y Tominaga, and H Ohno. Effect of terminal groups on the ionic conductivity of alpha,omega-dicharged poly(ethylene oxide) oligomers. *Solid State Ionics*, 86-8:325–328, 1996.

[40] G Zhou, I Khan, and J Smid. Solvent-free cation-conducting polysiloxane electrolytes with pendant oligo(oxyethylene) and sulfonate groups. *Macromolecules*, 26(9):2202–2208, 1993.

[41] Hiroyuki Ohno, Norihisa Kobayashi, Shinji Takeoka, Hajime Ishizaka, and Eishun Tsuchida. Larger cations can move faster in solid polymer electrolytes. *Solid State Ionics*, 40-41(Part 2):655–658, 1990.

[42] Eishun Tsuchida, Hiroyuki Ohno, Norihisa Kobayashi, and Hajime Ishizaka. Poly[(w-carboxy)oligo(oxyethylene) methacrylate] as a new type of polymeric solid electrolyte for alkali-metal ion transport. *Macromolecules*, 22(4):1771–1775, 1989.

[43] R J Klein and J Runt. Plasticized single-ion polymer conductors: Conductivity, local and segmental dynamics, and interaction parameters. *Journal of Physical Chemistry B*, 111(46):13188–13193, 2007.

[44] Robert J. Klein, Daniel T. Welna, Arlin L. Weikel, Harry R. Allcock, and James Runt. Counterion Effects on Ion Mobility and Mobile Ion Concentration of Doped Polyphosphazene and Polyphosphazene Ionomers. *Macromolecules*, 40(11):3990–3995, May 2007.

[45] M M Doeff and J S Reed. Li ion conductors based on laponite/poly(ethylene oxide) composites. *Solid State Ionics*, 113:109–115, 1998.

[46] Norihisa Kobayashi, Masahiro Uchiyama, and Eishun Tsuchida. Poly[lithium methacrylate-co-oligo(oxyethylene)methacrylate] as a solid electrolyte with high ionic conductivity. *Solid State Ionics*, 17(4):307–311, 1985.

[47] D Fragiadakis, S C Dou, R H Colby, and J Runt. Molecular mobility, ion mobility, and mobile ion concentration in poly(ethylene oxide)-based polyurethane ionomers. *Macromolecules*, 41(15):5723–5728, 2008.

[48] Gregory J. Tudryn, Wenjuan Liu, Shih-Wa Wang, and Ralph H. Colby. Counterion Dynamics in PolyesterSulfonate Ionomers with Ionic Liquid Counterions. *Macromolecules*, 44(9):3572–3582, May 2011.

[49] D.J Bannister, G.R Davies, I.M Ward, and J.E McIntyre. Ionic conductivities of poly(methoxy polyethylene glycol monomethacrylate) complexes with LiSO3CH3. *Polymer*, 25(11):1600–1602, November 1984.

[50] L. Charles Hardy and Duward F. Shriver. Preparation and electrical response of solid polymer electrolytes with only one mobile species. *Journal of the American Chemical Society*, 107(13):3823–3828, June 1985.

[51] S. Ganapathiappan, Kaimin Chen, and D. F. Shriver. A new class of cation conductors: polyphosphazene sulfonates. *Macromolecules*, 21(7):2299–2301, July 1988.

[52] B. Hird and A. Eisenberg. Sizes and stabilities of multiplets and clusters in carboxylated and sulfonated styrene ionomers. *Macromolecules*, 25(24):6466–6474, November 1992.

[53] Adi Eisenberg. Clustering of Ions in Organic Polymers. A Theoretical Approach. *Macromolecules*, 3(2):147–154, 1970.

[54] Adi Eisenberg and Joon-Seop Kim. *Introduction to Ionomers*. John Wiley & Sons, Inc, New York, 1998.

[55] D Teeters and R Frech. Temperature-dependent spectroscopic studies of poly(propylene oxide) and poly(propylene oxide)-inorganic salt complexes. *Solid State Ionics*, 18-19:271–276, January 1986.

[56] M. Kakihana, S. Schantz, and L. M. Torell. Raman spectroscopic study of ionion interaction and its temperature dependence in a poly(propylene-oxide)-based NaCF3SO3 polymer electrolyte. *The Journal of Chemical Physics*, 92(10):6271, May 1990.

[57] S. Schantz. On the ion association at low salt concentrations in polymer electrolytes; a Raman study of NaCF3SO3 and LiClO4 dissolved in poly(propylene oxide). *The Journal of Chemical Physics*, 94(9):6296, May 1991.

[58] S. Schantz, L. M. Torell, and J. R. Stevens. Ion pairing effects in poly(propylene glycol)salt complexes as a function of molecular weight and temperature: A Raman scattering study using NaCF3SO3 and LiClO4. *The Journal of Chemical Physics*, 94(10):6862, May 1991.

[59] Xinya Lu and R. A. Weiss. Phase Behavior of Blends of Poly(ethylene glycol) and Partially Neutralized Poly(acrylic acid). *Macromolecules*, 28(9):3022–3029, April 1995.

[60] Irina A. Nyrkova, Alexei R. Khokhlov, and Masao Doi. Microdomains in block copolymers and multiplets in ionomers: parallels in behavior. *Macromolecules*, 26(14):3601–3610, July 1993.

[61] Sachin Velankar and Stuart L. Cooper. Microphase Separation and Rheological Properties of Polyurethane Melts. 1. Effect of Block Length. *Macromolecules*, 31(26):9181–9192, December 1998.

[62] Robert D. Groot and Timothy J. Madden. Dynamic simulation of diblock copolymer microphase separation. *The Journal of Chemical Physics*, 108(20):8713, May 1998.

[63] M. A. J. van der Mee, R. M. A. LAbee, G. Portale, J. G. P. Goossens, and M. van Duin. Synthesis, Structure, and Properties of Ionic Thermoplastic Elastomers Based on Maleated Ethylene/Propylene Copolymers. *Macromolecules*, 41(14):5493–5501, July 2008.

[64] Hee-Tak Kim and Jung-Ki Park. Effects of cations on ionic states of poly(oligo-oxyethylene methacrylate-co-alkali metal acrylamidocaproate) single-ion conductor. *Solid State Ionics*, 98(3-4):237–244, June 1997.

[65] S Zhang. Molecular and anionic polymer and oligomer systems with microdecoupled conductivities. *Electrochimica Acta*, 45(8-9):1229–1236, January 2000.

[66] G M Mao, R F Perea, W S Howells, D L Price, and M L Saboungi. Relaxation in polymer electrolytes on the nanosecond timescale. *Nature*, 405(6783):163–165, 2000.

[67] A Triolo, V Arrighi, R Triolo, S Passerini, M Mastragostino, R E Lechner, R Ferguson, O Borodin, and G D Smith. Dynamic heterogeneity in polymer electrolytes. Comparison between QENS data and MD simulations. *Physica B*, 301(1-2):163–167, 2001.

[68] O Borodin and G D Smith. Molecular dynamics simulations of poly(ethylene oxide)/LiI melts. 2. Dynamic properties. *Macromolecules*, 33(6):2273–2283, 2000.

[69] C Y Ouyang, S Q Shi, Z X Wang, X J Huang, and L Q Chen. First-principles study of Li ion diffusion in LiFePO4. *Physical Review B*, 69(10), 2004.

[70] B Mos, P Verkerk, S Pouget, A van Zon, G J Bel, S W de Leeuw, and C D Eisenbach. The dynamics in polyethyleneoxide-alkali iodide complexes investigated by neutron spin-echo spectroscopy and molecular dynamics simulations. *Journal of Chemical Physics*, 113(1):4–7, 2000.

[71] P Carlsson, R Zorn, D Andersson, B Farago, W S Howells, and L Borjesson. The segmental dynamics of a polymer electrolyte investigated by coherent quasielastic neutron scattering. *Journal of Chemical Physics*, 114(21):9645–9656, 2001.

[72] O Borodin and G D Smith. Mechanism of ion transport in amorphous poly(ethylene oxide)/LiTFSI from molecular dynamics simulations. *Macromolecules*, 39(4):1620–1629, 2006.

[73] Peter G Bruce, editor. *Solid state electrochemistry - Edited by Peter G. Bruce*. Cambridge University Press, Cambridge, April 1995.

[74] Shih-Wa Wang, Wenjuan Liu, and Ralph H. Colby. Counterion Dynamics in Polyurethane-Carboxylate Ionomers with Ionic Liquid Counterions. *Chemistry of Materials*, 23(7):1862–1873, April 2011.

[75] Eisaku Hirasawa, Yoshimasa Yamamoto, Kenji Tadano, and Shinichi Yano. Effect of metal cation type on the structure and properties of ethylene ionomers. *Journal of Applied Polymer Science*, 42(2):351–362, January 1991.

[76] Y. Okamoto, T. F. Yeh, H. S. Lee, and T. A. Skotheim. Design of alkaline metal ion conducting polymer electrolytes. *Journal of Polymer Science Part A: Polymer Chemistry*, 31(10):2573–2581, September 1993.

[77] D Benrabah. Perfluorosulfonate-polyether based single ion conductors. *Electrochimica Acta*, 40(13-14):2259–2264, October 1995.

[78] Benoit Marsan and Martin Malservisi. Ionic conductivity studies of polymer electrolytes containing organosulfur species. *Electrochimica Acta*, 37(9):1645–1647, January 1992.

[79] G Mao, M L Saboungi, D L Price, Y S Badyal, and H E Fischer. Lithium environment in PEO-LiClO4 polymer electrolyte. *Europhysics Letters*, 54(3):347–353, 2001.

[80] G M Mao, M L Saboungi, D L Price, M B Armand, and W S Howells. Structure of liquid PEO-LiTFSI electrolyte. *Physical Review Letters*, 84(24):5536–5539, 2000.

[81] A Triolo, F Lo Celso, S Passerini, V Arrighi, R E Lechner, B Frick, and R Triolo. Segmental dynamics in polymer electrolytes. *Applied Physics A: Materials Science & Processing*, 74(0):s493–s495, 2002.

[82] C D Robitaille and D Fauteux. Phase-Diagrams and Conductivity Characterization of Some Peo-Lix Electrolytes. *Journal of the Electrochemical Society*, 133(2):315–325, 1986.

[83] L Edman, A Ferry, and M M Doeff. Slow recrystallization in the polymer electrolyte system poly(ethylene oxide)(n)-LiN(CF3SO2)(2). *Journal of Materials Research*, 15(9):1950–1954, 2000.

[84] J K Maranas. "Solid Polymer Electrolytes" in Dynamics of Soft Matter: Neutron Applications (In press).

[85] G M Mao, M L Saboungi, D L Price, M Armand, F Mezei, and S Pouget. alpha-relaxation in PEO-LiTFSI polymer electrolytes. *Macromolecules*, 35(2):415–419, 2002.

[86] Oleg Borodin and Grant D. Smith. Development of Quantum Chemistry-Based Force Fields for Poly(ethylene oxide) with Many-Body Polarization Interactions. *The Journal of Physical Chemistry B*, 107(28):6801–6812, July 2003.

[87] E Staunton, Y G Andreev, and P G Bruce. Factors influencing the conductivity of crystalline polymer electrolytes. *Faraday Discussions*, 134:143–156, 2007.

[88] Y G Andreev, P Lightfoot, and P G Bruce. Structure of the polymer electrolyte poly(ethylene oxide)(3): LiN(SO2CF3)(2) determined by powder diffraction using a powerful Monte Carlo approach. *Chemical Communications*, 18:2169–2170, 1996.

[89] J D Londono, B K Annis, A Habenschuss, O Borodin, G D Smith, J Z Turner, and A K Soper. Cation Environment in Molten Lithium Iodide Doped Poly(ethylene oxide). *Macromolecules*, 30(23):7151–7157, 1997.

[90] Z Gadjourova, Y G Andreev, D P Tunstall, and P G Bruce. Ionic conductivity in crystalline polymer electrolytes. *Nature*, 412(6846):520–523, 2001.

[91] Peter G Bruce. Coordination chemistry in the solid state. *Philosophical Transactions of the Royal Society of London Series aMathematical Physical and Engineering Sciences*, 354(1706):415–436, 1996.

[92] S. H. Chung, Y. Wang, S. G. Greenbaum, D. Golodnitsky, and E. Peled. Uniaxial Stress Effects in Poly(ethyleneoxide)-LiI Polymer Electrolyte Film: A [sup 7]Li Nuclear Magnetic Resonance Study. *Electrochemical and Solid-State Letters*, 2(11):553–555, November 1999.

[93] Peter V. Wright, Y. Zheng, D. Bhatt, T. Richardson, and G. Ungar. Supramolecular order in new polymer electrolytes. *Polymer International*, 47(1):34–42, September 1998.

[94] Alasdair M Christie, Scott J Lilley, Edward Staunton, Yuri G Andreev, and Peter G Bruce. Increasing the conductivity of crystalline polymer electrolytes. *Nature*, 433(7021):50–3, January 2005.

[95] Zlatka Stoeva, Isabelle Martin-Litas, Edward Staunton, Yuri G Andreev, and Peter G Bruce. Ionic conductivity in the crystalline polymer electrolytes PEO6:LiXF6, X = P, As, Sb. *Journal of the American Chemical Society*, 125(15):4619–26, April 2003.

[96] Josef Barthel. *Physical chemistry of electrolyte solutions : modern aspects*. Steinkopf ;;Springer, Darmstadt, New York, 1998.

[97] Raymond M. Fuoss and Charles A. Kraus. Properties of Electrolytic Solutions. IV. The Conductance Minimum and the Formation of Triple Ions Due to the Action of Coulomb Forces1. *J. Am. Chem. Soc.*, 55(6):2387–2399, 1933.

[98] Masashi Hojo. Elucidation of specific ion association in nonaqueous solution environments. *Pure and Applied Chemistry*, 80(7):1539–1560, 2008.

[99] David J. Roach, Shichen Dou, Ralph H. Colby, and Karl T. Mueller. Nuclear Magnetic Resonance Investigation of the Dynamics in Poly(Ethylene Oxide) Based Lithium Polyether-ester-sulfonate Ionomers. *Manuscript in preparation*.

[100] M F Lu, J Runt, and P Painter. An Infrared Spectrocopic Study of a Polyester Copolymer Ionomer Based on Poly(ethylene oxide). *Macromolecules*, 42(17):6581–6587, 2009.

[101] K-J Lin and J K Maranas. Comparison of PEO-based ionomer and PEO/salt - A molecular dynamics simulation study. *Manuscript in preparation*.

[102] K-J Lin and J K Maranas. The interplay of ion crosslinking, free ion content and polymer mobility in PEO based single ion conductors. *Manuscript in preparation*.

[103] S H Zhang, S C Dou, R H Colby, and J Runt. Glass transition and ionic conduction in plasticized and doped ionomers. *Journal of Non-Crystalline Solids*, 351(33-36):2825–2830, 2005.

[104] E De Luca, T A Waigh, M Monkenbusch, J S Kim, and H S Jeon. Neutron spin echo study of the dynamics of micellar solutions of randomly sulphonated polystyrene. *Polymer*, 48(14):3930–3934, 2007.

[105] A Paciaroni, M Casciola, E Cornicchi, M Marconi, G Onori, M Pica, and R Narducci. Temperature-dependent dynamics of water confined in Nafion membranes. *Journal of Physical Chemistry B*, 110(28):13769–13776, 2006.

[106] J C Perrin, S Lyonnard, and F Volino. Quasielastic neutron scattering study of water dynamics in hydrated nafion membranes. *Journal of Physical Chemistry C*, 111(8):3393–3404, 2007.

[107] A A Pivovar and B S Pivovar. Dynamic behavior of water within a polymer electrolyte fuel cell membrane at low hydration levels. *Journal of Physical Chemistry B*, 109(2):785–793, 2005.

[108] K A Page, J K Park, R B Moore, and V G Sakai. Direct Analysis of the Ion-Hopping Process Associated with the alpha-Relaxation in Perfluorosulfonate Ionomers Using Quasielastic Neutron Scattering. *Macromolecules*, 42(7):2729–2736, 2009.

[109] NIST Center for Neutron Research - Neutron scattering lengths and cross sections, 2011.

[110] J R D Copley and J C Cook. The Disk Chopper Spectrometer at NIST: a new instrument for quasielastic neutron scattering studies. *Chemical Physics*, 292(2-3):477–485, 2003.

[111] A Meyer, R M Dimeo, P M Gehring, and D A Neumann. The high-flux backscattering spectrometer at the NIST Center for Neutron Research. *Review of Scientific Instruments*, 74(5):2759–2777, 2003.

[112] E Mamontov and K W Herwig. A time-of-flight backscattering spectrometer at the Spallation Neutron Source, BASIS. *The Review of scientific instruments*, 82(8):085109, August 2011.

[113] R T Azuah, L R Kneller, Y Qiu, P L W Tregenna-Piggott, C M Brown, J R D Copley, and R M Dimeo. DAVE: A comprehensive software suite for the reduction, visualization, and analysis of low energy neutron spectroscopic data. *J. Res. Natl. Inst. Stand. Technol*, 114(6):341–358, 2009.

[114] G Williams and D C Watts. Non-Symmetrical Dielectric Relaxation Behaviour Arising from a Simple Empirical Decay Function. *Transactions of the Faraday Society*, 66(565P), 1970.

[115] C X Chen, P Depa, V G Sakai, J K Maranas, J W Lynn, I Peral, and J R D Copley. A comparison of united atom, explicit atom, and coarse-grained simulation models for poly(ethylene oxide). *Journal of Chemical Physics*, 124(23), 2006.

[116] K L Ngai and C M Roland. Unusual component dynamics in poly(ethylene oxide)/poly(methyl methacrylate) blends as probed by deuterium NMR. *Macromolecules*, 37(8):2817–2822, 2004.

[117] V G Sakai, J K Maranas, Z Chowdhuri, I Peral, and J R D Copley. Miscible blend dynamics and the length scale of local compositions. *Journal of Polymer Science Part B-Polymer Physics*, 43(20):2914–2923, 2005.

[118] J Maranas. The effect of environment on local dynamics of macromolecules. *Current Opinion in Colloid & Interface Science*, 12(1):29–42, February 2007.

[119] J Rault. Origin of the Vogel-Fulcher-Tammann law in glass-forming materials: the alpha-beta bifurcation. *Journal of Non-Crystalline Solids*, 271(3):177–217, 2000.

[120] R. Bergman, F. Alvarez, A. Alegra, and J. Colmenero. The merging of the dielectric α- and β-relaxations in poly-(methyl methacrylate). *The Journal of Chemical Physics*, 109(17):7546, November 1998.

[121] M L Saboungi, D L Price, G M Mao, R Fernandez-Perea, O Borodin, G D Smith, M Armand, and W S Howells. Coherent neutron scattering from PEO and a PEO-based polymer electrolyte. *Solid State Ionics*, 147(3-4):225–236, 2002.

[122] V G Sakai, C X Chen, J K Maranas, and Z Chowdhuri. Effect of blending with poly(ethylene oxide) on the dynamics of poly(methyl methacrylate): A quasi-elastic neutron scattering approach. *Macromolecules*, 37(26):9975–9983, 2004.

[123] J Sacristan, C X Chen, and J K Maranas. Role of effective composition on dynamics of PEO-PMMA blends. *Macromolecules*, 41(14):5466–5476, 2008.

[124] William W Graessley. *Polymeric Liquids & Networks: Structure and Properties*. Taylor & Francis Books, Inc, New York, 2004.

[125] C Labreche, I Levesque, and J Prudhomme. An appraisal of tetraethylsulfamide as plasticizer for poly(ethylene oxide)-LiN(CF3SO2)(2) rubbery electrolytes. *Macromolecules*, 29(24):7795–7801, 1996.

[126] E Donth. The size of cooperatively rearranging regions at the glass transition. *Journal of Non-Crystalline Solids*, 53(3):325–330, 1982.

[127] A Bouridah, F Dalard, D Deroo, and M B Armand. Potentiometric measurements of ionic transport parameters in poly(ethylene oxide)-LiX electrolytes. *Journal of Applied Electrochemistry*, 17(3):625–634, 1987.

[128] Michel Armand. Polymer solid electrolytes - an overview. *Solid State Ionics*, 9-10(Part 2):745–754, 1983.

[129] M R Tant, K A Mauritz, and G L Wilkes. *Ionomers: Synthesis, Structure, Properties and Applications*. Springer, Berlin, 1997.

[130] Peter G. Bruce and Colin A. Vincent. Effect of ion association on transport in polymer electrolytes. *Faraday Discussions of the Chemical Society*, 88:43, January 1989.

[131] R J Klein, S H Zhang, S Dou, B H Jones, R H Colby, and J Runt. Modeling electrode polarization in dielectric spectroscopy: Ion mobility and mobile ion concentration of single-ion polymer electrolytes. *Journal of Chemical Physics*, 124(14), 2006.

[132] J. Bastek, N.A. Stolwijk, Th. K.-J. Köster, and L. van Wüllen. Systematics of salt precipitation in complexes of polyethylene oxide and alkali metal iodides. *Electrochimica Acta*, 55(4):1289–1297, January 2010.

Kokonad Sinha

CONTACT INFORMATION
115 Fenske Lab
University Park, PA 16802
E-mail: kus160@psu.edu
Phone: (814) 863-2879

EDUCATION

The Pennsylvania State University, University Park, PA USA

Ph.D., Chemical Engineering, May 2012 (GPA: 3.56)

Indian Institute of Technology - Madras, Chennai, Tamil Nadu, India

Master of Technology, Chemical Engineering, Spring 2006 (GPA: 9.74)

Bachelor of Technology, Chemical Engineering, Spring 2006 (GPA: 8.22)

PUBLICATIONS

Sinha, K.; Maranas, J.K. "Favorable scenarios for ion transport based on polymer dynamics in PEO based single conductors (working title)"
Manuscript in preparation, Spring 2012

Sinha, K.; Maranas, J.K. "Dynamic patterning in PEO based single ion conductors for Li ion batteries (working title)"
Manuscript in preparation, Fall 2011

Sinha, K.; Maranas, J.K. "Segmental Dynamics and Ion Association in PEO-Based Single Ion Conductors"
Macromolecules **2011**, 44(13), pp5381-5391.

CONFERENCES

American Physical Society:
March 2011, Dallas, TX; March 2010, Portland, OR; March 2009, Pittsburgh, PA. (Oral)

American Institute of Chemical Engineers:
November 2008, Philadelphia, PA. (Oral)

Gordon Research Conference - Polymer Physics:
July 2010. South Hadley, MA. (Poster)

Materials Research Symposium - Dynamics of Soft Matter:
December 2008. Boston, MA. (Poster)

AWARDS

The Larry Duda Award for Outstanding Graduate Student Performance in Chemical Engineering, sponsored by Arkema, Inc. *2010*

National Talent Search Scheme Scholarship, organized by the National Council of Educational Research and Training, India. *1999-2006*